EXPERIMENTAL INVESTIGATION ON THE OUT-OF-PLANE BEHAVIOUR OF CONCRETE MASONRY INFILLED RC FRAMES

by

Reza Sepasdar

Submitted in partial fulfilment of the requirements
for the degree of Master of Applied Science

at

Dalhousie University
Halifax, Nova Scotia
April 2017

TABLE OF CONTENTS

LIST OF TABLES

LIST OF FIGURES

ABSTRACT

Previous studies on masonry infilled frames have shown that if an infill is built in tight contact with the bounding frame, the out-of-plane behaviour is governed by a phenomenon called arching action. This causes masonry infills to have much greater out-of-plane strength than conventional flexural walls. However, the literature review yielded a small number of studies and on limited material and geometric parameters of masonry infilled frames. Although there are several existing analytical methods for calculating the out-of-plane strength, their efficacy has not been thoroughly examined. While the American standard MSJC 2013 contains a semi-empirical equation for out-of-plane strength calculation for masonry infills of simple conditions, the Canadian standard CSA S304-14 provides no specific provisions but suggests the use of first-principle mechanics for design.

This study was motivated to augment the existing experimental database on out-of-plane behaviour and strength of masonry infills and to assess the efficacy of existing analytical methods for infill out-of-plane strength calculation. A total of four masonry infilled reinforced concrete (RC) frame specimens was tested with different parameters. One was considered as a control specimen; one was built with a window opening in the infill; and the other two had sustained damage caused by either prior in-plane or out-of-plane loading. Of two specimens with prior damage, one was first subjected to in-plane loading until occurrence of a major diagonal crack, and then tested under out-of-plane pressure to failure. The other was first subjected to out-of-plane pressure until occurrence of a major horizontal crack, and then tested under in-plane loading to failure. The experimental results were presented and discussed in terms of load vs. displacement response, cracking pattern, and failure mode for each specimen and the effect of parameters was studied. The effectiveness of existing analytical methods for out-of-plane strength calculation was examined using test results of experimental programs carried out by various researchers.

Experimental results showed that prior damage sustained from in-plane loading resulted in reduction in the out-of-plane strength, and the more significant the damage, the higher the reduction. However, prior damage in the form of a central horizontal crack sustained from out-of-plane loading showed negligible effect on the in-plane strength of the infill. The presence of infill opening resulted in a reduction in the out-of-plane strength and displacement of the infill. The out-of-plane failure of all specimens was characterized by web shear failure of masonry units of the infill.

None of the existing methods was shown to provide consistently accurate strength estimate over the entire data set. Both gross conservatism and overestimation were observed for certain group of results. Comparing to the other methods evaluated for strength calculation, MSJC 2013 performed better still with a high COV. The only method that accounts for prior in-plane damage effect provided inconsistent predictions of strength for damaged specimens.

LIST OF ABBREVIATIONS AND SYMBOLS USED

ABBREVIATIONS

CMUs	Concrete masonry units
COV	Coefficient of variation
IF-D	Infilled frame with prior damage
IF-ND	Infilled frame with no damage
IF-W-ND	Infilled frame with window opening and no damage
LVDT	Linear variable differential transformer
RC	Reinforced concrete
URM	Unreinforced masonry

SYMBOLS

A_0	Area of openings in wall panel
A^{eq}	Area equivalent cross-section
A_c	Area of concrete section
A_p	Area of wall panel without opening
A_s^{eq}	Area of equivalent steel section
b_w	Actual thickness of the infill
C	Clamping compressive force
d_v	Effective depth of a masonry wall in direction of shear considered
C_h, C_v	Horizontal, vertical clamping compressive force
E	Modulus of elasticity

E_b, E_c	Bounding beam, bounding column modulus of elasticity
E_f	Bounding frame modulus of elasticity
E_m	Modulus of elasticity of masonry
EI	Flexural stiffness of weakest member of the bounding frame
f_c	Maximum stress at contact surface after arching action is enabled
f_c'	Compressive strength of concrete
f_m'	Compressive strength of masonry
F_{cr}	First crack load of the infilled frame under in-plane loading
F_{cr}^{ana}	Analytical first crack load of the infilled frame under in-plane loading
F_r	Modification factor that depends on whether or not the opening is blast-resisting
F_{strt}	The load in the diagonal strut
F_{ult}	Ultimate load of the infilled frame under in-plane loading
g_0	Axial shortening of the infill
g_0^h, g_0^v	Horizontal, vertical axial shortening
G_b, G_c	Bounding beam, bounding column shear modulus
h	Height of the infill
I_b, I_c	Bounding beam, bounding column moment of inertia in the plane of infill
I_{cr}	Moment of inertia of the cracked section
I_g	Gross moment of inertia
J_b, J_c	Bounding beam, bounding column torsional constant in the plane of infill
l	Length of the infill
M_{rh}, M_{rv}	Horizontal, vertical bending moment resistant

P_{cr}	First crack pressure of the infill under out-of-plane loading
P_d	Axial compressive load on the section considered
P_{ult}	Ultimate pressure of the infill under out-of-plane loading
q, q_{ana}	Out-of-plane strength of the infill obtained from analytical method
q'	Resistance of the infill without opening
q_h, q_v	Horizontal, vertical arching strength obtained from analytical method
R_1	A reduction factor accounting for prior in-plane damage
R_2	A reduction factor accounting for bounding frame stiffness
t	Thickness of the infill
t_e	Effective thickness of the infill
V_f	Factored shear at the section considered
V_r	Shear resistance of the infill
w	Width of the diagonal strut
x_{yh}, x_{yv}	Horizontal, vertical arching out-of-plane displacement
θ	Angle whose tangent is the infill height-to-length aspect ratio
α	A measure of relative stiffness of the bounding beam
α_h, α_l	Vertical, horizontal contact length of the frame and the diagonal strut
β	A measure of relative stiffness of the bounding column
ϵ_m	Strain of the infill corresponding to axial shortening
$\epsilon_m^h, \epsilon_m^v$	Horizontal, vertical strain of the infill corresponding to axial shortening
λ	A measure of wall slenderness ratio
γ	A factor that accounts for depth of compression

γ_g	Factor to account for partially grouted and ungrouted walls
ϕ_m	Resistance factor for masonry
Δ_0	Midspan deflection of the infill in one-way arching condition
Δ_{cr}	First crack displacement of the infill under out-of-plane loading
Δ_{ult}	Displacement at ultimate load of the infill under out-of-plane loading
δ	Applied displacement of the infilled frame under in-plane loading
δ_{cr}	First crack displacement of the infilled frame under in-plane loading
δ_{cr}^{ana}	Analytical first crack displacement of the infilled frame under in-plane loading
δ_{ult}	Displacement at ultimate load of the infilled frame under in-plane loading

ACKNOWLEDGEMENTS

First and foremost, I would like to express my sincere gratitude to my supervisor, Dr. Yi Liu, for her guidance throughout my project and for her continuous support during my studies at Dalhousie University. This thesis would have not been possible without her irreplaceable contribution.

I wish to recognize the contribution of financial assistance by the Canadian Concrete Masonry Producers Association and the Natural Sciences and Engineering Research Council of Canada.

I would like to thank Dr. Pedram Sadeghian and Dr. Andrew Corkum for reviewing this thesis and providing valuable feedbacks.

I would like to thank my fellow colleagues Ryan Steeves, Reza Rahimi, Ehsan Nasiri, and Chongyang Wang for helping me in carrying out the experiment.

I would like to thank the departmental technicians Mr. Brian Kennedy, Mr. Blair Nickerson, Mr. Brian Liekens, and the mason Gerry Hubley for their assistance and contribution during the experiment.

Finally, I would like to thank my family for their endless love, support, and encouragement.

CHAPTER 1 INTRODUCTION

1.1 BACKGROUND

Masonry materials and construction have progressed through several stages of development. Masonry clay brick was predominately used prior to 1900s. With the introduction of concrete in early 1900s, concrete masonry was introduced to the construction. The concrete block was cheaper than cut stones and required less labor to lay than bricks and use of concrete masonry advanced masonry construction into a modern era. Over the twentieth-century masonry blocks were manufactured with much higher strength and various types, and together with the introduction of steel reinforcement into masonry, masonry remained as a competitive construction material among steel and concrete for both residential and commercial construction. Historically, the "rules of thumb", were the only available methods for masonry design until 1950s. The development of building codes for engineering design of masonry structures began in late 1950s. The first unified provisions for masonry design in Canada were introduced in the National Building Code of Canada (NBCC) in 1965 and improved and expanded in 1970 and 1975 editions. Although based on the allowable stress concept, the design provisions were considered a large step forward from the "rules of thumb". The methodology of ultimate limit state design was introduced in 1990s for masonry and has been adopted in design codes and standards ever since in both Canada and United States. This has aligned masonry design methodology with that of other main construction materials (concrete, steel, timber) and enabled masonry to remain as a predominant construction material in modern days. At present, the governing standards

for masonry design are the Canadian Standard Association CSA S304-14 (2014) in Canada and Masonry Standard Joint Committee MSJC 2013 in the US.

1.2 OUT-OF-PLANE BEHAVIOUR OF MASONRY INFILLS

A masonry infilled frame is either a concrete or steel frame with a masonry wall built within and it is used either as a partition to separate spaces or cladding to complete a building envelope (Figure 1.1). Although the inherent large in-plane stiffness of masonry walls can provide the lateral stiffness required in a seismic design, the industry practice has been to treat the infill as non-structural element and design the frame for both lateral and gravity loads. However, the practice has shown that when infills are built tight against their bounding frames, interaction between the infill and its bounding frame will make behavioural characteristics of the infill different from regular masonry walls without confinement. One such example is out-of-plane behaviour and strength of infills which is different from masonry flexural walls without confinement. The out-of-plane strength of flexural walls relies on its bending capacity which is in turn dependent on the tensile strength of the mortar joint while the out-of-plane behaviour of infill walls is characterized by a phenomenon called “arching action”. When a wall is butted up against the frame acting as rigid supports, in-plane compressive forces are induced in the wall as it bends under out-of-plane forces, and these compressive forces can delay cracking and subsequent arching of the wall. The arching action was shown to increase the out-of-plane capacity of masonry infills significantly, in some cases, 2 to 3 times higher than its flexural capacity. The more recent research showed that the “arching action” was dependent on the masonry compressive strength, panel dimensions, and boundary conditions between the infill and

the frame. Development of arching action can enhance the stability of infills even after the ultimate capacity was achieved. However, parameters in previous studies were limited and although arching action phenomenon was well described, no quantitative relationships were established to define the out-of-plane strength in relation to all influential parameters for practical design. In practice, the Canadian masonry design standard CSA S304-14 provides no specific design provisions for the out-of-plane strength of infill walls but suggests that the first principle mechanics be relied on for analysis. The American masonry design standard MSJC 2013 contains a semi-empirical strength equation for masonry infills subjected to out-of-plane loading, which was largely based on experimental results obtained by three research groups (Dawe and Seah 1989; Angel 1994; Klingner et al. 1996).

It is noted that while considerable research has been conducted in the area of in-plane behaviour of masonry infilled frames, the research on the out-of-plane behaviour of masonry infills is very limited and research results are scarce in the literature. Furthermore, in-plane and out-of-plane behaviour may have some level of interaction in the event of earthquake. It is conceivable that the in-plane damage sustained in the infill could affect its out-of-plane strength and vice versa. However, the potential interaction of in-plane and out-of-plane behaviour of masonry infills has received little research attention. Also, the amount of research on the effect of window opening on the out-of-plane behaviour of masonry infills is limited. In view of the above, this research was carried out to provide a better understanding of out-of-plane behaviour of masonry infills in general, as well as on how in-plane/out-of-plane damage influences out-of-plane/in-plane strength of infills.

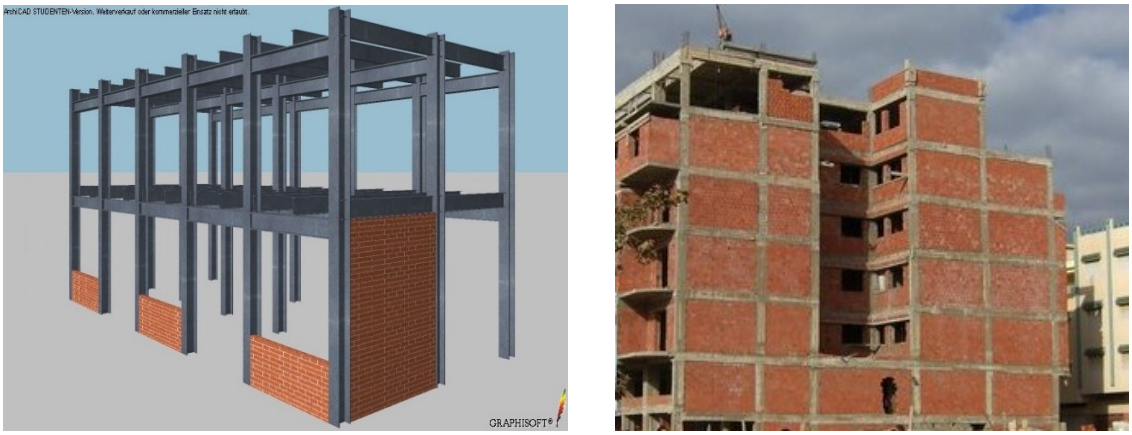

(a) (b)

Figure 1.1 Example of Masonry Infill Walls

(a) Steel moment resisting frame with brick masonry partitions (world house encyclopedia); (b) Reinforced concrete frame with brick masonry infills (Scawthorn, C.)

1.3 RESEARCH OBJECTIVES

This research involved an experimental investigation of the out-of-plane behaviour and strength of masonry infills with a focus on the effect of infill opening and prior damage. The objectives are as follows:

1. To augment the existing experimental database on the out-of-plane behaviour of masonry infilled RC frame specimens.

2. To analyze the effect of tested parameters on the behaviour and strength of the infills.

3. To examine the efficacy of existing analytical methods including code provisions using test results.

1.4 DOCUMENT ORGANIZATION

This thesis comprises six chapters. Chapter 1 contains an introduction along with objectives of this research; Chapter 2 presents a literature review on the out-of-plane behaviour of masonry infilled frames including various methods of calculating the out-of-plane strength, North American masonry design codes, and previous experimental studies; Chapter 3 describes the procedure of the experimental program in detail, including the construction of masonry infilled RC frames, in-plane and out-of-plane test setup, and auxiliary tests of the materials used; Chapter 4 presents and analyzes the experimental results; Chapter 5 compares the experimental results with the analytical values obtained using the design codes and various analytical methods; Chapter 6 presents a summary of the research and conclusions from this study.

CHAPTER 2 LITERATURE REVIEW

2.1 INTRODUCTION

The research is to investigate the out-of-plane behaviour and strength of masonry infilled RC frames with a focus on the masonry infill. The following sections present a summary of general behaviour of infilled frames, current code practice in North America for design of infills, and previous studies conducted in the area of infilled frames with particular attention paid to the effect of prior in-plane damage and infill opening. This literature review focuses on RC frames, although the relevant researches on steel frames are also reported.

2.2 OUT-OF-PLANE BEHAVIOUR OF INFILLED FRAMES

2.2.1 General

As mentioned earlier, previous research conducted on the out-of-plane behaviour of infill walls is limited and within available studies, several methods were reported for the out-of-plane loading including blast loading, shaking table, and static pressure while majority studies used the setup of a single-bay single-storey infilled frame loaded by static uniform pressure.

One of the earliest studies on the out-of-plane behaviour of infill walls was done by Monk (1958) using blast loading to assess the damage expected in different types of blast up to atomic blast. Gabrielsen (1975) tested a series of full scale infilled panels under the blast loading to assess the out-of-plane strength and behaviour. However, blast loading test is

expensive and also requires special facilities and thus is usually done by defence and military agencies.

Another method for dynamic testing of infill specimens is by using shaking tables (Henderson et al. 2003; Meisl et al. 2007; Rabinovitch 2011). Shaking tables are the best means of obtaining the seismic response of a structure by simulating a specific recorded ground motion. Henderson et al. (2003) conducted an extensive shake-table test of large- and small-scale unreinforced masonry infills. They found that the unreinforced masonry infills are more ductile and more efficient in carrying both out-of-plane and in-plane loads than what building codes specify. Meisl et al. (2007) studied the effects of ground motion type and quality of construction on the rocking response of unreinforced masonry walls (URMs) after they cracked at the mid-height under out-of-plane inertial forces using a shaking table. The parameters they studied were observed not to have a significant effect on the peak response of the walls. Rabinovitch and Madah (2011) conducted unidirectional shake-table tests of masonry infill walls to study their response to out-of-plane dynamic loads and proposed a finite element model for numerical simulation of infill walls.

Static testing of infill walls has been shown to have an acceptable accuracy to reflect dynamic properties of the infilled system (Dawe and Seah 1989; Angel 1994; Flanagan and Bennett 1999). The static loading can be applied by either concentrated loading through hydraulic actuators (Hill 1993; Hak 2014), or by uniform out-of-plane pressure on the surface of the panels via airbags. The latter is the most common method of static out-of-plane testing of infill walls and has been used by many researchers.

2.2.2 Arching Action

As mentioned earlier, the key characteristics of out-of-plane behaviour of an infill is the potential development of arching action with the surrounding frame. If a wall is built in tight contact against its bounding frame while the frame member is considered rigid, an out-of-plane displacement of the wall will induce an in-plane compressive force within the wall. This force results in arching within the thickness of the wall which will drastically increase the cracking load. The further deformation of the wall is followed by the occurrence of flexural cracks at the supports (bounding frame member), and horizontal cracks within the wall panel at the location of maximum moments, after which the wall is pushed against the supports and creates thrust forces at each end (Drysdale and Hamid 2005). Figure 2.1 illustrates the one-way arching (or three-hinged arch) behaviour of a wall supported on only two boundaries. Once arching action is enabled, the out-of-plane strength of the wall is dependent on the compressive strength of the mortar rather than its tensile strength.

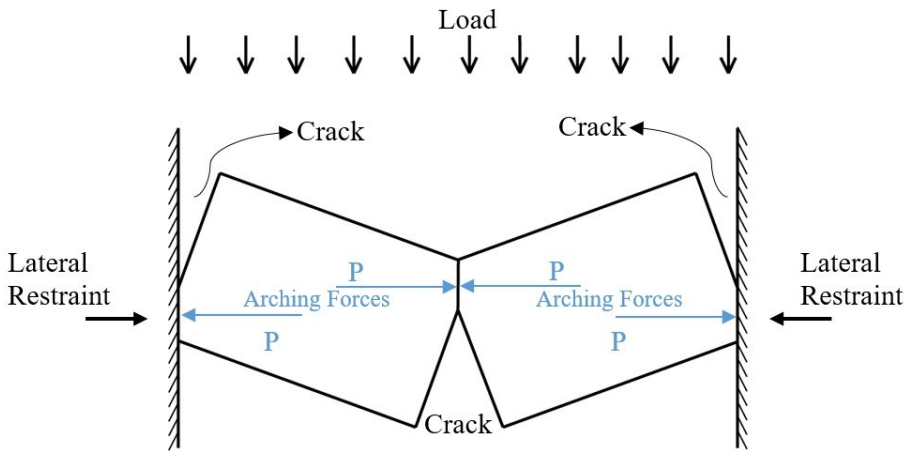

Figure 2.1 One-Way Arcing of Masonry Walls

Arching action in masonry walls was first studied by McDowell et al. (1956) and they proposed an equation for calculating out-of-plane pressure based on equilibrium conditions with clamping force developed at the compressive faces at the frame-to-infill boundary and at the midheight of the infill after the infill undergoes cracking and rigid body rotation. This method is discussed in detail in later sections.

To demonstrate the effect of arching action on the out-of-plane strength, an infill supported by four frame members and subjected to out-of-plane pressure was analyzed using yield line theory. Detailed calculation is shown in Appendix B using the infilled frame geometry and property of this experimental study. It is shown that for a regular infill or an infill with a central opening, consideration of arching action resulted in an increase in the out-of-plane strength about 500% to 600% in comparison with a yield line analysis.

2.2.3 Experimental Studies

Gabrielsen et al. (1975, 1976, 1977) conducted an experimental program to study the response of masonry walls subjected to uniform blast loads. Their experiment included full scale masonry walls bounded by steel frames subjected to blast waves in a big shock tunnel. The walls exhibited a load carrying capacity of roughly twice their corresponding flexural capacity. The walls also had the ability to resist moderate reversed cyclic loading.

Dawe and Seah (1989) conducted experiments on the out-of-plane behaviour of nine large scale concrete block masonry infilled steel frame specimens. One of their specimens had a central opening with 19% area of the infill. They reported that the presence of the opening resulted in about 10% reduction in the out-of-plane strength of the specimen and less ductility after the cracking occurred in the infill.

Frederiksen (1992) tested sixteen scaled clay brick infills bounded by steel tube frames under out-of-plane loading using an airbag. Three types of brick were used in their experiment and the main objective was to study the effect of infill-to-frame interfacial conditions by placing different materials in gaps between the infill and the frame at all boundaries instead of mortar. They concluded that the effect of bound type on the out-of-plane strength and cracking patter is negligible so long the infill is in tight contact with the bounding frame.

Angel (1994) conducted experiments on the out-of-plane behaviour of seven masonry infilled RC frames. The parameters he studied included wall thickness, mortar type, and unit type. They concluded that the out-of-plane strength depended on the compressive strength of the infill rather than its tensile strength, and was highly affected by the slenderness ratio of the wall. They also reported that the prior in-plane cracking reduced the out-of-plane strength of the panels by a factor as high as two.

Flanagan and Bennett (1999) conducted a series of in-plane, out-of-plane, and combined in-plane and out-of-plane experiments for a single-storey, single-bay clay tile infilled steel frame. They reported that the prior in-plane loading resulted in some strength reduction and higher deflections under uniform out-of-plane loading, however the arching was still formed which allowed the infill to maintain a substantial capacity. The combined loadings were achieved by pushing the infill to a certain displacement under in-plane/out-of-plane loading, and testing the infill to failure under out-of-plane/in-plane loading while holding the initial loading constant. It was reported that the presence of in-plane load reduced the out-of-plane pressure capacity, and the presence of out-of-plane load slightly increased the in-plane stiffness although the ultimate in-plane load remained unchanged.

Dafnis et al. (2002) conducted an experimental program to study the effect of gap resulted from shrinkage of the mortar, on the arching behaviour and stability of brick masonry walls. The gaps had both different sizes and different lengths on top of the infills. Six specimens were tested using a shaking table. All of the specimens were fix supported on top and bottom, meeting the condition of a one-way arching. One of their specimens was built with a central opening with about 7.5% of the wall area with no gap on top. They reported that the opening did not alter the dynamic response of the wall and no local effect around the opening especially at corners was reported. The relative displacement in the gap affected the stability of the walls, although for small gaps (< 3mm) the arching action still developed.

Griffith and Vaculik (2007) studied the out-of-plane behaviour of eight clay brick masonry wall specimens subjected to airbag pressure. The infills were assumed simply supported at the top and bottom, and fix-supported on sides, which corresponded to the horizontal arching action condition. The parameters included the presence of window opening, infill aspect ratio, and axial load. Two of their specimens with a height to length aspect ratio of 0.625 had an eccentrically positioned opening with 10% area of the wall. The other two specimens had an aspect ratio of 1.00 with a central opening with 16% area of the wall. They reported that the presence of the opening did not affect the ultimate strength of any of their specimen and only decreased the post cracking deformations. The presence of axial load was shown to increase the out-of-plane strength of the specimens.

Hak et al. (2014) conducted five out-of-plane cyclic tests on full-scale, single-storey, single-bay RC frame specimens with masonry clay block infills. The out-of-plane loading was applied at six discrete locations across the width of the infill using a hydraulic jack.

They suggested that the out-of-plane strength of infill walls may be expressed as a function of in-plane damage but without providing any quantitative correlations.

Furtado et al. (2016) conducted out-of-plane tests on three masonry infill walls bounded by RC frames to investigate the in-plane damage effect on the out-of-plane behaviour of infills. It was found that the out-of-plane strength of the undamaged specimen was about four times greater than the damaged specimen which also showed a higher out-of-plane deformation. The initial stiffness of the damaged specimen under out-of-plane loading was significantly smaller than the other specimens. The prior in-plane damage was also shown to affect the cracking pattern and failure mode of the specimen when subjected to out-of-plane loading.

Akhoundi et al. (2016) studied the out-of-plane behaviour of three brick masonry infilled RC frame specimens under uniform cyclic out-of-plane pressure. They found that the presence of opening decreased the initial stiffness by 12% while no significant reduction in the out-of-plane strength was observed.

2.2.4 Analytical Methods

Two methodologies have been used in developing analytical equations to calculate the out-of-plane strength of masonry infills bounded by either steel or RC frames. The existing proposed equations are based on either one or the other method. Early analytical methods were largely developed based on first principles of mechanics considering the arching action as shown in Figure 2.2 while later analytical equations (after 1989) were based on statistical analysis of the test results.

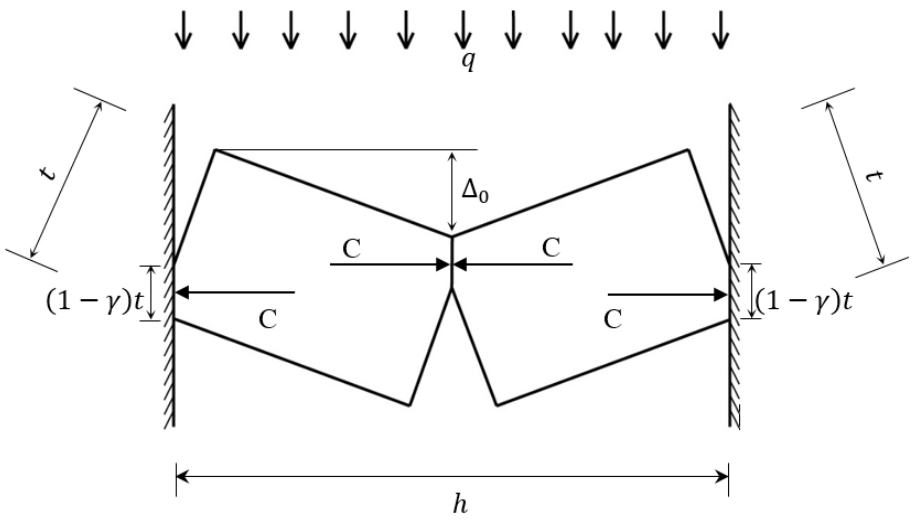

Figure 2.2 Arching Action Parameter in Mechanics of Rigid Arching

According to the mechanics of rigid arching in walls, McDowell et al. (1956) proposed the following equation to calculate the out-of-plane resistance of masonry walls under one-way arching condition:

$$q = \frac{8C}{h^2}(\gamma t - \Delta_0) \qquad [2.1]$$

where γ is a factor that accounts for the depth of the compression zone, t and h are the thickness and the height of the wall respectively, Δ_0 is the midspan deflection of the wall, and C is the thrust or clamping compression force per unit length of the wall which can be estimated as:

$$C = f_c(1 - \gamma)t \qquad [2.2]$$

where f_c is the stress over the compression zone which is assumed to be constant. The midspan deflection of the wall by considering axial shortening due to compressive arching forces in the wall is calculated from:

$$\Delta_0 = \frac{g_0 h}{4\gamma t} \qquad [2.3]$$

where g_0 is the axial shortening of the wall due to the arching forces.

British Standards Institution BS 5628 "Code of practice for use of masonry" (2005) suggested that γ be taken as 0.9 and f_c be considered as the compressive strength of masonry wall. Neglecting any deflection Δ_0=0, Eqn [2.1] can be simplified as follows:

$$q = \frac{8C}{h^2}(\gamma t) \qquad [2.4]$$

The equations based on mechanics of arching action apply only to infills after cracking. Therefore, design with these arching equations is an ultimate limit state design, not a design for service loads. The procedure of using this method for two-way arching conditions proposed by Drysdale and Hamid (2005) is explained in Appendix A.

Dawe and Seah (1989) performed nine large-scale, out-of-plane static pushover test on ungrouted, unreinforced masonry infill panels bounded by steel frames using an airbag. Parameters included the effects of boundary supports, joint reinforcement, panel thicknesses, panel opening, and characteristics of construction. They developed an empirical relationship based on their test results to calculate the out-of-plane strength of infill walls built in tight contact at all four boundaries against surrounding frames. In this method, the uniform out-of-plane pressure, q, that an infill can withstand is determined as:

$$q = 4.5 f_m'^{0.75} t^2 \left(\frac{\alpha}{l^{2.5}} + \frac{\beta}{h^{2.5}}\right) \qquad [2.5]$$

in which f'_m is the masonry compressive strength (kPa), t is the infill gross cross-section thickness (mm), h is the infill height (mm), and l is the infill length (mm). The parameters α and β account for the relative stiffness of the bounding columns and the bounding beam respectively, and are calculated as:

$$\alpha = \frac{1}{h}(E_c I_c h^2 + G_c J_c t h)^{0.25} < 50 \quad [2.6]$$

$$\beta = \frac{1}{l}(E_b I_b l^2 + G_b J_b t l)^{0.25} < 50 \quad [2.7]$$

where E is the modulus of elasticity of steel (MPa), I is the moment of inertia in the plane of the infill (mm^2), G is the shear modulus (MPa), and J is the torsional constant (mm^2), In which the subscript b and c are used for beam and columns material properties respectively.

Angel (1994) developed an analytical method based on his test results to consider the effect of prior in-plane damage on the out-of-plane strength of masonry infilled RC frames as:

$$q = \frac{2f'_m}{\left(\frac{h}{t}\right)} R_1 R_2 \lambda \quad [2.8]$$

where λ is a dimensionless parameter that is a function of the wall slenderness ratio (h/t). R_1 is a reduction factor accounting for prior in-plane damage and R_2 is a reduction factor for bounding frame stiffness obtaining from:

$$R_1 = \left[0.958 - 0.144\left(\frac{h}{l}\right)\right]^{\frac{\delta}{2\delta_{cr}}} \quad [2.9]$$

$$R_2 = 0.357 + 2.49\times10^{-14}EI \leq 1.0 \qquad [2.10]$$

in which δ_{cr} is the lateral drift of the frame corresponding to occurrence of first crack on the infill surface under in-plane loading, δ is the maximum lateral drift the infill has experienced, and EI is the flexural stiffness of weakest member of the frame ($N.mm^2$). This method was later adopted by Federal Emergency Management Agency FEMA 273 (1997) as follows:

$$q = \frac{0.7f'_m}{\left(\frac{h}{t}\right)}\lambda \qquad [2.11]$$

As seen in Eqn [2.11], a value of 0.7 instead of 2 was used in Eqn [2.8]. The reason is that FEMA 273 presents a lower-bound strength equation which accounts for prior in-plane damages by considering a reduction of 42% in the strength and also takes a value of 0.61 for R_2 (Flanagan and Bennett 1999).

Flanagan and Bennett (1999) further expanded the equation to show for the common slenderness ratios which are between 10 and 30, λ can be approximated as:

$$\lambda = 0.154\exp\left(-0.0985\frac{h}{t}\right) \qquad [2.12]$$

It should be noted that this method is the only one that accounts for damage due to prior in-plane loadings.

Klinger et al. (1996) improved the method that was first developed by Cohen and Laing (1956) by extending it to two-way arching. The out-of-plane pressure q is obtained as:

$$q = \frac{8}{h^2 l}\left\{M_{rv}[(l-h) + h\ln(2)] + M_{rh}\left(\frac{x_{yv}}{x_{yh}}\right)\ln\left(\frac{1}{1-h/2}\right)l\right\} \quad [2.13]$$

where M_{rv}, the moment resistance corresponding to vertical arching, is calculated as:

$$M_{rv} = \frac{0.85 f'_m}{4}\left(t - x_{yv}\right)^2 \quad [2.14]$$

In which x_{yv} is the displacement of the infill wall (corresponding to vertical arching) at the point of failure (mm), which is calculated as:

$$x_{yv} = \frac{t f'_m}{1000E\left[1 - \frac{h}{2\sqrt{(h/2)^2 + t^2}}\right]} \quad [2.15]$$

where E is the modulus of elasticity of the masonry (MPa). The term M_{rh} in Eqn [2.13] is calculated from Eqn [2.14] by replacing x_{yv} with x_{yh}, and x_{yh} is calculated from Eqn [2.15] by substituting h with l.

Mays et al. (1998) developed an equation to calculate the out-of-plane capacity of reinforced concrete wall panels with openings as:

$$\frac{q}{q'} = 1 + F_r\left(\frac{A_0}{A_p}\right) \quad [2.16]$$

in which q is the resistance of the wall panel with openings, q' is the resistance of the wall panel without opening, A_0 is the area of openings, A_p is the area of the wall panel without opening, and F_r is a modification factor that depends on whether or not the opening is blast-resistant. Blast-resistant openings are assumed to transfer the applied pressure to the wall panel as line loads along the opening boundaries, while non-resistant-openings are assumed

not to carry any out-of-plane load. For blast-resisting and non-blast-resistant central window openings, they suggested a value of -3.07 and -1.00 respectively for F_r. Although this formulation was developed for reinforced concrete walls, Flanagan and Bennett (1999) suggested that it can be used for evaluation of out-of-plane strength of unreinforced masonry infills with openings as well, however, more experimental results are needed to confirm its validity.

Flanagan and Bennett (1999) modified the method developed by Dawe and Seah (1989) by using test results obtained by researchers including Dawe and Seah (1989), Frederiksen (1992), Angel (1994), and Flanagan and Bennett (1999). In this method, the out-of-plane capacity of an infill is calculated as:

$$q = 4.1 f_m'^{0.75} t^2 \left(\frac{\alpha}{l^{2.5}} + \frac{\beta}{h^{2.5}}\right) \quad [2.17]$$

in which the parameters α and β are obtained from:

$$\alpha = \frac{1}{h}(E_c I_c h^2)^{0.25} < 50 \quad [2.18]$$

$$\beta = \frac{1}{l}(E_b I_b l^2)^{0.25} < 50 \quad [2.19]$$

If the slenderness ratio is less than 8 for an infill, the thickness of the infill should be considered as $1/8$ of the infill height in the presented formulation. They also proposed a formulation to calculate the deflection of the centre of the infill wall at the peak load as:

$$\frac{\Delta_{\text{ult}}}{h} = \frac{0.002\left(\frac{h}{t}\right)}{1 + \sqrt{1 - 0.001\left(\frac{h}{t}\right)^2}} \quad [2.20]$$

in which the Δ_{ult} is the deflection of the centre of the infill corresponding to ultimate load. This formulation is valid for slenderness ratios up to 25.

2.2.5 Code Practice in North America

2.2.5.1 CSA S304.14

The Canadian Masonry Standard CSA S304.14 does not contain any provisions for the out-of-plane strength calculation of masonry infills or arching action in masonry walls.

2.2.5.2 MSJC 2013

MSJC 2013 adopts the equations proposed by Flanagan and Bennett (1999), which was originally developed by Dawe and Seah (1989), as follows:

$$q = 105 f_m'^{0.75} t^2 \left(\frac{\alpha}{l^{2.5}} + \frac{\beta}{h^{2.5}} \right) \quad [2.21]$$

where α and β are obtained from:

$$\alpha = \frac{1}{h} (E_c I_c h^2)^{0.25} < 35 \quad [2.22]$$

$$\beta = \frac{1}{l} (E_b I_b l^2)^{0.25} < 35 \quad [2.23]$$

It must be noted that in these equations imperial units are used (*lb* and *in*) and q is calculated in lb/ft^2 unit. When the bounding frame is made from different columns (or beams) cross-sections, average values for properties shall be used. In the case of a single-storey frame, the properties of the top beam shall be used in the calculation. It is noted that equations presented above are essentially same as Eqn [2-17]-[2-19] but formulated in imperial units.

According to MSJC 2013, when a side (or a top gap) exists, a one-way arching may still develop and in such a case, the corresponding β (for side gap) or α (for top gap) shall be taken as zero.

2.4 CONCLUDING REMARKS

Compared with in-plane behaviour of masonry infills, the out-of-plane behaviour is much less researched. Although a number of experimental studies have been conducted, the number of specimens and studied parameters were limited which led to a small existing database of test results. Consequently, analytical equations developed based on existing test data are not thoroughly validated for different infill materials, geometries, and boundary conditions. This research is conducted to augment the existing database on the out-of-plane behaviour of masonry infills and to examine the efficacy of existing analytical equations using test results.

CHAPTER 3 EXPERIMENTAL PROGRAM

3.1 GENERAL

The experimental program was designed to investigate the out-of-plane behaviour and strength of concrete masonry infills bounded by RC frames. Effect of infill opening as well as prior damage were two parameters considered in this study. All specimens were constructed with the same general geometry but different parameters reflecting the opening and prior damage.

Along with testing of the infilled frame specimens, auxiliary tests for obtaining the material properties of concrete masonry units (CMUs), mortar, masonry prisms, concrete cylinders, and reinforcing steel were also performed. Detailed descriptions of the infilled frame specimens, test set-up, testing procedures, and auxiliary tests are presented in the following sections.

3.2 INFILLED FRAME SPECIMENS

Table 3.1 presents a summary of the infilled frame specimens. A total of four infilled frame specimens were tested in this experimental phase, including one control specimen with no prior damage and opening (IF-ND), one specimen with a central window opening of 17% of the infill area (IF-W-ND), and two specimens (IF-D1 and IF-D2) with prior damages. All masonry infills were built in tight contact at all boundaries with the bounding frames to enable the arching action. Specimen IF-D1 was first subjected to in-plane loading to the onset of diagonal cracking on the surface of the infill and then the in-plane loading was removed. The specimen was subsequently subjected to the out-of-plane pressure to failure.

Specimen IF-D2 was first subjected to the out-of-plane pressure to the onset of horizontal cracking at infill's midheight and then the out-of-plane loading was removed. The specimen was subsequently tested under in-plane loading to the ultimate capacity of the infilled frame. It was observed during the test that the infill remained largely intact at this point except some crushing at loaded corners. It was then decided to test the specimen again under out-of-plane loading to complete failure. The loading sequence is identified in the table and the intended prior damage is indicated in parenthesis.

Table 3.1 Summary of Frame Specimens

Number	Specimen ID	In-Plane (Prior Damage)	Out-of-Plane (Prior Damage)	Window Opening-to-Infill Area Ratio
1	IF-ND	No	Loaded to failure	N/A
2	IF-W-ND	No	Loaded to failure	17%
3	IF-D1	([1]Diagonal cracking)	[2]Loaded to failure	N/A
4	IF-D2	[2]Loaded to ultimate	([1]Horizontal cracking) [3]Loaded to failure	N/A

The dimensions for all frame specimens are shown in Figure 3.1. An experimental program was performed by Hu (2015), and continued by Steeves (2016) in the same research group on the in-plane behaviour of infilled RC frames. In order to make a meaningful comparison between in-plane and out-of-plane behaviour, the geometry and reinforcing details of their specimens were adopted in this study. The geometry of the infill yielded a height-to-length aspect ratio of about 0.73. The specimen IF-W-ND was made with a central opening of 584 *mm* by 395 *mm*. The infills were constructed using custom-made, half-scale standard

200 *mm* CMUs laid in running bond. Thus, all infills had a slenderness ratio (*h/t*) of 10.9. All of the specimens were unreinforced and ungrouted except for the specimen with opening which was grouted only in the cells surrounding the opening as required by CSA A179-14. The nominal dimensions of the stretchers and half blocks used in this experiment are shown in Figure 3.2. The stretcher blocks were cut in half to make the half blocks.

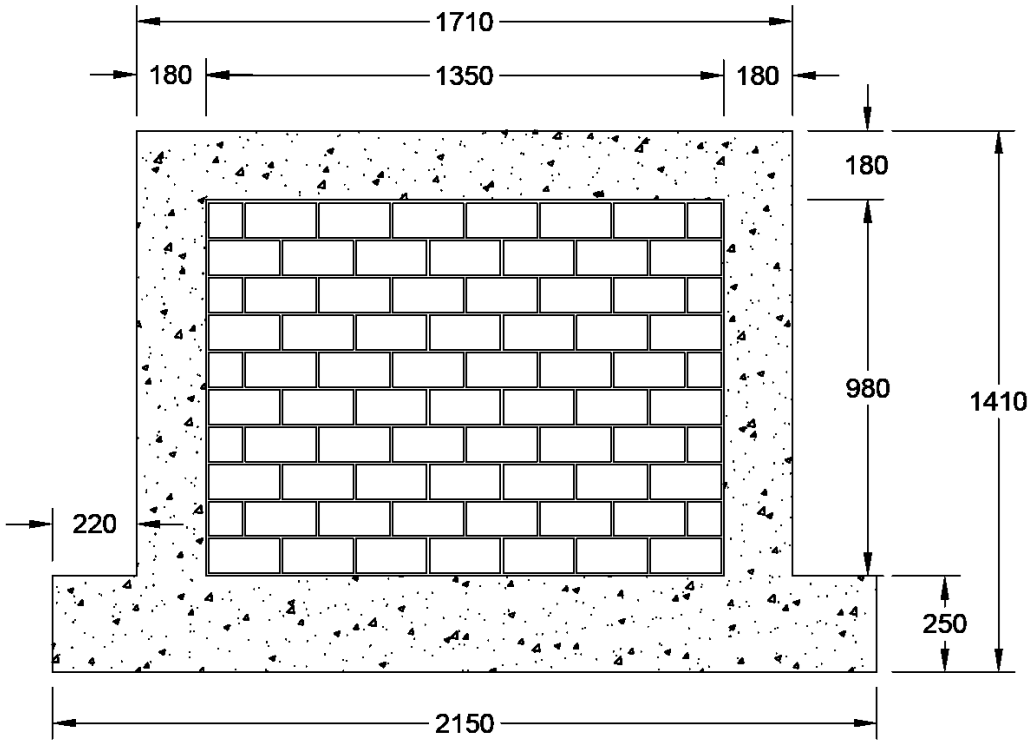

Figure 3.1 Geometric Properties of Infilled Frame Specimens (unit: *mm*)

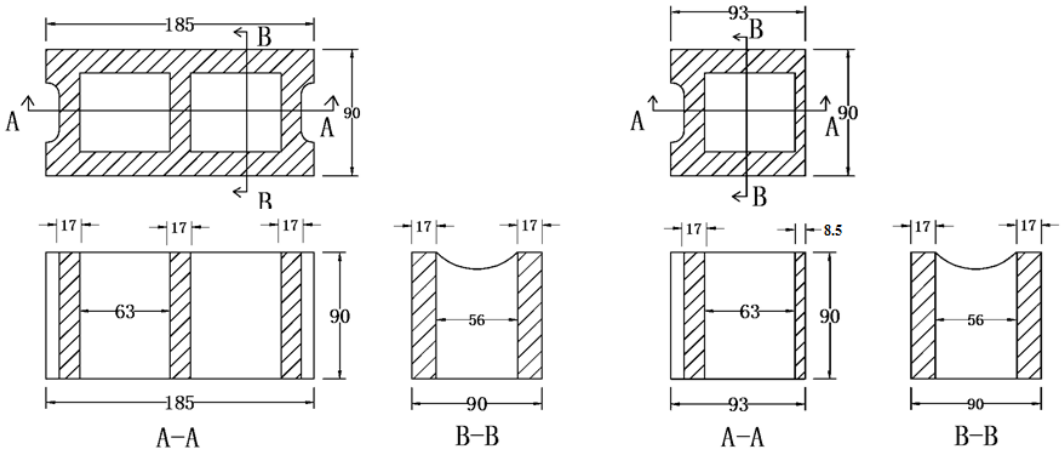

(a) Stretcher block (b) Half block

Figure 3.2 Details of Half-Scaled CMUs (unit: *mm*)

The frame beam and columns had a 180 *mm* square section reinforced with four 10M deformed rebars and 10M stirrups spaced at 100 *mm* centre-to-centre. The base beam had a 250 *mm* by 250 *mm* square cross-section reinforced with four 15M longitudinal rebars and 10M stirrups with a spacing of 100 *mm* centre-to-centre. In addition, four 300 *mm* by 300 *mm* L-shaped made from 10M rebars were used to make the top beam-column corners stronger. The concrete cover on rebars for all the frame members was 25 *mm*. Details of the reinforcement are shown in Figure 3.3.

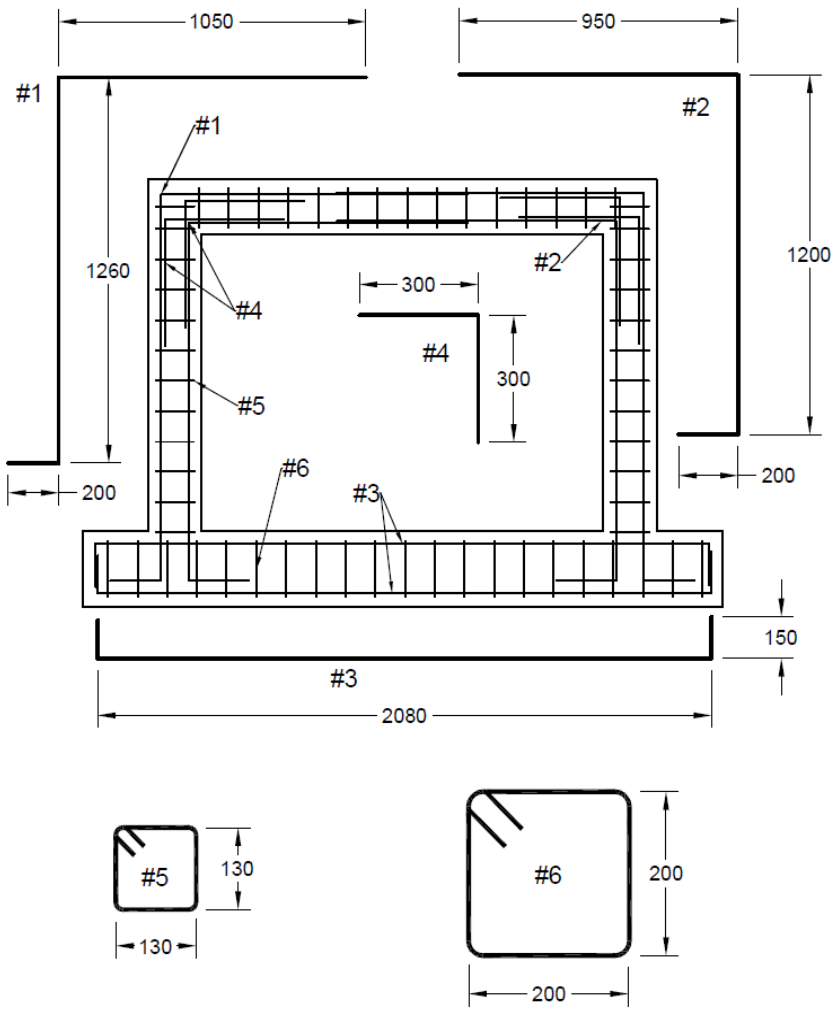

Figure 3.3 Details of Reinforcement in RC Frames (unit: *mm*)

3.2.1 Construction of RC Frames

The construction of RC frames was comprised of four major stages (Figure 3.4 to Figure 3.12) including: building concrete formworks, forming reinforcement steel cages, placing the reinforcements into the forms, and casting concrete.

The forms were constructed by cutting boards into the required dimensions and then fastening them together to form the specified geometry, after which, the reinforcement

cages were placed inside the formwork (Figures 3.4-3.5). In order to ensure a 25 *mm* concrete cover, plastic chairs were utilized around reinforcement cage (Figure 3.6). The tubes shown in Figures 3.6 and 3.7 were part of out-of-plane loading fixture. The tubes were placed in beam and the base so that a reaction panel could later be installed on the frame by using the holes they created. The ready-mix concrete with a specified compressive strength of 25 *MPa* and maximum aggregate size of 12 *mm* was used. The concrete was poured in two batches, one on July 15, 2016 for the specimens IF-ND, IF-D1, and IF-W-ND, and the other on July 19, 2016 for the specimen IF-D2. The slump test was performed before casting concrete in accordance with ASTM C143/C143M (2015) Standard Test Method for Slump of Hydraulic-Cement Concrete, which showed falling heights of 160 *mm* and 155 *mm* respectively for the two batches, meeting the required 150 *mm*. During pouring, a vibrator was used to ensure that all voids around the rebars and the form surfaces were filled with concrete (Figure 3.10), after which, the concrete surface was smoothed using concrete trowels. At the same time with pouring the specimens, 100 *mm* by 200 *mm*, and 150 *mm* by 300 *mm* concrete cylinders were poured and vibrated using a vibrating table in accordance with ASTM C39/C39M (2016) (Figure 3.12). All specimens and cylinders were moist cured under the same condition (using plastic covers) until the 14^{th} day after pouring which was followed by air curing till the testing day.

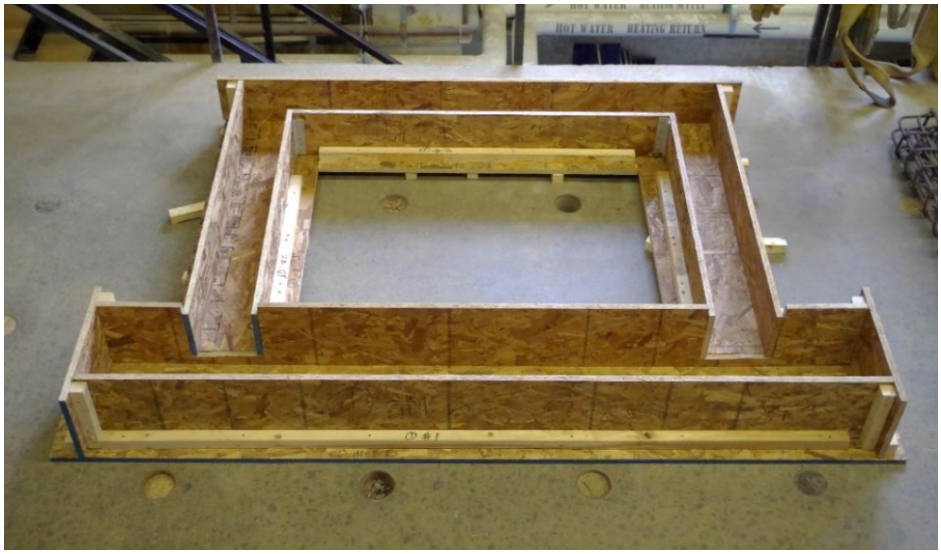

Figure 3.4 Overview of Formwork

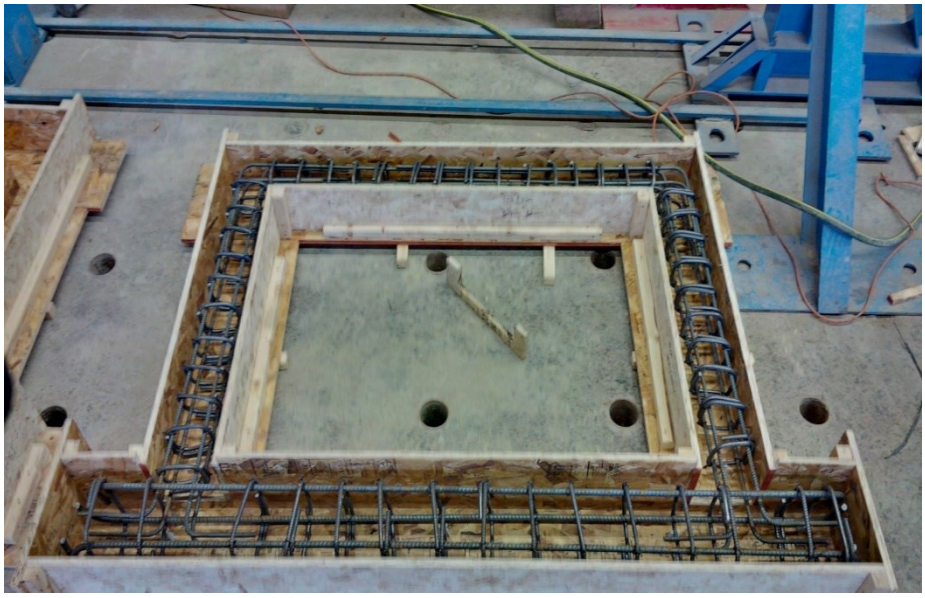

Figure 3.5 Overview of Formwork with Reinforcement

Figure 3.6 Formwork with Reinforcement, Chairs, and Tube Detail

Figure 3.7 Formwork with Reinforcement, and Tube Detail

Figure 3.8 Details of Formwork with Reinforcement

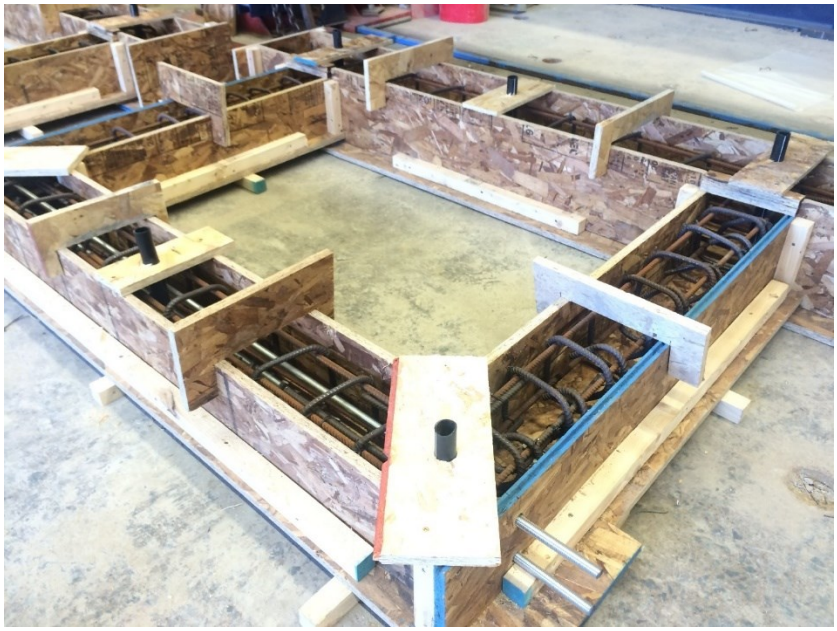

Figure 3.9 Frame Specimen Ready for Pouring Concrete

Figure 3.10 Concrete Pouring and Vibrating

Figure 3.11 Curing of Concrete

Figure 3.12 Pouring and Vibrating Cylinders

3.2.2 Construction of Masonry Infill Walls

The masonry infill walls were built in two batches on the 1st of September 2016 by an experienced mason to the standard of construction practice. The specimens IF-D1 and IF-D2 were constructed with the first batch, and the specimens IF-ND and IF-W-ND were constructed with the second batch. The process of building the walls are illustrated in Figure 3.13. The half blocks needed for running bond pattern were obtained by cutting the stretcher block in half using a concrete saw (a). Before constructing the wall, the columns and base were carefully marked in order to achieve the specified mortar width between the units and between the wall and the boundaries (b). Then, the units were carefully placed following the reference marks and the mortar was applied only on the blocks face shell for

both the bed joints and the head joints (c). After placing each row of blocks, it was checked to ensure that the wall was leveled using a level and plump device (d). For the specimen IF-W-ND, the block cells in the courses beside and above the opening were grouted as illustrated in Figure (e). Along with construction of the walls, masonry prisms and mortar cubes were built and cured under the same condition as the walls for 28 days. After that, all the specimens were air cured until the day of testing.

(a) Obtaining Half Blocks

(b) Marking Frames

(c) Application of Mortar

(d) Leveling Block Rows

(e) Opening Construction Details

(f) Running Bond Pattern

Figure 3.13 Construction of Masonry Infill Walls

3.3 OUT-OF-PLANE TEST SETUP

The application of out-of-plane uniform pressure on the infill panels was achieved using an airbag. A self-equilibrating loading system was designed to apply the transverse load as shown in Figure 3.14. The airbag was housed between a reaction panel and the masonry infill. The reaction panel was connected to the RC frames using threaded rods through those pre-embedded tubes. The reaction panel was made of a 15 *mm* thick plywood board stiffened with steel hollow sections (HSS) as shown in Figure 3.14. The steel horizontal beams had three holes aligned with the holes made on the beam and the base of the RC frame to facilitate the connection of the reaction panel to the RC frame using threaded rods. The specimens were tightly clamped to the strong floor using two W-section beams on each end of the frame beam stems (Figure 3.15).

Figure 3.14 Out-of-Plane Test Setup

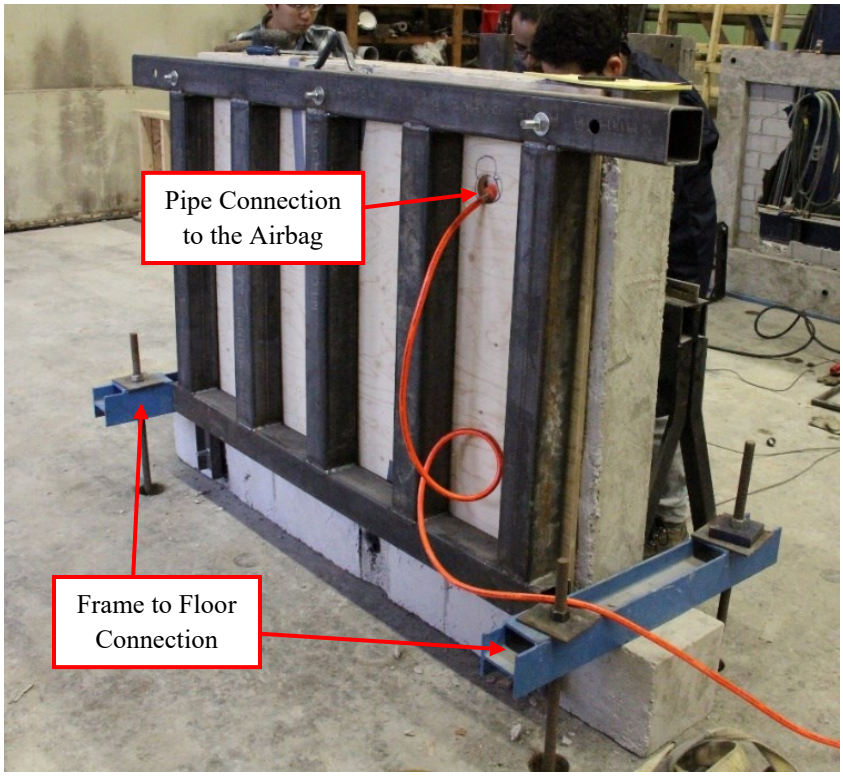

Figure 3.15 Out-of-plane Setup Details

The airbag was connected to a pressure transducer to measure and record the air pressure inside the airbag as seen in Figure 3.16. In addition to the pressure transducer, a pressure gauge was also used to read the air pressure and two readings from transducer and pressure gauge were checked throughout the test for consistency. An air compressor was used to inflate the airbag.

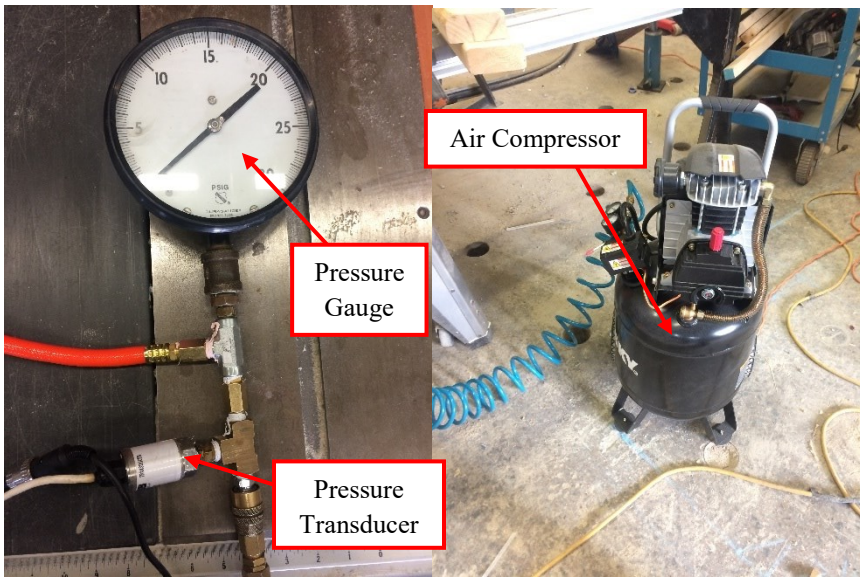

Figure 3.16 Pressure Gauge, Pressure Transducer and Air Compressor

To measure and record the out-of-plane displacement of the infill, four linear variable differential transformers (LVDT) were employed (Figure 3.17): one LVDT was used to measure the displacement at the centre of the infill; two LVDTs were used to measure the displacement at the centres of right and left half of the wall respectively; one LVDT was used to record the displacement of the centre of the top half of the wall. For the specimen with opening, four LVDTs were used to measure the displacements of the centre of each side of the opening as illustrated in Figure 3.18.

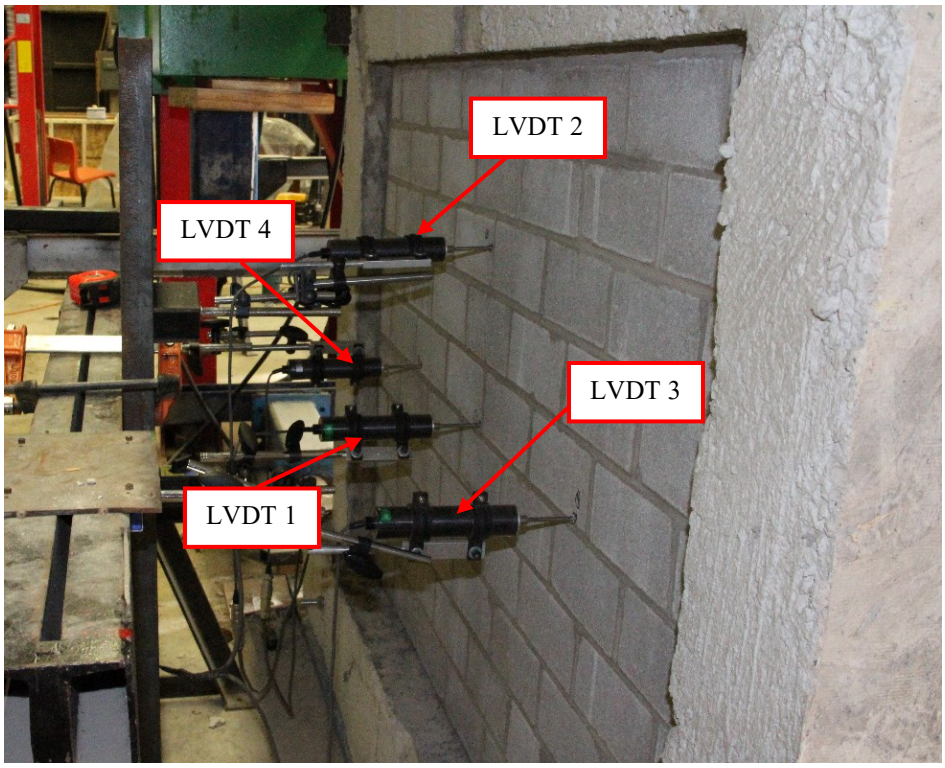

Figure 3.17 Locations of LVDTs

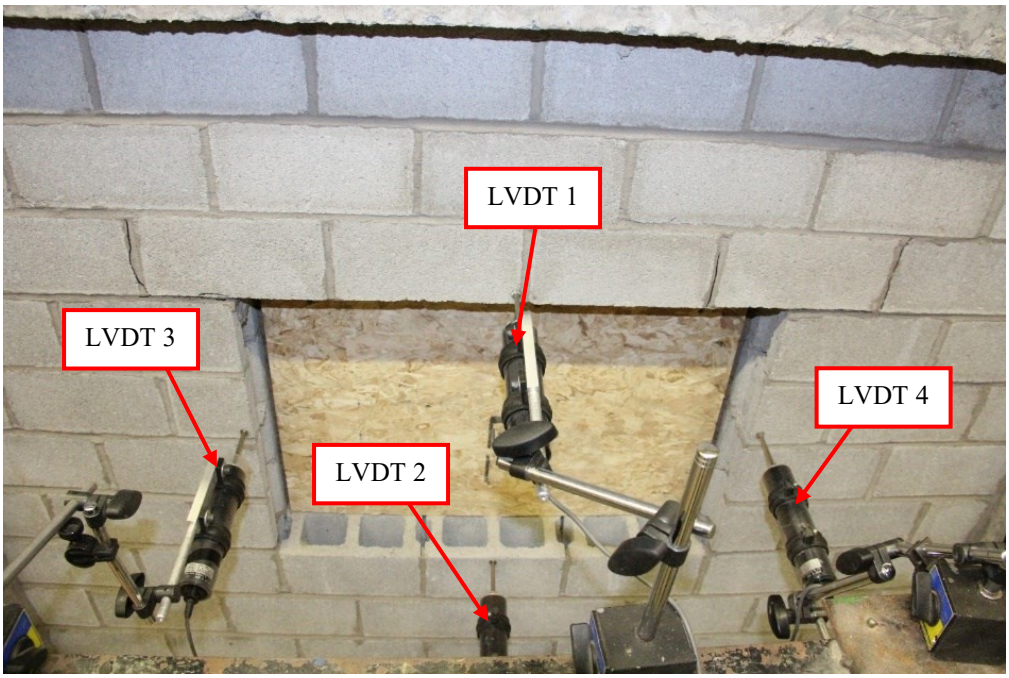

Figure 3.18 Locations of LVDTs for the Specimen with Opening

3.4 IN-PLANE TEST SETUP

The in-plane loading was required for specimens IF-D1 and IF-D2. This loading was applied monotonically using a hydraulic jack with a capacity of 250 *kN*. As shown in Figures 3.19 and 3.20, the hydraulic jack was attached to the column of an independent reaction frame. A load cell was mounted at the end of the jack to measure the applied load. To prevent local crushing of concrete at the point of loading, a steel plate was placed between the load cell and the specimen to evenly distribute the load. The specimen was tightly clamped to the strong floor in the same way as the out-of-plane test setup (Figure 3.21 and Figure 3.22). The potential in-plane sliding of the specimen base was further restrained using hydraulic rams braced against the columns of the reaction frame (Figure 3.23).

Figure 3.19 In-Plane Test Setup

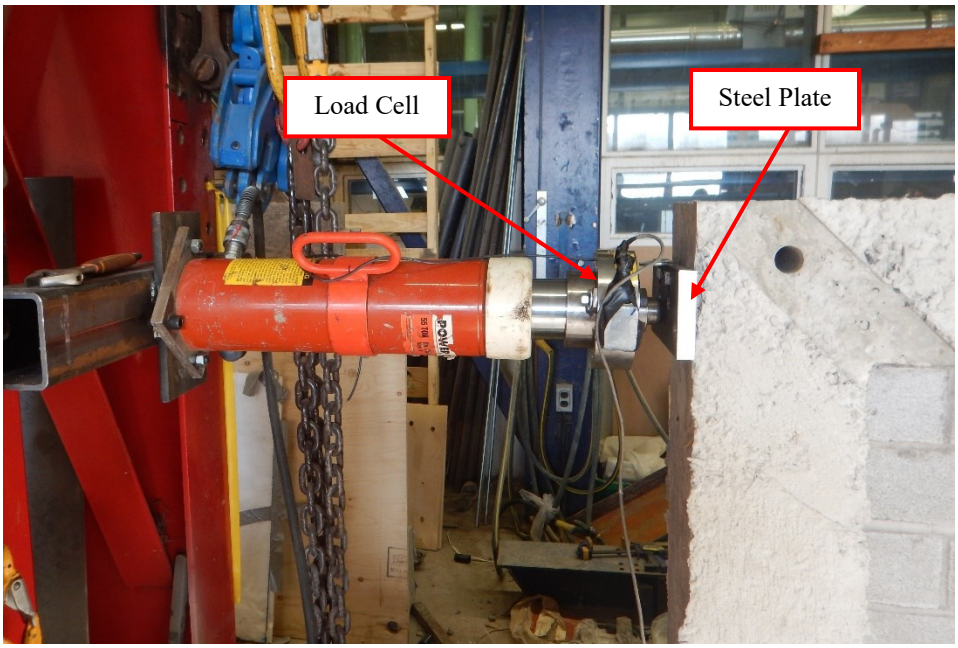

Figure 3.20 Hydraulic Jack Connection to Test Specimen

Figure 3.21 Frame to Floor Connection Top View

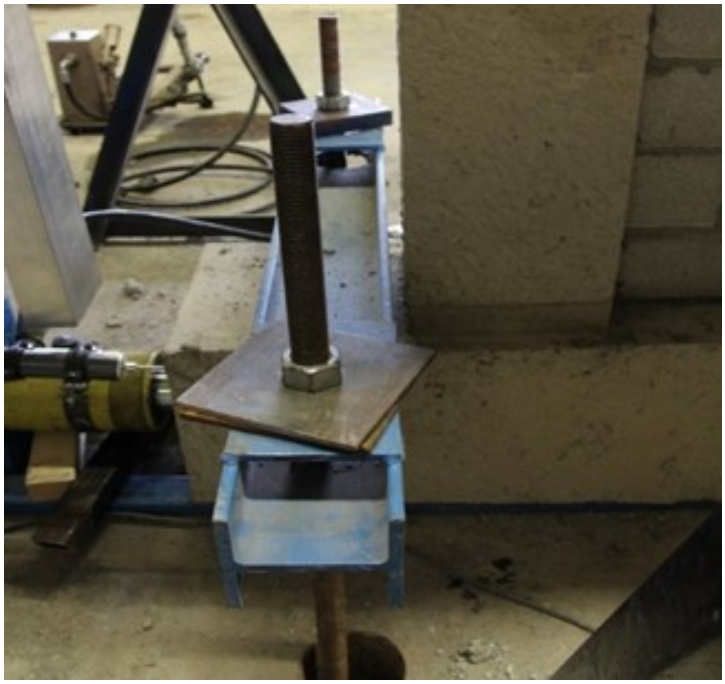

Figure 3.22 Frame to Floor Connection Side View

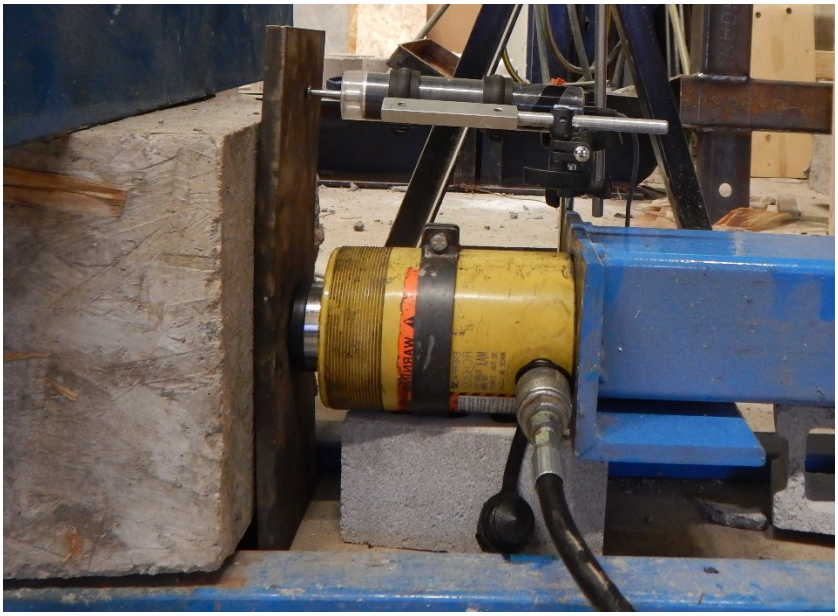

Figure 3.23 Hydraulic Jack Bracing the Base Beam

Four LVDTs were used to record the displacements. LVDT 1 and LVDT 2 were used to measure the in-plane lateral displacement of the top beam and the base respectively (Figure 3.24 and Figure 3.25), while LVDT 3 and LVDT 4 were to measure the potential out-of-plane displacement of the centres of the top beam and the infill under the in-plane loading (Figure 3.26).

Figure 3.24 Placement of LVDT 1

Figure 3.25 Placement of LVDT 2

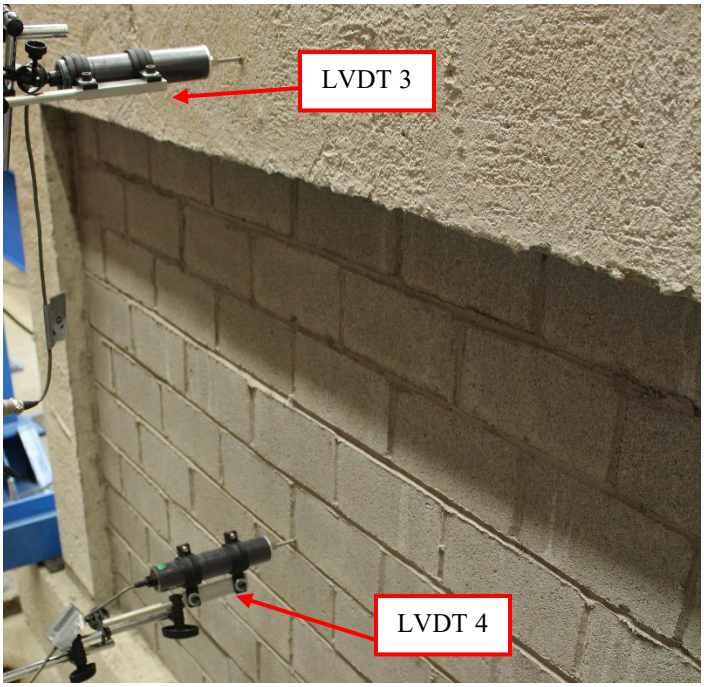

Figure 3.26 Placement of LVDT 3 and LVDT 4

3.6 TESTING PROCEDURES

3.6.1 Out-of-Plane Test

In the case of out-of-plane loading, the specimen was first clamped down to the strong floor. The airbag and reaction panel were then mounted in place where the reaction panel was bolt-connected to the RC frame. The LVDTs were then carefully placed and the airbag was connected to the pressure transducer and air compressor. Before testing, all devices were checked to confirm that they function properly. The LVDTs and the pressure transducer were set to record the displacement and pressure with an interval of 0.1 seconds using an electronic data acquisition system. The pressure was applied at a rate of 1 *kPa* per minute until the failure of the infills. During testing, initiation and propagation of cracking

as well as final failure mode were monitored and recorded throughout the loading history.

3.6.2 In-Plane Test

Note that specimen IF-D1 was first subjected to monotonic in-plane loading to the onset of diagonal cracking, and the specimen IF-D2 was tested to failure under in-plane loading after subjected to out-of-plane loading to the onset of cracking. During the in-plane loading stage, these specimens were placed in position and centered with respect to the hydraulic loading jack. A preliminary inspection was then performed to confirm the LVDTs and the load cell functionality. The LVDTs and the load cell were set to record the displacement and the load at every 0.1 seconds using an electronic data acquisition system. The lateral load was applied at a rate of 6 *kN* per minute until the desirable damage or ultimate load were reached in the specimens. During the loading, cracks were detected and marked, and their patterns were identified by carefully monitoring the specimen different surfaces.

3.7 AUXILIARY TESTS

Auxiliary tests were carried out to define the material properties of different components of the infilled frame specimens including CMUs, mortar, masonry prism, concrete, and reinforcing steel. Each test was performed in accordance with the corresponding American Standard Test Method ASTM.

3.7.1 CMUs

Three randomly selected blocks were used to determine the compressive strength and physical properties of CMUs including moisture content, percentage absorption, and

density in accordance with ASTM C140/C140M (2016) Standard Test Methods for Sampling and Testing Concrete Masonry Units and Related Units. To obtain the compressive strength, the blocks were tested using Instron universal testing machine as illustrated in Figure 3.27. The blocks were end capped using fiberboards to ensure a uniform stress distribution when loaded.

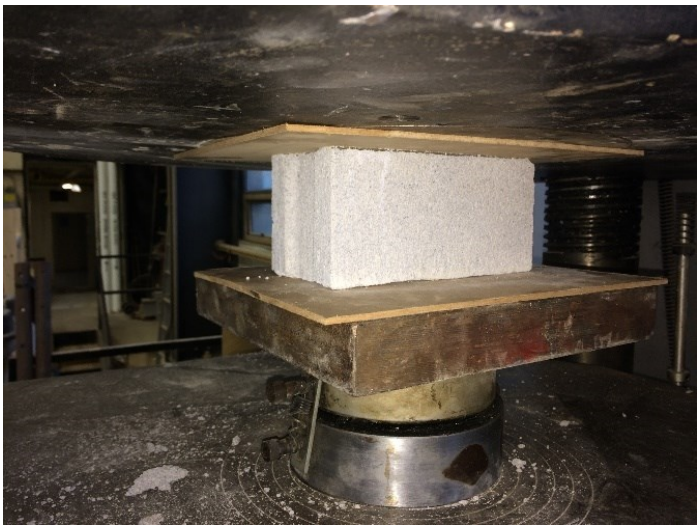

Figure 3.27 Compression Test Setup for CMUs

3.7.2 Mortar

The mortar used to construct the infill walls was Type S mortar. This mortar was obtained using a mixture of Type N mortar, Portland cement, and sand in a volume ratio of 1:3:12. Two batches of mortar were mixed for the construction of infill walls and mortar cubes. A total of twelve cubes were poured in a non-absorbent mold and after 48 hours, they were demoulded and half of them (three for each batch) were cured for 28 days in hydrated lime water whereas the other half were cured in the same condition as the infills. The compressive testing of each set of cubes was performed using the Instron compression machine as seen in Figure 3.28 on the day of testing the corresponding specimens. All

curing and testing procedures were in accordance with ASTM C270 (2014) Standard Specification for Mortar for Unit Masonry.

Figure 3.28 Compression Test Setup for Mortar Cubes

3.7.3 Masonry Prisms

A total of ten, 5-course high hollow masonry prisms were fabricated at the same time as the construction of infill walls and tested as per ASTM C1314 (2016) Standard Test Method for Compressive Strength of Masonry Prisms. The prisms were cured under the same condition as the masonry infill walls. The prisms were constructed by applying mortar only to the face shell of the masonry blocks, identical to the construction of the infill walls. The compressive testing of the prisms was conducted using the Instron universal testing machine and the specimens were capped with fiberboards similar to the testing of concrete blocks as illustrated in Figure 3.29.

Figure 3.29 Compression Test Setup for Prisms

3.7.4 Concrete

The ready mix concrete with a specified compressive strength of 25 *MPa* was used in construction of the RC frames. The frames were cast in two batches on the July 15th 2016 and July 19th 2016 respectively. For each batch, six 100×200 *mm* and three 150×300 *mm* cylinders were also poured. The small cylinders were tested on the 14th day and 28th day for compressive strength. The large cylinders were tested on the day of testing the frame specimens to obtain both compressive strength and modulus of elasticity of the concrete. All the cylinders were tested using the Instron universal testing machine as seen in Figure 3.30. The construction and testing procedure of concrete cylinders were as per

ASTM C39/C39M (2016) Standard Test Method for Compressive Strength of Cylindrical Concrete Specimens.

Figure 3.30 Compression Test Setup for Concrete Cylinders

3.7.5 Reinforcing Steel

Reinforcing steel data was collected from Hu (2015) and was used in this study since the reinforcement used in both studies was from the same batch. Three steel coupons were cut from randomly selected 10M longitudinal rebars and tested using the Inston universal testing machine to obtain material properties in accordance with ASTM E8 (2008) Standard Test Methods for Tension Testing of Metallic Materials. Details of the reinforcing coupons

used are presented in Figure 3.31. Figure 3.32 shows the test setup where an extensometer was mounted on the coupon to measure the strain during the loading.

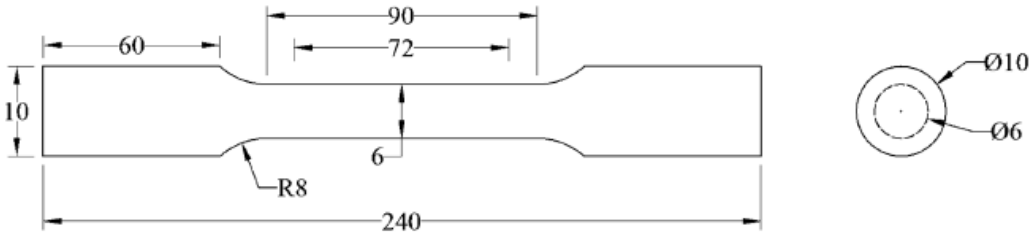

(a) Steel Coupon Dimensions (b) Cross-Section

Figure 3.31 Steel Coupon Detailing (Hu 2015) (unit: *mm*)

Figure 3.32 Tension Test Setup for Reinforcing Steel (Hu 2015)

CHAPTER 4 EXPERIMENTAL RESULTS

4.1 INTRODUCTION

In this chapter the results from auxiliary tests and infilled specimen tests are presented and discussed. The auxiliary test results include mechanical properties of CMUs, mortar, masonry prisms, concrete cylinders, and reinforcing steel. The infilled specimen results are presented in terms of load vs. displacement responses with discussion focused on strength and failure pattern of each specimen. The effect of prior damage and window opening on the specimen behaviour and strength is also discussed.

4.2 AUXILIARY TEST RESULTS

In the following sections, procedures and results for each auxiliary test are presented. They include physical properties and compressive strength of CMUs, compressive strength of mortar cubes, compressive strength of masonry prisms, modulus of elasticity and compressive strength of concrete cylinders, and tensile strength of steel reinforcement.

4.2.1 CMUs

Three randomly selected CMUs were used to determine the physical properties of CMUs including net area, weight, density, absorption rate, and moisture content. The dimensions of the selected CMUs were measure and the resulting mean net area was calculated to be 9128 mm^2 as depicted in Figure 4.1. The absorption, moisture content, and density of blocks were measured as per ASTM C140/C140M (2015). For each CMU block, the received weight was first measured. The block was then immersed in the water and the

immersed weight was subsequently measured. The block was kept in the water for 24 hours, after which point, it was removed from the water and the weight was measured after being surface dried with a towel. This weight was denoted as the saturated weight. The block was then kept in an oven at 100°*C* for 24 hours and at that point, the dry weight was measured. The obtained weights were then utilized to determine the absorption, moisture content, and density. The average absorption was calculated to be 139.8 *kg/m* with a coefficient of variation (CV) of 0.9%. The average moisture content was calculated to be 4.5% with a CV of 9.1%. The average density was determined to be 2037.2 kg/m^3 with a CV of 1.3%. Based on the provisions required by CAN/CSA A165 (2015) Standard for Masonry Units, a standard 200 *mm* hollow block, shall have a density greater than 2000 kg/m^3, a moisture content smaller than 45% for a relative humidity of 75% or bigger, and an absorption smaller than 175 kg/m^3. As seen in the presented results in Table 4.1, the average obtained properties meet the required criteria.

Table 4.1 CMU Physical Properties

ID	Received Weight (*g*)	Immersed Weight (*g*)	Saturated Weight (*g*)	Dry Weight (*g*)	Absorption (kg/m^3)	Absorption (%)	Moisture Content (%)	Density (kg/m^3)
A	1621.2	931.5	1727.9	1616.7	139.0	6.9	4.0	2026.5
B	1613.4	925.3	1718.3	1608.1	141.3	6.8	4.8	2068.5
C	1633.6	941.3	1741.0	1628.3	139.1	6.9	4.7	2016.8
				Avg.	139.8	6.9	4.5	2037.2
				CV (%)	0.9	0.5	9.1	1.3

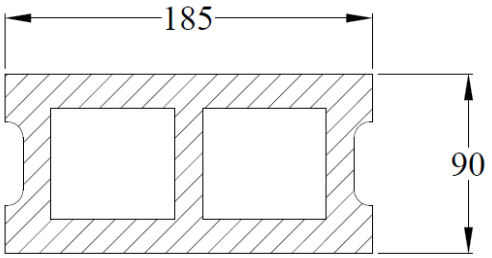

Figure 4.1 Net Area of the CMU Block (unit: mm)

The mechanical properties of CMUs are summarized in Table 4.2 and the testing procedure was described in Chapter 3. The net area of 9128 mm^2 was used in the calculation of the compressive strength. The average compressive strength was obtained to be 12.8 *MPa* with a CV of 6.8%. Conical shear followed by face shell spalling was observed to be the predominant failure mode of CMUs as illustrated in Figure 4.2.

Table 4.2 Mechanical Properties of CMUs

ID	Ultimate Load (*kN*)	Compressive Strength (*MPa*)
CMU1	125.8	13.8
CMU2	118.4	13.0
CMU3	107.0	11.7
	Avg.	12.8
	CV (%)	6.8

Figure 4.2 Typical Failure Mode of the CMUs

4.2.2 Mortar

Specimens IF-D1 and IF-D2 were constructed using mortar batch A, whereas specimens IF-ND and IF-W-ND were constructed using batch B. A summary of the test results is provided in Table 4.3 and Table 4.4. Table 4.3 lists results of mortar cubes cured in lime water (in accordance with ASTM C270) and Table 4.4 lists results of those cured in the same condition as the infills. For specimens cured in the lime water, mortar batch A had a compressive strength of 21.6 MPa with a CV of 7.2%, while the mortar batch B had a compressive strength of 20.4 MPa with a CV of 8.2%. The CVs for both mortar batches satisfy the limit specified by CSA S304-14 (<15%), indicating the consistency of mortar strength. For specimens cured in the same condition as the infills, mortar batch A had a compressive strength of 17.6 MPa with a CV of 20.0%, while mortar batch B had a compressive strength of 17.7 with a CV of 22.5%. This shows that mortar cubes cured in the same condition as infills (air cured) attained lower strength and the CVs were much

greater. It should be noted that the lime water curing was specified in the ASTM specification. A typical failure pattern for mortar cubes is illustrated in Figure 4.3, which showed crushing on surfaces and splitting vertical cracks through the height.

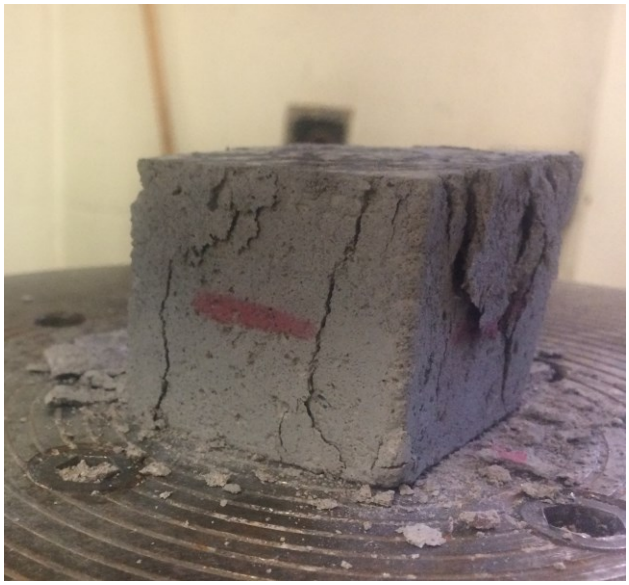

Figure 4.3 Typical Failure Mode of the Mortar Cubes

Table 4.3 Compressive Strength of Mortar Cubes Cured in Lime Water

ID	Length (*mm*)	Width (*mm*)	Area (mm^2)	Ultimate Load (*kN*)	Compressive Strength (*MPa*)
Mortar Batch A (for IF-D1 and IF-D2)					
MLA1	50.0	50.2	2510	59.2	23.6
MLA2	50.4	50.6	2550	50.6	19.8
MLA3	50.1	50.7	2540	54.5	21.4
				Avg.	21.6
				CV(%)	7.2
Mortar Batch B (for IF-ND and IF-W-ND)					
MLB1	50.4	50.1	2525	47.4	18.8
MLB2	50.6	50.2	2540	56.2	22.1
MLB3	50.7	50.6	2565	52.2	20.3
				Avg.	20.4
				CV(%)	8.2

Table 4.4 Compressive Strength of Mortar Cubes Cured in the Same Condition as the Walls

ID	Length (*mm*)	Width (*mm*)	Area (mm^2)	Ultimate Load (*kN*)	Compressive Strength (*MPa*)
Mortar Batch A (for IF-D1 and IF-D2)					
MWA1	50.1	50.2	2515	35.5	14.1
MWA2	50.0	51.2	2560	45.2	17.6
MWA3	50.1	50.5	2530	53.6	21.2
				Avg.	17.6
				CV(%)	20.0
Mortar Batch B (for IF-ND and IF-W-ND)					
MWB1	50.2	50.3	2525	33.4	13.2
MWB2	50.4	50.1	2525	47.7	18.9
MWB3	50.7	50.2	2545	53.1	20.9
				Avg.	17.7
				CV(%)	22.5

4.2.3 Masonry Prisms

Two batches of prisms A and B correspond to mortar batches A and B were constructed. Each batch consisted of five, 5-high prisms. The mortar was applied only to the face shells of prisms simulating the manner in which the masonry wall infill was constructed. Therefore, the net area for compressive strength calculation excluded the area of the webs, resulting in the effective area of 6290 mm^2, as shown in Figure 4.4. A summery of the test results is presented in Table 4.5. The average compressive strength for batch A was 9.7 *MPa* with a CV of 11.7%, and the average compressive strength for batch B was 9.4 *MPa*

with a CV of 9.2%. The CVs of both batches were well below the required CV limit of 15%. Figure 4.5 shows the typical failure pattern of the prisms which was characterized by vertical splitting cracks through both face shells and webs of the prisms.

Table 4.5 Masonry Prism Compressive Test Results

Prism Batch A (for IF-D1 and IF-D2)			Prism Batch B (for IF-ND and IF-W-ND)		
ID	Ultimate Load (kN)	f'_m (MPa)	ID	Ultimate Load (kN)	f'_m (MPa)
PA1	67.4	10.7	PB1	60.9	9.7
PA2	52.8	8.3	PB2	62.1	9.9
PA3	69.4	11.0	PB3	50.2	8.0
PA4	56.1	8.9	PB4	55.7	8.9
PA5	59.1	9.4	PB5	66.2	10.5
	Avg.	9.7		Avg.	9.4
	CV(%)	11.7		CV(%)	9.2

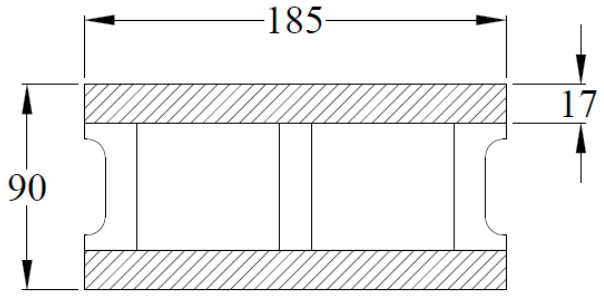

Figure 4.4 Effective Cross-Sectional Area of Prisms

Figure 4.5 Typical Failure Mode of Masonry Prisms

4.2.4 Concrete

Two batches of concrete A and B were used in construction of RC frames. The concrete batch A was used in the construction of specimens IF-ND, IF-D1, and IF-W-ND whereas the specimen IF-D2 was constructed with batch B. Concrete cylinders from both batches were made and tested at the following days of curing: 14 days, 28 days, and the day of infilled specimens testing. The modulus of elasticity of concrete was also determined at the day of infilled specimen testing. A summary of the test results is shown in Table 4.6. As expected, the concrete strength increased with the curing time, and overall, the batch B attained a slightly higher strength than the batch A. On the day of testing, the batch A showed an average compressive strength of 38.5 *MPa* with a CV of 0.6% and an average elastic modulus of 16911 *MPa* with a CV of 2.4%. The batch B showed an average

compressive strength of 42.2 *MPa* with a CV of 4.6% and an average elastic modulus of 20357 *MPa* with a CV of 7.8%. The typical failure mode of the concrete cylinders was conical shear failure as shown in Figure 4.6. The determination of the modulus of elasticity is illustrated in Figure 4.7 where the slope of the initial linear elastic portion of a typical stress vs. strain curve of the concrete cylinders is used.

Table 4.6 Concrete Cylinder Compression Tests Results

Concrete Batch A (for IF-ND, IF-W-ND, and IF-D1)									
14 Days	Ultimate Load (kN)	f_c' (MPa)	28 Days	Ultimate Load (kN)	f_c' (MPa)	120 Days	Ultimate Load (kN)	f_c' (MPa)	E (MPa)
A1	194.0	24.7	A4	278.8	35.5	A7	682.7	38.6	17247
A2	175.1	22.3	A5	288.2	36.7	A8	684.4	38.7	16342
A3	207.3	26.4	A6	275.7	35.1	A9	674.7	38.2	17145
Avg.		24.5			35.8			38.5	16911
CV(%)		8.4			2.3			0.6	2.4
Concrete Batch B (for IF-D2)									
14 Days	Ultimate Load (kN)	f_c' (MPa)	28 Days	Ultimate Load (kN)	f_c' (MPa)	120 Days	Ultimate Load (kN)	f_c' (MPa)	E (MPa)
B1	233.9	29.8	B4	304.2	38.7	B7	781.0	44.2	19083
B2	206.2	26.2	B5	267.6	34.1	B8	755.3	42.7	22160
B3	246.0	31.3	B6	290.6	37.0	B9	712.0	40.3	19829
Avg.		29.1			36.6			42.2	20357
CV(%)		8.9			6.4			4.6	7.8

Figure 4.6 Typical Failure Mode of Concrete Cylinders

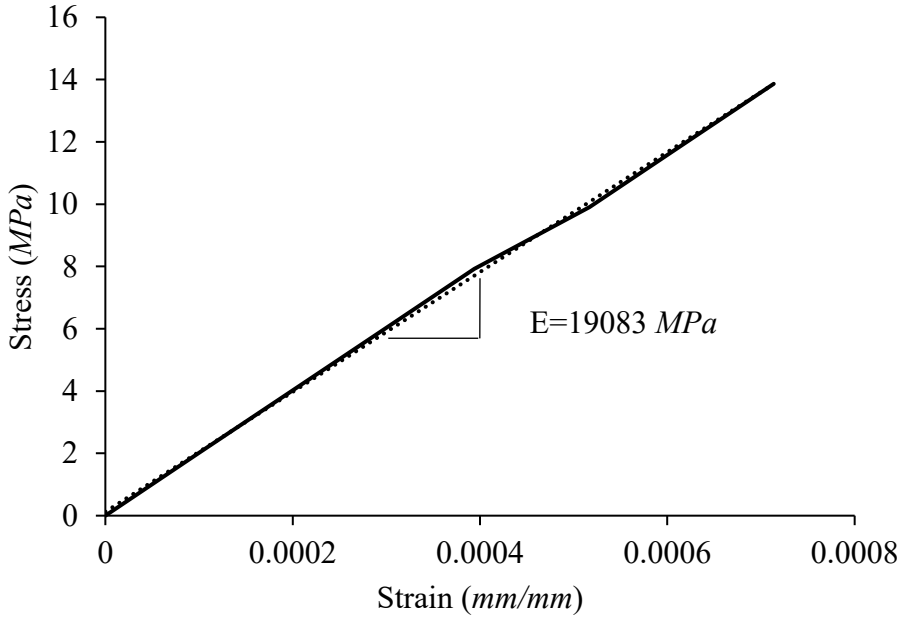

Figure 4.7 Initial Stress vs. Strain Curve of Concrete Cylinders under Compression (B7)

4.2.5 Summary of Auxiliary Test Results

Since the steel reinforcement used in this experiment was from the same batch as a previous experimental program conducted by Hu (2015) of the same research group, the mechanical properties of steel reinforcement obtained in that program were used in this study. A summary of auxiliary test results for each masonry infilled frame specimen is provided in Table 4.7.

Table 4.7 Summary of Auxiliary Test Results

Component	Property	IF-ND	IF-W-ND	IF-D1	IF-D2
CMUs	Strength (*MPa*)	12.8	12.8	12.8	12.8
Mortar	Strength (*MPa*)	20.4	20.4	21.6	21.6
Masonry Prism	Strength (*MPa*)	9.4	9.4	9.7	9.7
	Elastic Modulus (*MPa*)	7990	7990	8245	8245
Concrete	Strength (*MPa*)	38.5	38.5	38.5	42.2
	Elastic Modulus (*MPa*)	16911	16911	16911	20357
Reinforcement (Hu 2015)	Yield Strength (Ultimate Strength) (*MPa*)	446 (665)	446 (665)	446 (665)	446 (665)
	Elastic Modulus (*MPa*)	247357	247357	247357	247357

4.3 INFILLED FRAME SPECIMEN RESULTS

The following sections describe the behaviour, strength, and failure mode for each specimen. Note that all specimens were built in tight contact at all boundaries with the bounding frames to enable arching action.

4.3.1 Specimen IF-ND

This specimen was designed as the control specimen (without prior damage or opening). The pressure vs. out-of-plane displacement curve for the central LVDT (the one with the largest recorded displacements) is shown in Figure 4.8. The development of cracking through loading history is shown in Figure 4.9. Figure 4.10 shows the out-of-plane displacement curves for LVDTs along the central horizontal axis. Figure 4.8 shows that the behaviour of this specimen up to the onset of tensile cracking around the centre of the infill is linear. As indicated in Figure 4.9, the first crack was a horizontal crack with the length of about four blocks at the centre of the infill at the load of 26.8 *kPa* (about 40% of the ultimate pressure) and out-of-plane displacement of 0.4 *mm*. The pressure and displacement correspond to this point is defined as cracking pressure, P_{cr}, and cracking displacement, Δ_{cr}, respectively. With the increase of pressure, the central crack began to expand horizontally. At the pressure of about 45 *kPa* and central out-of-plane displacement of 2 *mm*, diagonal cracking began to develop from each end of the horizontal crack. As load continued to increase, the central crack began to widen and diagonal cracks propagated towards each corner of the infill to form a yield line pattern for the specimen.

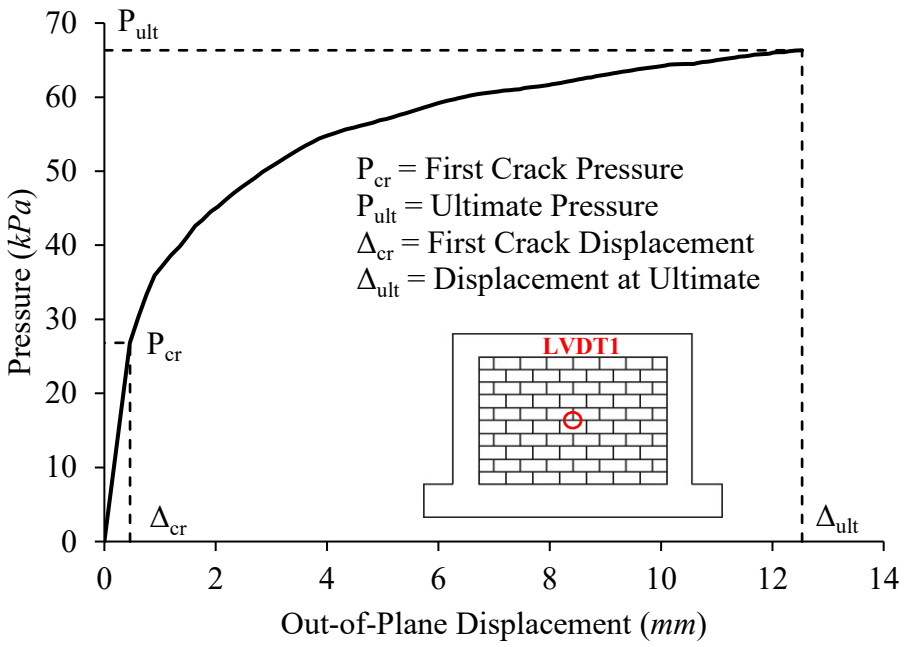

Figure 4.8 Pressure vs. Out-of-Plane Displacement Curve of Specimen IF-ND

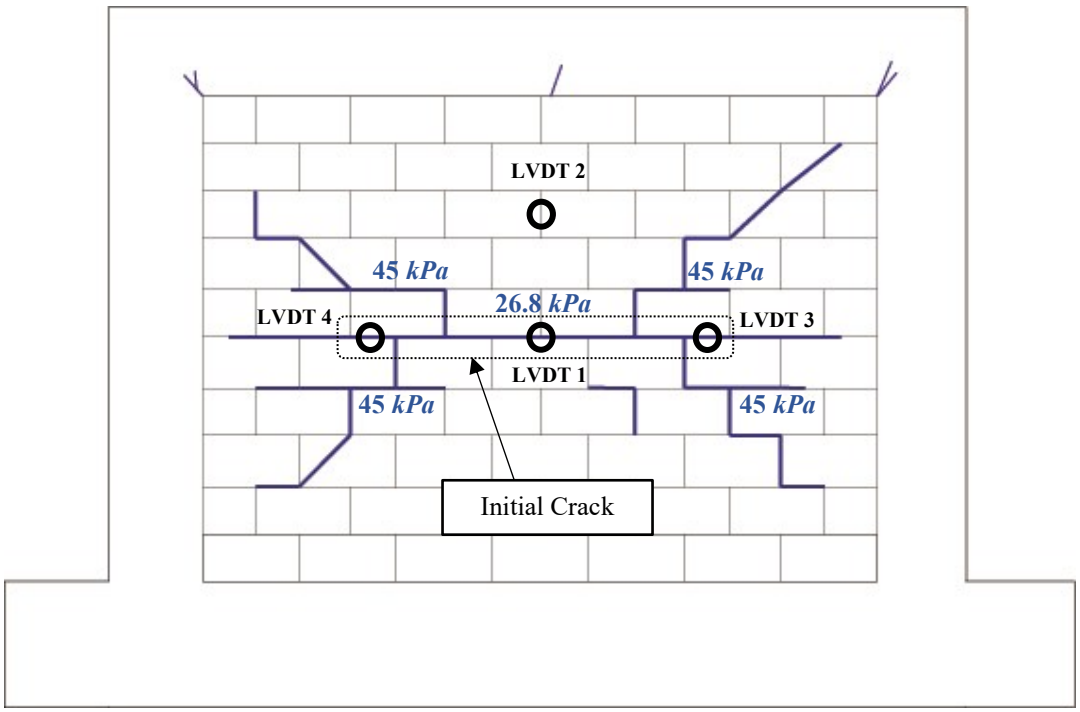

Figure 4.9 The Cracking Pattern of IF-ND before Failure

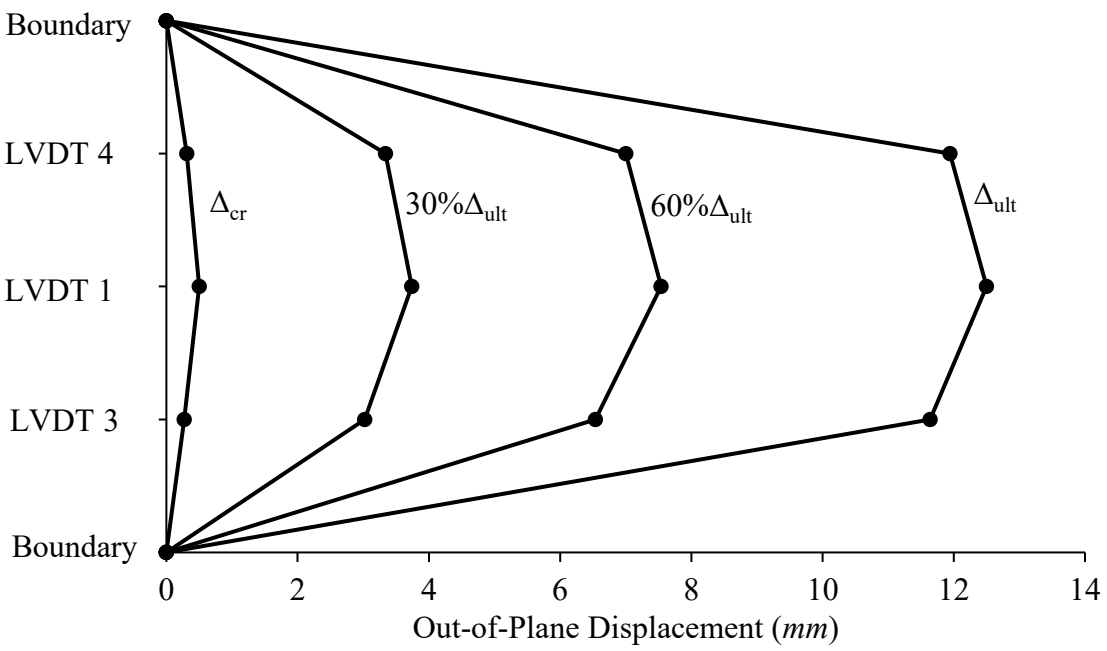

Figure 4.10 Out-of-Plane Displacement Curves of IF-ND for the Horizontal LVDTs

At this point, a number of small hairline cracks appeared mostly on the top corners of the infill as well as the beam of the bounding frame, indicating that the arching action was enabled which caused forces on the bounding frame. It is noted that the formation of cracks on the infill was either at the block-mortar interface or through the face shell of the units. The infill eventually failed at the load of 66.3 *kPa* and central out-of-plane displacement of 12.5 *mm*. The pressure and displacement correspond to this point are termed the ultimate pressure, P_{ult}, and displacement at ultimate, Δ_{ult}, respectively. Sudden out-of-plane collapse of the infill was the final failure mode of this specimen. Figure 4.11 depicts the failure mode showing the remnants after the infill collapsed. The failure was appeared to be a result of web shear failure of almost all of the collapsed masonry units as seen in Figure 4.12. During the loading, no drop in pressure was recorded and after the onset of initial cracking, the curve showed some deviation from linearity with increasing nonlinearity till

failure. According to Figure 4.10, the results of the LVDT 3 and LVDT 4 (Figure 4.9) showed that the behaviour of the infill with respect to the vertical centre line was fully symmetrical, indicating the uniform application of the pressure. At the point of failure, displacements of the side LVDTs (LVDT 3 and 4) were only about 4.7% smaller than the central LVDT (LVDT 1), and the ratio of the displacement of the top LVDT (LVDT 2, halfway between the LVDT 1 and the top of the infill) and the central LVDT was approximately 0.45. This indicates that the upper and lower segments defined the central crack experienced more or less rigid body movement.

Figure 4.11 Failure Mode of Specimen IF-ND

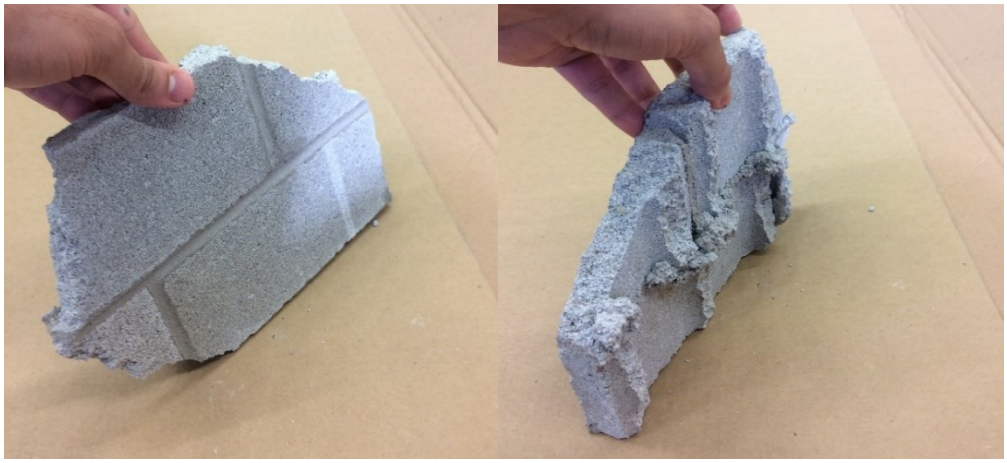

Figure 4.12 The Typical Web Shear Failure of Masonry Units for Specimen IF-ND

4.3.2 Specimen IF-W-ND

This specimen had a 17% central window opening with an aspect ratio of 1.5 and was tested for out-of-plane loading under uniform pressure. The pressure vs. out-of-plane displacement curve for the LVDT with largest recorded displacements (LVDT 3) is depicted in Figure 4.13. The development of cracking through loading history is shown in Figure 4.14. Figure 4.15 and Figure 4.16 show the out-of-plane displacement curves of the specimen for the LVDTs along the central vertical and horizontal axes respectively. This specimen showed a more or less linear behaviour up to about 55% of the ultimate pressure (23.7 *kPa*). The visible cracking began to form thereafter from both top corners of the opening as two horizontal cracks with the length of a half block at each side at an out-of-plane displacement of 0.6 *mm*. The onset of cracking was not accompanied by any marked drop in pressure or decrease in the stiffness of the curve, and the behaviour still remained linear. With the increase of pressure, those cracks expanded towards top corners of the infill. At a load of about 35 *kPa*, those cracks reached the top corners of the infill. At the pressure of about 37 *kPa*, a series of small horizontal and vertical cracks began to develop

on both sides of the opening which marked the onset of nonlinearity in the curve. As the pressure increased, the side cracks gradually expanded in both size and number, which resulted in significant reduction in the slope of the curve until, at the pressure of 43.7 *kPa* and out-of-plane displacement of 4.3 *mm*, the infill reached the ultimate strength. Similar to specimen IF-ND the formation of cracks on the infill was either at the block-mortar interface or through the face shell of the units. At this point, the pressure stabilized for about 15 seconds after undergoing about 0.5 *mm* displacement without any increase or decrease in pressure. Afterwards, the pressure started to decline with a negative slope until at the pressure of 40 *kPa* (about 89% of the ultimate pressure) and at out-of-plane displacement of 6.75 *mm* the collapse occurred. Similar to specimen IF-ND, the out-of-plane collapse of the infill was sudden and volatile as shown in Figure 4.17.

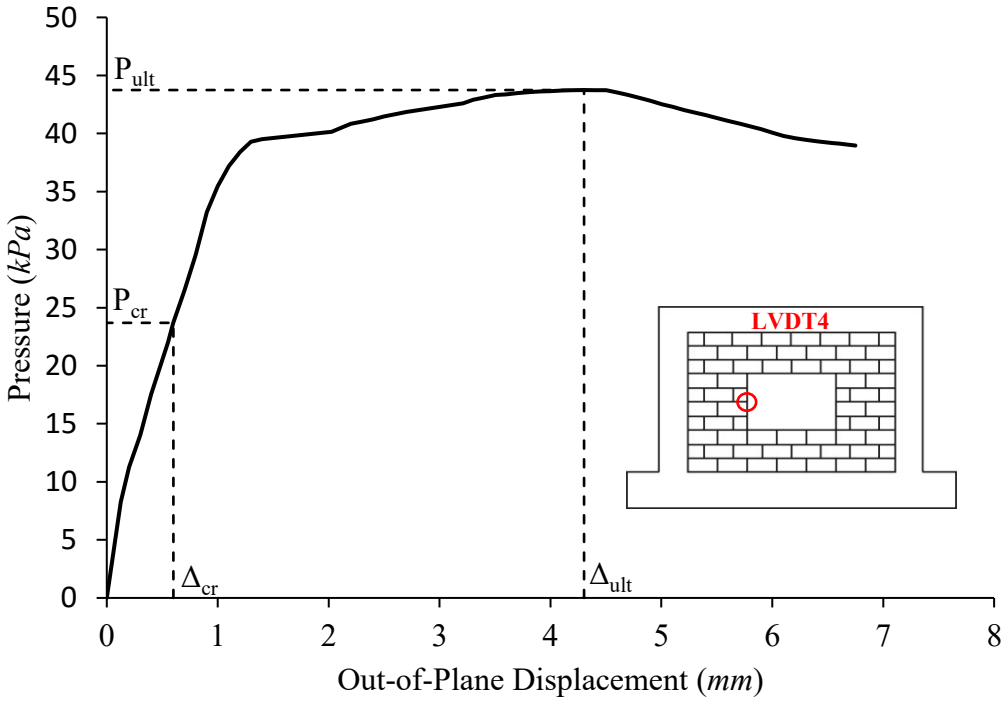

Figure 4.13 Pressure vs. Out-of-Plane Displacement Curve of Specimen IF-W-ND

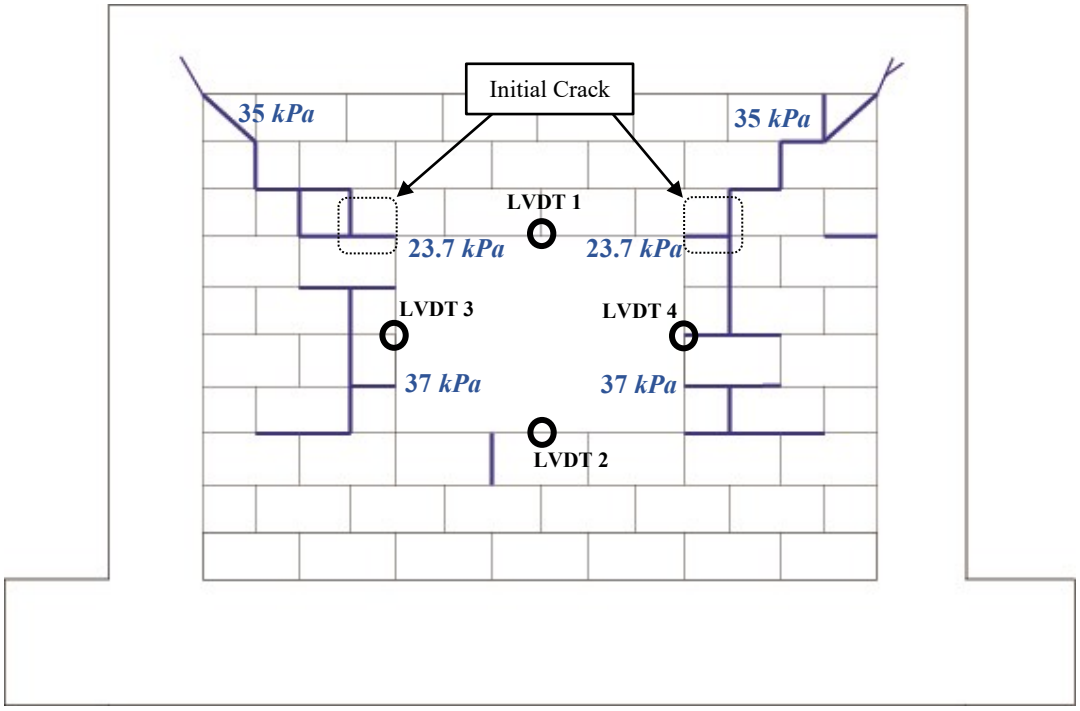

Figure 4.14 The Cracking Pattern of IF-ND Before Failure

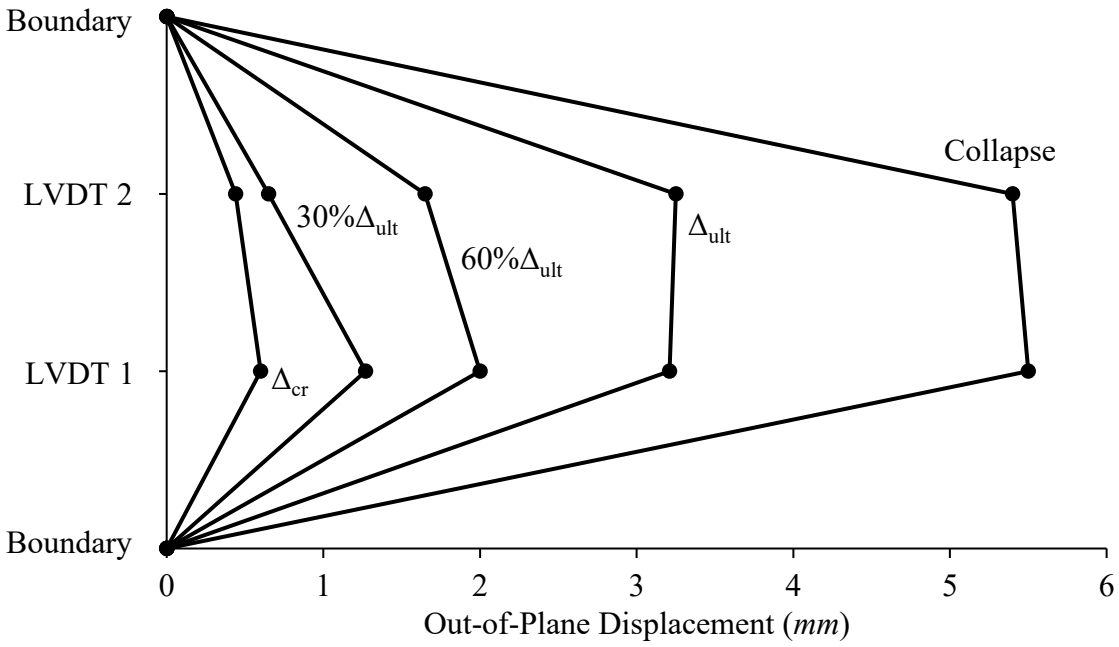

Figure 4.15 Out-of-Plane Displacement Curves of IF-W-ND for Vertical LVDTs

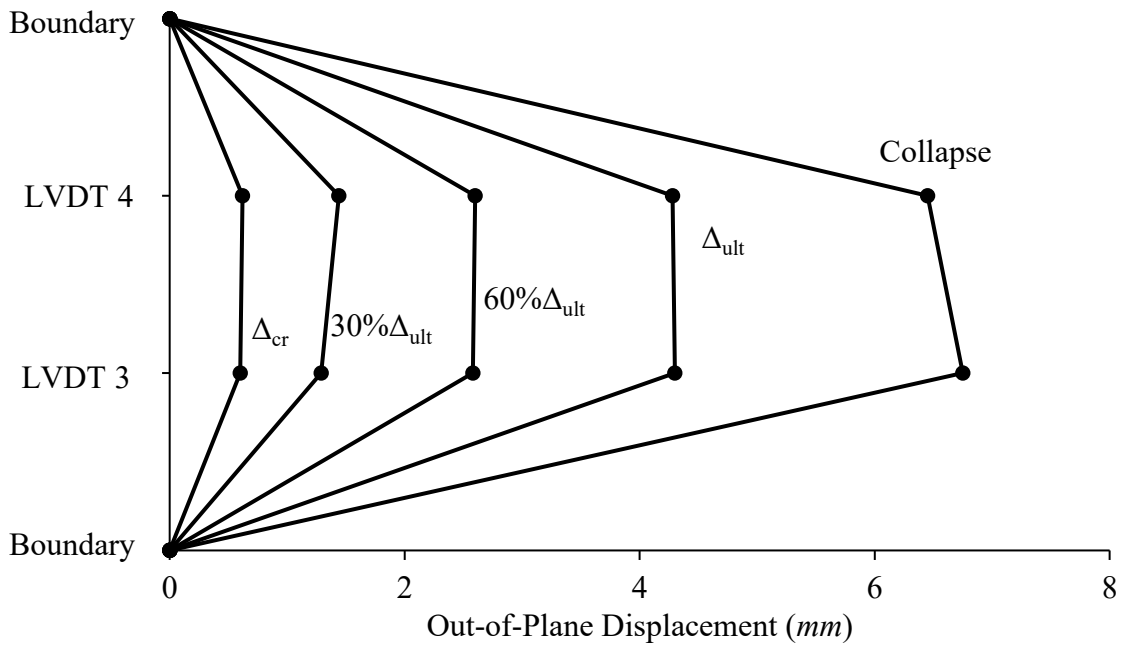

Figure 4.16 Out-of-Plane Displacement Curves of IF-W-ND for Horizontal LVDTs

Figure 4.18 illustrates the failure mode of the specimen from the windward side of the wall after the airbag and reaction frame were removed. The collapse of the infill was resulted from web shear failure of the masonry units (Figure 4.19). The failure occurred in 89 seconds after the infill reached its ultimate strength. Only a few small hairline cracks similar to specimen IF-ND were produced on the top corners of the beam of the bounding frame. The high similarity between the results of side LVDTs (Figure 4.16) until the point of failure was an indication of symmetrical behaviour with respect to central vertical axis of the infill.

Figure 4.17 Failure Mode of Specimen IF-W-ND

Figure 4.18 Failure Mode of Specimen IF-W-ND (Back View)

Figure 4.19 Web Shear Failure of Masonry Units

4.3.3 Specimen IF-D1

This specimen was first subjected to in-plane loading to the onset of a major diagonal cracking on both surfaces of the infill. At that point, the in-plane loading was removed and the wall was tested to failure under out-of-plane pressure. The load vs. lateral displacement of this specimen under the in-plane loading is shown in Figure 4.20. It shows that the specimen developed a major diagonal cracking at a load of 107.4 *kN* with a lateral displacement of 6.5 *mm*. The load and lateral displacement correspond to this point was termed cracking load, F_{cr}, and cracking displacement, δ_{cr}, respectively. Figure 4.21 illustrates the diagonal cracking produced under prior in-plane loading for both surfaces of the infill. Small separation of the infill from the bounding frame at unloaded corners and

also small hairline cracks on top and bottom corners of the frame were also observed. After the in-plane loading was removed, the frame returned to its initial position but the produced cracks remained unclosed and visible. The out-of-plane displacements of the infill during the in-plane loading, which was recorded by LVDT 3 and LVDT 4, were negligible.

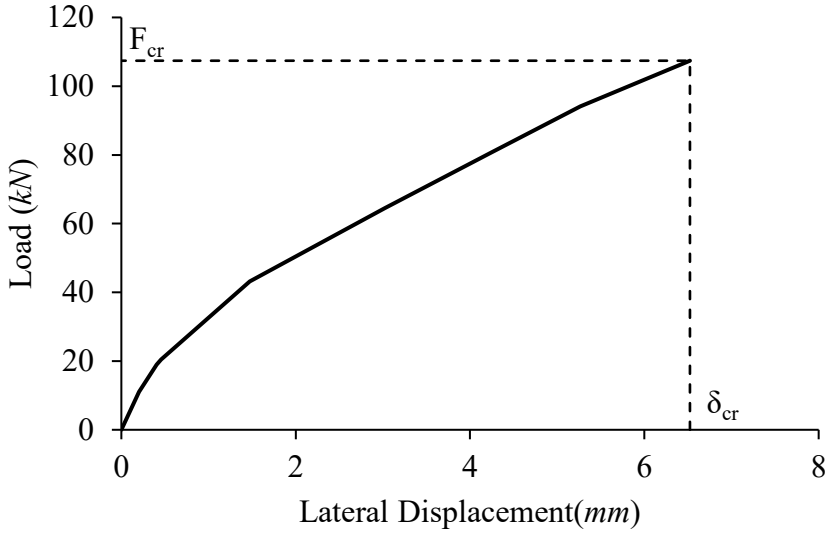

Figure 4.20 Load vs. Lateral Displacement of Specimen IF-D1 under In-Plane Loading

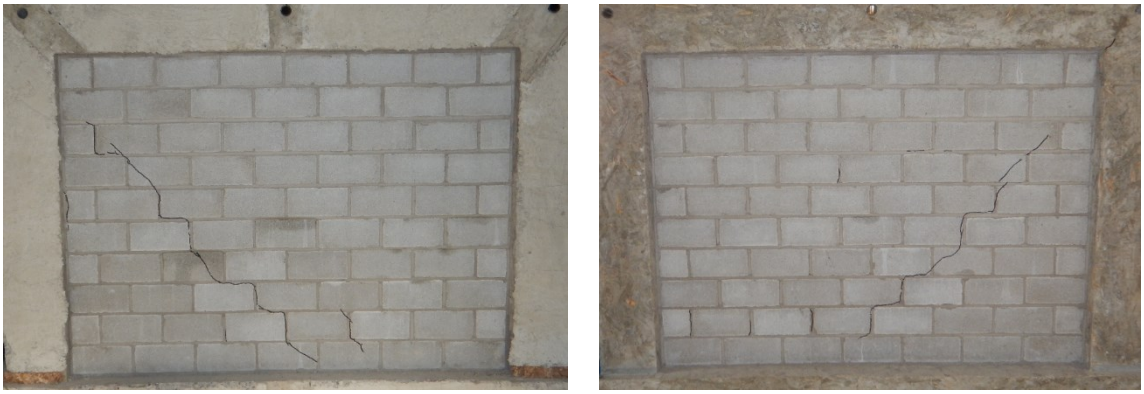

(a) Front View (b) Back View

Figure 4.21 Prior In-Plane Damage for Specimen IF-D1

The pressure vs. out-of-plane displacement for the central LVDT is shown in Figure 4.22 and the development of cracks during the history is shown in Figure 4.23. Figure 4.24 shows the out-of-plane displacement curves of the specimen for the LVDTs along the central horizontal axis. The first crack due to out-of-plane loading occurred at a pressure of 14.6 *kPa* (about 33% of the ultimate pressure), which was a central horizontal crack with the length of four blocks. The behaviour of the specimen until the occurrence of this crack was linear. With the increase of pressure, the horizontal crack began to widen and expand from both sides which resulted in a reduction in the slope of the curve to about 40% of the initial slope. At about 58% of the ultimate pressure, the curve began to show significant nonlinearity as the new cracks developed on the surface of the infill. At about 37.3 *kPa* (84% of the ultimate pressure), starting from one and half blocks away from the right and left end of the infill, diagonal cracks began to form from the central horizontal crack towards the corners of the infill. At about 38 *kPa*, another horizontal crack started to develop at one block course above the previous horizontal crack. At about 40 *kPa*, new cracks formed at the top-left portion of the infill (the location of prior diagonal cracks from in-plane loading). The specimen reached its ultimate strength at 44.4 *kPa* pressure at a central out-of-plane displacement of 6.6 *mm*, and 28 seconds later, the infill collapsed out of the bounding frame. As seen in Figure 4.23, the LVDT at the zone of prior damage (LVDT 4) experienced more displacement than the LVDT at the other side of the infill without prior damage (LVDT 3).

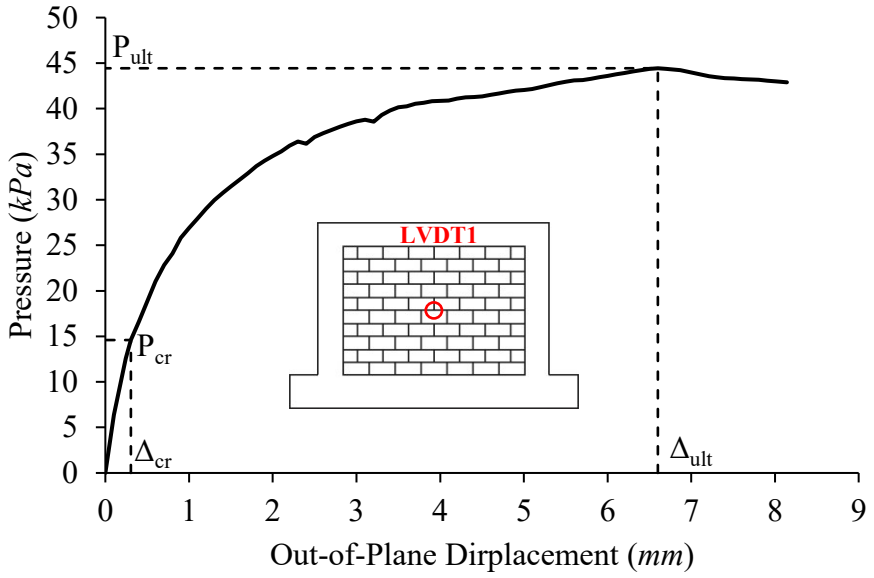

Figure 4.22 Pressure vs. Out-of-Plane Displacement Curve of Specimen IF-D1 under Out-of-Plane Loading

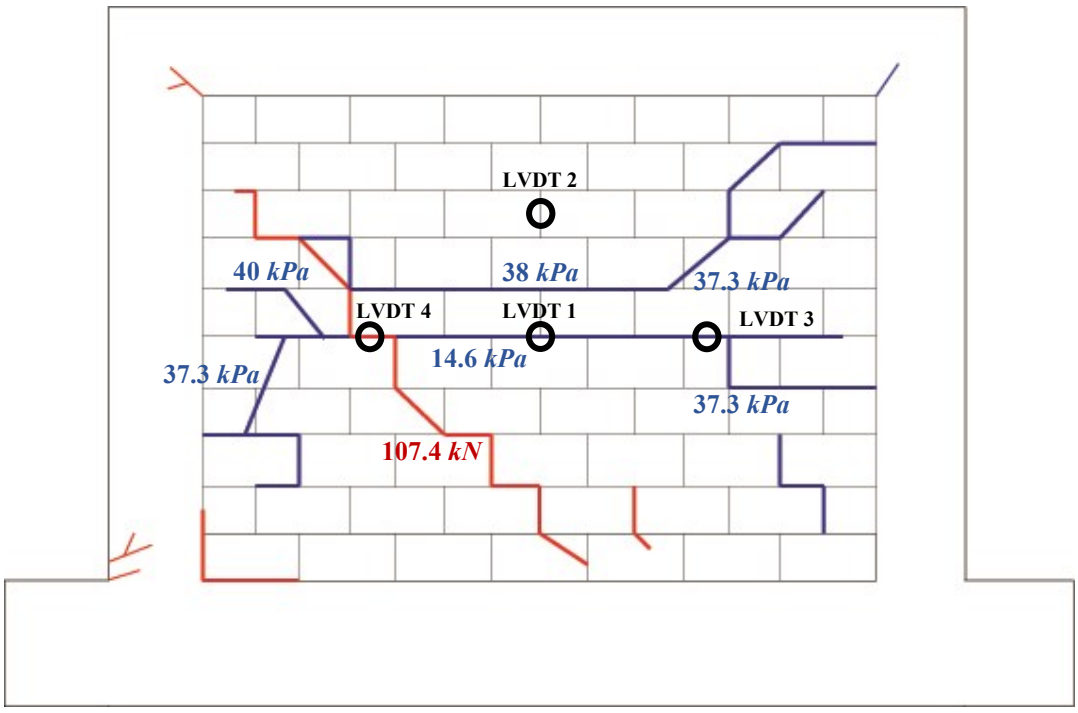

Figure 4.23 The Cracking Pattern of IF-D1 before Failure (Red Colour: Prior In-Plane Damage, Blue Colour: Out-of-Plane Cracking)

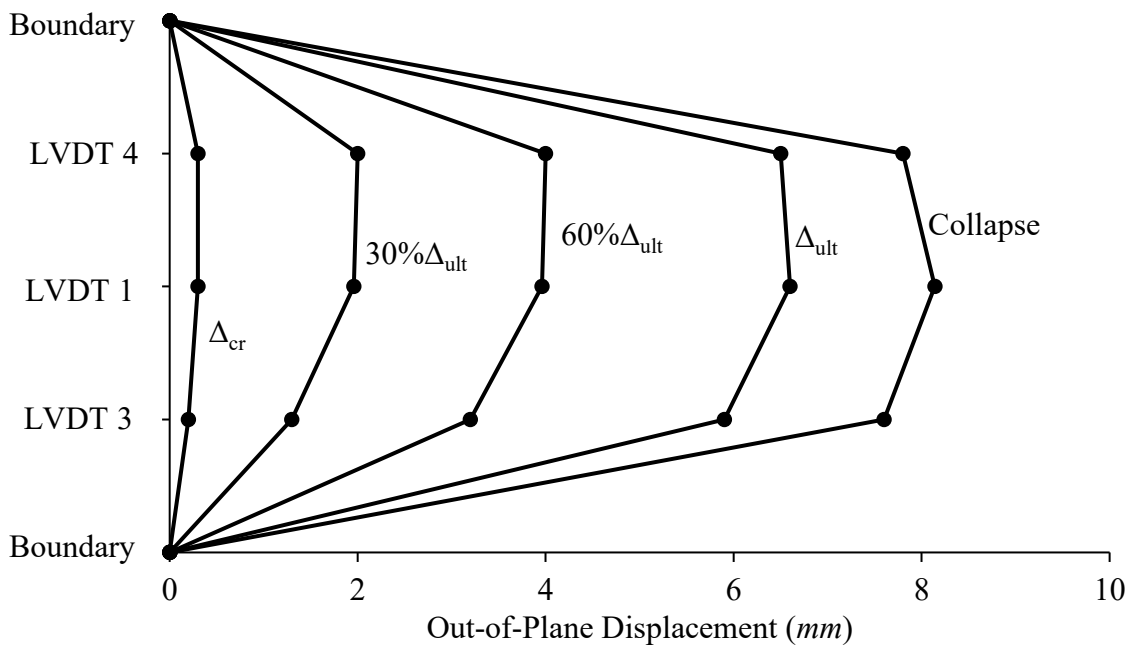

Figure 4.24 Out-of-Plane Displacement Curves of IF-D1 for Horizontal LVDTs

The failure mode of this specimen is shown in Figure 4.25. Similar to the previous specimens, the failure was characterized by web shear failure of the masonry units as seen in Figure 4.26. During the out-of-plane loading only one small hairline crack was observed at the inner side of top right corner of the bounding frame.

Figure 4.25 Failure Mode of Specimen IF-D1

Figure 4.26 Web Shear Failure of Masonry Units for Specimen IF-D1

4.3.4 Specimen IF-D2

This specimen was designed to study the effect of out-of-plane damage on the in-plane behaviour of the system. To this purpose, specimen IF-D2 was first subjected to out-of-plane loading until the observation of a major tensile crack, after which point the out-of-plane load was removed and the specimen was tested under in-plane loading to the ultimate capacity of infilled frame. At this point, the infill was observed to be largely intact, except some minor crushing at the loaded corners. Therefore, it was then decided to test the specimen again under out-of-plane loading to complete failure.

The pressure vs. out-of-plane displacement of this specimen under the 1st round of out-of-plane loading is depicted in Figure 4.27. At a pressure of 26.0 *kPa* corresponding to an out-of-plane displacement of 0.4 *mm*, a horizontal crack with the length of about five blocks occurred at one block course above the centre of the infill as shown in Figure 4.28. After this point the pressure was removed and the crack remained.

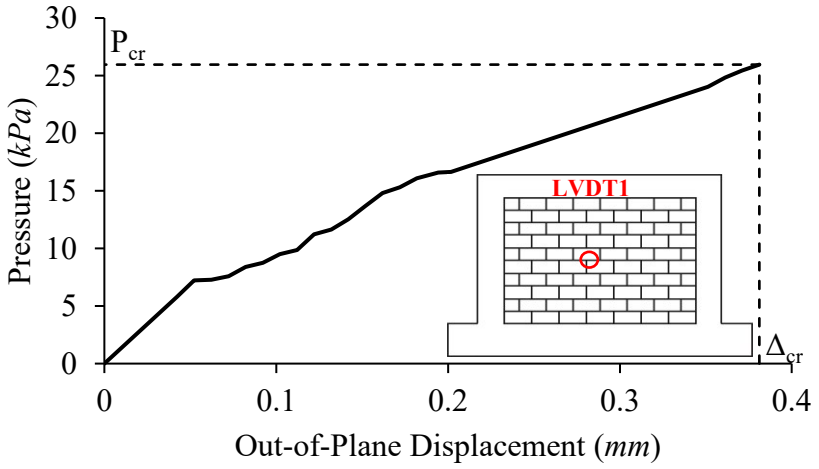

Figure 4.27 Pressure vs. Out-of-Plane Displacement Curve of IF-D2 under the 1st Round of Out-of-Plane Loading

Figure 4.28 Prior Out-of-Plane Damage for Specimen IF-D2

Figure 4.29 depicts the load vs. lateral displacement of the infilled system under the subsequent in-plane loading. The load at which point the first crack developed on the infill surface, $\boldsymbol{F_{cr}}$, and the maximum load the infilled system resisted, $\boldsymbol{F_{ult}}$, with their corresponding lateral displacements, $\boldsymbol{\delta_{cr}}$ and $\boldsymbol{\delta_{ult}}$ are shown on the figure. The behaviour was almost linear up to 28 *kN* (20% of the ultimate load) when a hairline crack occurred on the left-top corner of the bounding frame. With the increase of load, separation of the infill from the bounding frame at unloaded corners was observable at about 41 *kN* which gradually expanded during the loading. At about 60 *kN*, additional cracks began to form on the outer side of the bottom corner of the left column. The onset of diagonal cracking on both surfaces of the infill occurred at the load of 113.3 *kN* (about 80% of the ultimate load) and lateral displacement of 8.7 *mm* as illustrated in Figure 4.30.

The analytical diagonal cracking load and displacement of the infilled frame was also calculated using equivalent diagonal strut method (CSA S304.14). The calculations of diagonal cracking strength and width of diagonal strut in accordance with CSA S304.14, and the method of obtaining cracking load and displacement of the infilled system are

explained in Appendix C. The cracking load and displacement of the infilled frame was obtained to be 39.98 *kN* and 0.92 *mm* respectively. This point is also shown in Figure 4.29 (in red). Comparing this point with the cracking point obtained from the experimental observation, it seem to suggest that the diagonal cracking might have started to develop at about 40 *kN*. In this case, the cracks were either very small or developed within the thickness of the infill. The first major diagonal crack was observed at about 113 kN experimentally. After the diagonal crack appeared, more cracks occurred on the infill surfaces and the bounding frame, and the diagonal cracks gradually expanded towards the bottom right corner of the infill. The specimen reached its ultimate strength at a load of 139.3 *kN* and lateral displacement of 16.9 *mm*, accompanied by corner crushing of the infill, and local crushing of a number of blocks along the top portion of the diagonal crack. The load was stabilized for about 3 *mm* after the ultimate, with the occurrence of additional cracks (mostly below the top portion of diagonal crack) and onset of corner crushing, the load began to decline. At the load of 90.4 *kN* (65% of the ultimate load) and lateral displacement of 26.6 *mm*, the in-plane load was removed. At that point, although the in-plane strength was reached, no major crushing of the infill was observed and the infill remained mainly intact. The specimen at failure is depicted in Figure 4.30. The out-of-plane displacement of the frame during the in-plane loading was quite negligible. It also appeared that the cracks produced during the in-plane loading did not connect with the central horizontal crack (from prior out-of-plane loading) or vice versa. Upon removal of the in-plane loading, no new cracks were formed and previous cracks remained open.

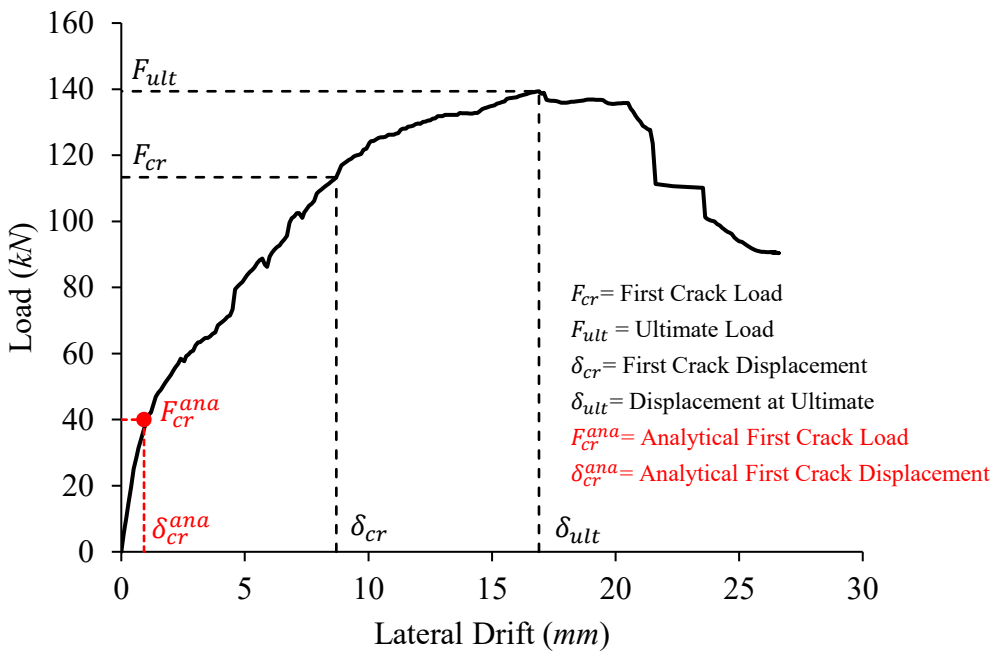

Figure 4.29 Load vs. Lateral Displacement Curve of Specimen IF-D2 under In-plane Loading

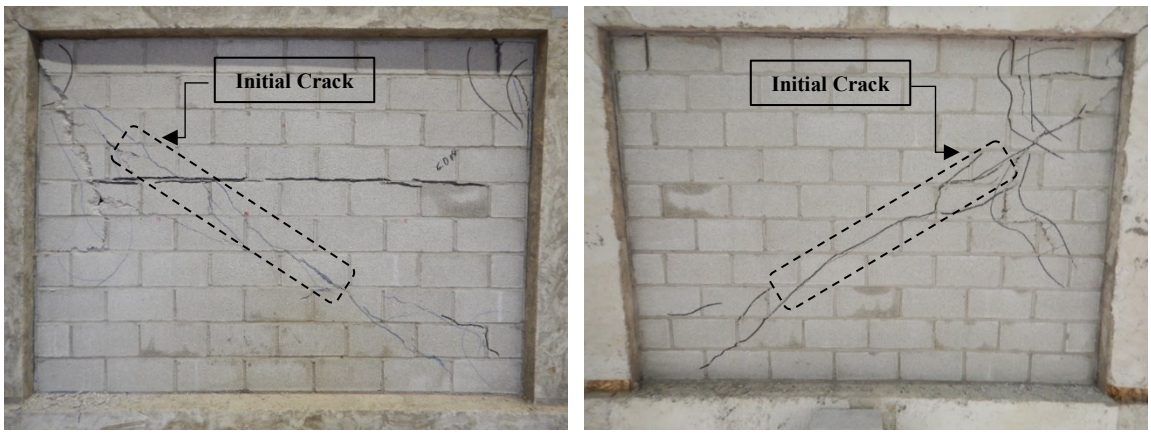

(a) Front View (b) Back View

Figure 4.30 In-plane Failure Mode of Specimen IF-D2

The pressure vs. out-of-plane displacement curve for the central LVDT (with largest displacement records) is illustrated in Figure 4.31 and the cracking pattern of this specimen before failure is illustrated in Figure 4.32. Figure 4.33 shows the out-of-plane displacement curves of the specimen for the LVDTs along the central horizontal axis under both rounds of out-of-plane loading. The behaviour of this specimen was nonlinear throughout the loading history. As loading increased, the prior cracks on the infill surface gradually widened until the failure of the infill occurred. The only new crack occurred on the surface of the infill was a vertical crack above the previous horizontal central crack at the load of 24.8 *kN* (94% of the ultimate pressure) and out-of-plane displacement of 7.6 *mm*. The ultimate of the infill was reached at a pressure of 26.4 *kPa* and out-of-plane displacement of 9.9 *mm*. The collapse of infill happened at a load of 26.0 *kPa* and out-of-plane displacement of 11.0 *mm*. As seen in Figure 4.33, the out-of-plane displacement of the infill is not symmetrical and the zone of prior cracks experienced more out-of-plane displacement.

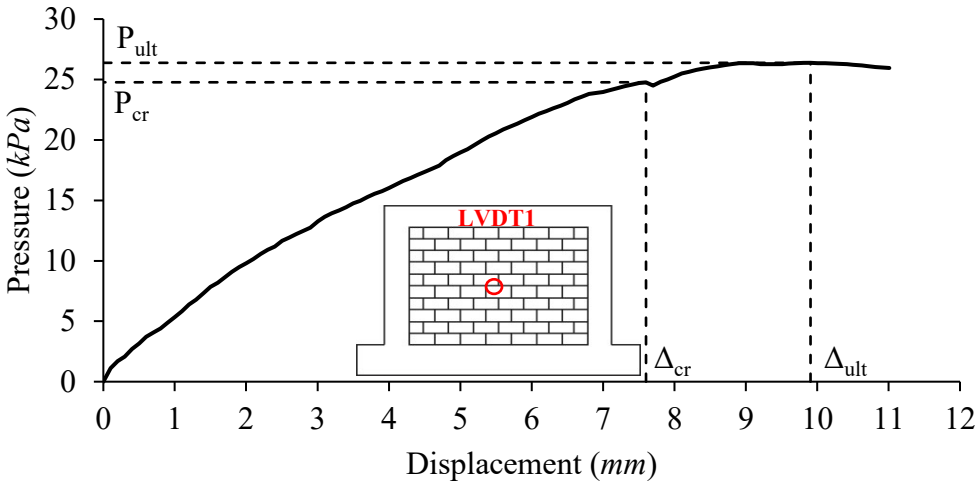

Figure 4.31 Pressure vs. Out-of-Plane Displacement Curve of IF-D2 under the Second Round of Out-of-Plane Loading

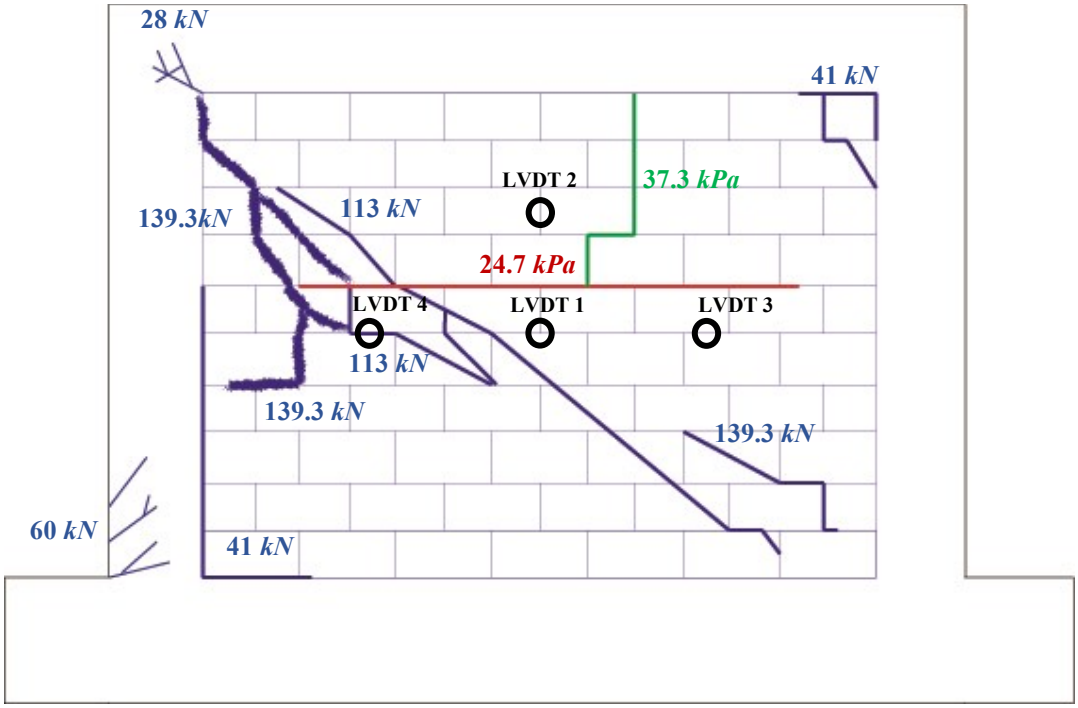

Figure 4.32 Crack Pattern of Specimen IF-D2 before Failure (Red Colour: 1st Round of Out-of-Plane Crack; Blue Colour: In-Plane Cracks; Green Colour: 2nd round of Out-of-Plane Cracks)

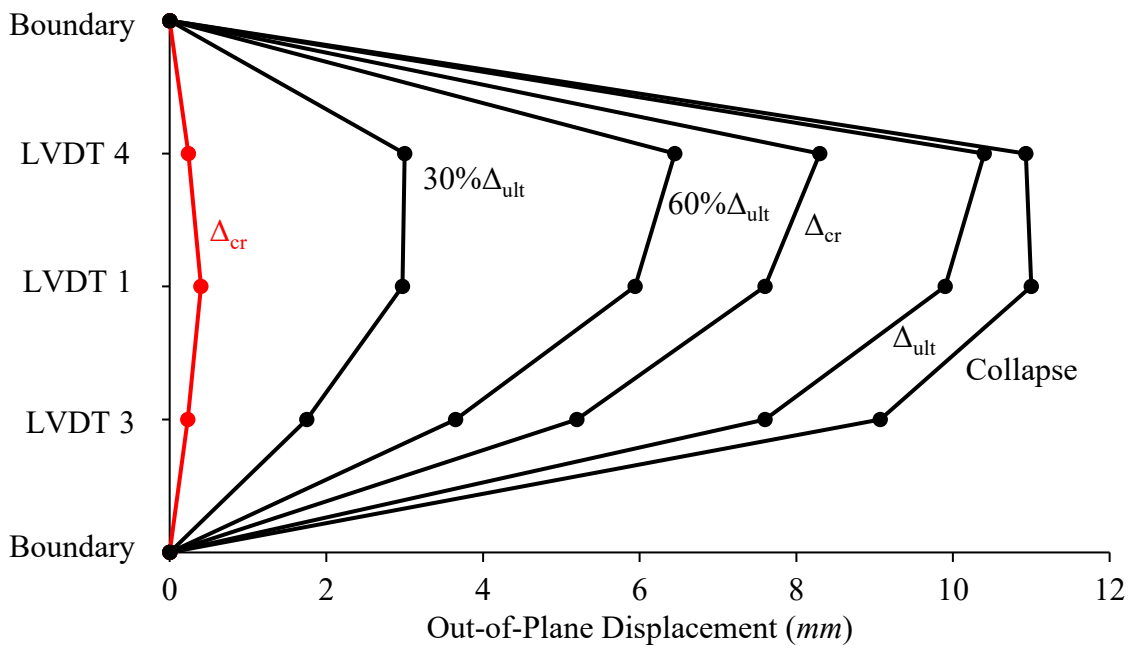

Figure 4.33 Out-of-Plane Displacement Curves of Specimen IF-D2 for the Horizontal LVDTs (Red Colour: 1st Round of Out-of-Plane Loading; Black Colour: 2nd round of Out-of-Plane Loading)

Figure 4.34 depicts the failure mode of this specimen under the second round of out-of-plane loading which was a sudden out-of-plane collapse of the entire infill. A close-up view of failed masonry units again showed the web shear failure characteristics while some portion of the infill remained as a whole after the failure.

The development of cracks on the surface of this specimen under both in-plane and out-of-plane loadings was either at the block-mortar interface or at the face shell of the blocks, except for the in-plane test, the development of cracks near the ultimate load was characterised by crushing of the mortar joint and blocks near the loaded corners.

Figure 4.34 Out-of-Plane Failure Mode of Specimen IF-D2

4.3.5 Summary of Infilled Specimen Results

Table 4.8 presents a summary of the test results of infilled specimens. The values shown in brackets represent those obtained during the prior damage loading stage. The loading sequence is indicated with number 1, 2, and 3. An evaluation of effect of specimen parameters is presented in the following sections.

Table 4.8 Summary of Test Results of Infilled Specimen

Loading	Component	IF-ND	IF-W-ND	IF-D1	IF-D2	
In-Plane (Prior)	F_{cr} (kN)	-	-	(107.4[1])	113.3[2]	
	δ_{cr} (mm)	-	-	(6.5[1])	8.7[2]	
	F_{ult} (kN)	-	-	-	139.3[2]	
	δ_{ult} (mm)	-	-	-	16.9[2]	
Out-Of-Plane (Prior)	P_{cr} (kPa)	26.8	23.7	14.6[2]	(26.0[1])	24.8[3]
	Δ_{cr} (mm)	0.5	0.6	0.3[2]	(0.4[1])	7.6[3]
	P_{ult} (kPa)	66.3	43.7	44.4[2]	-	26.4[3]
	Δ_{ult} (mm)	12.5	4.3	6.6[2]	-	9.9[3]

4.4 EFFECT OF WINDOW OPENING

Figure 4.35 illustrates the pressure vs. out-of-plane displacement curves of specimens IF-ND and IF-W-ND for studying the effect of opening. The displacements used in this case were the maximum displacement recorded (central LVDT 1 for IF-ND, and left LVDT 3 for IF-W-ND). Figure 4.36 further demonstrates the pressure vs. out-of-plane displacement curves of top and left LVDTs for both specimens. The locations of top and side LVDTs for IF-ND and IF-W-ND had about 40 *mm* difference to accommodate the opening. It is noted that (as mentioned before), the out-of-plane displacements of IF-ND along the central horizontal crack were almost the same. Thus, the left side LVDTs of IF-ND and IF-W-ND can be directly compared (Figure 4.36 (a)). For the top LVDT comparison (Figure 4.36 (b)), the out-of-plane displacement of IF-ND was adjusted to be measured at the same location as the top LVDT of IF-W-ND assuming the upper segment of IF-ND had a rigid

body rotation about the top boundary.

Figure 4.35 shows that the presence of opening resulted in a 12% reduction in cracking load and a 34% reduction in ultimate load. The specimen with opening failed at a much smaller displacement. It should be pointed out that a plywood panel (485 *mm* by 660 *mm*) was used to cover the opening for the application of the pressure from the airbag. It is believed that the plywood panel enabled distribution of air pressure over to the area away from the opening and the infill had essentially less area to resist the pressure, which led to a reduction in the strength. As seen in Figure 4.35 and Figure 4.36, the reduction in strength was more significant after the onset of cracking. Referring to Figure 4.9 and Figure 4.14, they show that due to the presence of opening, development of cracking differed and so did the development of arching action. It may be deduced that the specimen with opening had incomplete arching action. The initial slope of the linear portion of the curves in Figure 4.36, showed a 65% and 21% reduction for left and top LVDTs, respectively, caused by the opening.

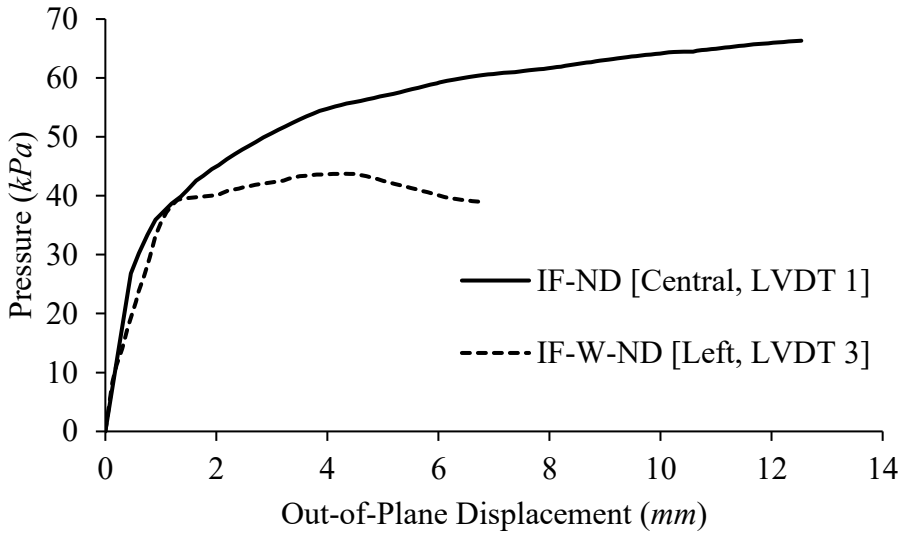

Figure 4.35 Pressure vs. Maximum Out-of-Plane Displacement Curves of IF-ND and IF-W-ND

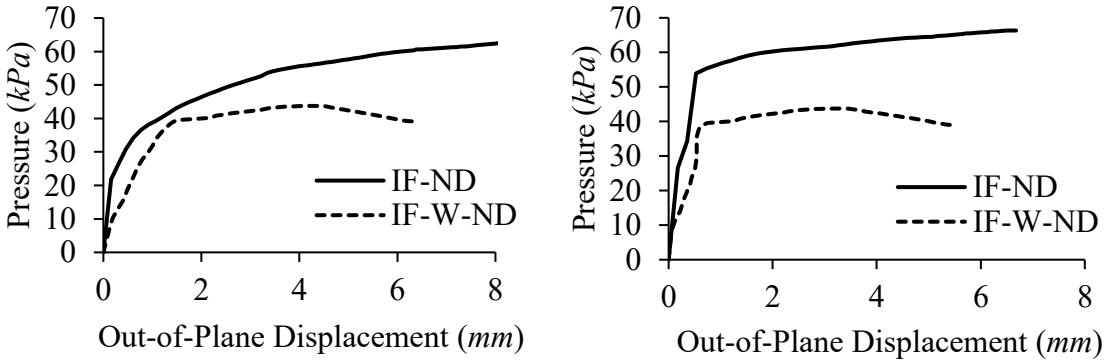

(a) Left LVDT (b) Top LVDT

Figure 4.36 Pressure vs. Out-of-Plane Displacement Curves of IF-ND and IF-W-ND

4.5 EFFECT OF PRIOR DAMAGE

Figure 4.37 illustrates the in-plane load vs. lateral displacement of specimens IF-D1 and IF-D2. A specimen IFNG from an earlier experimental program conducted by Hu (2015)

of the same research group was also included for comparison. The specimen IFNG had the same geometry and similar material properties as specimens tested in this program. Note that specimen IF-D2 had sustained a midheight horizontal crack from the out-of-plane loading. The initial behaviour of specimen IF-D2 up to about 60 *kN* was almost identical to IFNG. A deviation showing a drop in stiffness in IF-D2 observed after this point was attributed to the prior damage of the horizontal crack. However, the ultimate load of IF-D2 was 4% greater than IFNG and reached at a greater lateral displacement. Referring to Table 4.8 and earlier discussion, the prior out-of-plane loading for IF-D2 to generate a horizontal crack was about 40% of its ultimate out-of-plane strength. Furthermore, none of the cracks occurred during the in-plane test of IF-D2 was observed to become connected to the prior central crack. The above observations suggest that the effect of the prior out-of-plane damage defined by a central crack (40% of the ultimate strength) on the in-plane behaviour was insignificant.

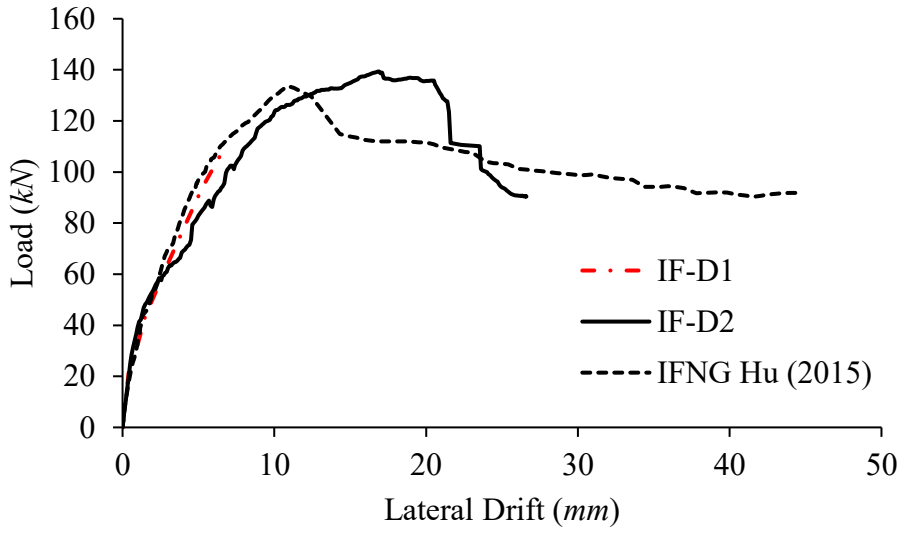

Figure 4.37 Load vs. Lateral Displacement Curves of IF-D1, IF-D2 and IFNG (Hu 2015) under In-Plane Loading

Figure 4.38 depicts the pressure vs. central out-of-plane displacement curves of specimens IF-ND, IF-D1, and IF-D2 for evaluation of the effect of prior in-plane damage on the out-of-plane behaviour. The pressure vs. out-of-plane displacement curves of the top, left, and right LVDTs for all three specimens are also illustrated in Figure 4.39. Note that in the mentioned figures, specimen IF-D1 has sustained a prior in-plane damage in the form of diagonal cracking and specimen IF-D2 has reached its in-plane ultimate strength before being subjected to out-of-plane loading.

Referring to Table 4.8, the prior in-plane loading for IF-D1 was about 75% of its ultimate in-plane capacity. The comparison between IF-ND and IF-D1 showed that the prior in-plane damage in the form of diagonal cracking (75% of the in-plane ultimate strength) resulted in a 33% reduction in the out-of-plane ultimate strength of the infill and 47% reduction in the displacement at ultimate. The cracking strength was also decreased by 46%. The initial slope of IF-D1 had about 17% reduction. With regards to the results of left and right LVDTs, the displacement at ultimate for the left LVDT (at the location of prior in-plane crack) was 10% greater than the right LVDT. Based on the results of all four LVDTs, it can be seen that the pressure vs. displacement curves of IF-D1 and IF-ND followed the same behavioural trend at different locations of infill. In terms of cracking, the ultimate cracking patterns of both specimens were similar except that the prior in-plane damage delayed the formation of new cracks on the left-top portion of the infill (at the location of prior damage) and also another horizontal crack developed above the centre of IF-D1 before failure. The ultimate failure mode of IF-ND and IF-D1 was similar and was characterized by sudden collapse of the infill caused by web shear failure of masonry units.

Comparing to IF-ND, the ultimate strength and displacement of IF-D2 under the second

round of out-of-plane loading had 60% and 21% reductions respectively. As the infill has exhausted its in-plane capacity before this test, the initial slope of the pressure vs. out-of-plane displacement curve of IF-D2 was substantially smaller than IF-ND. The deformation of the infill was accompanied by widening of previous cracks rather than formation of new cracks. The comparison of the results of all LVDTs of IF-ND and IF-D2 again confirms that IF-D2 had much lower stiffness at all locations of the infill. Further, Figure 4.39 (b) and (c), and also Figure 4.33 show that the maximum out-of-plane displacement reached for the left LVDT was 38% greater than the right LVDT, which indicates that the zone of prior in-plane cracks underwent larger out-of-plane displacement. The ultimate failure of IF-ND and IF-D2 was sudden crushing of the infill caused by web shear failure of the masonry units. Noting that IF-D2 has reached its in-plane capacity before subjected to the second round of out-of-plane loading, it suggests that the prior in-plane damage characterized by specimen's reaching its in-plane capacity resulted in a 60% reduction in specimen's out-of-plane strength.

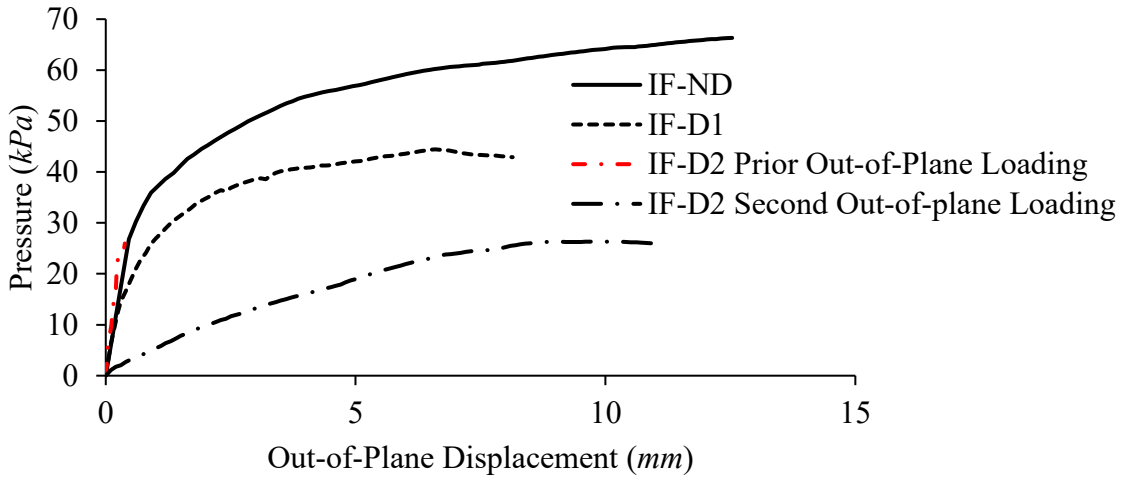

Figure 4.38 Pressure vs. Centre Out-of-Plane Displacement Curves of IF-ND, IF-D1, and IF-D2

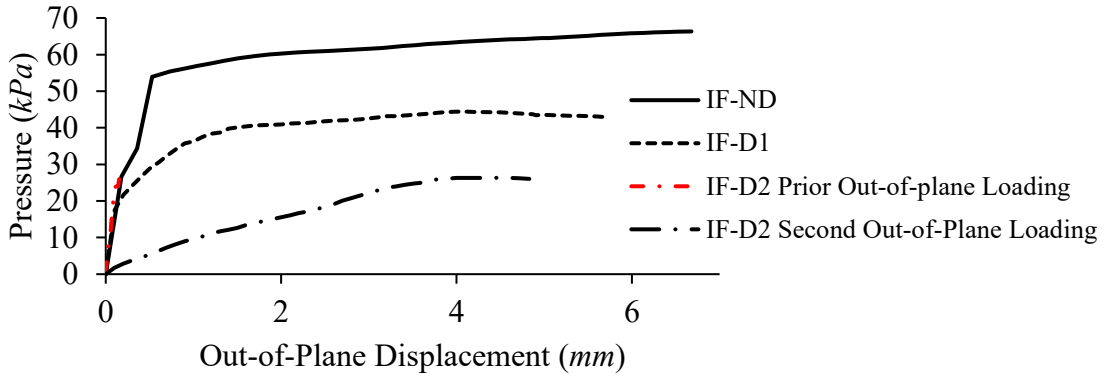

(a) Top LVDT

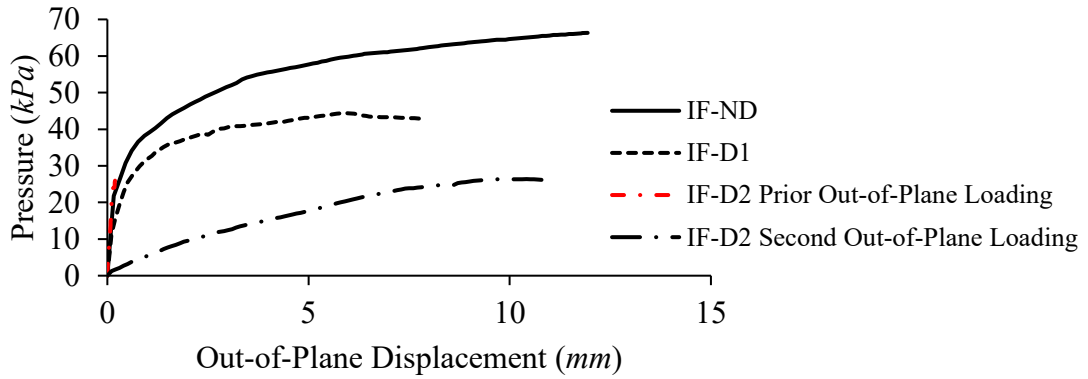

(b) Left LVDT

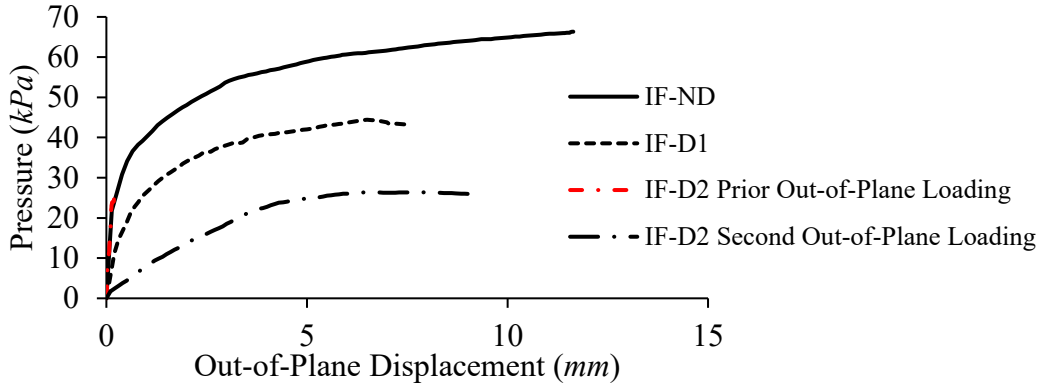

(c) Right LVDT

Figure 4.39 Pressure vs. Out-of-Plane Displacement Curves of IF-ND, IF-D1, and IF-D2

CHAPTER 5 EVALUATION OF ANALYTICAL METHODS

5.1 INTRODUCTION

In this chapter, several existing analytical methods for out-of-plane strength calculations presented in Chapter 2 are assessed using the experimental results obtained in this study as well as those available in literature.

5.2 EXISTING METHODS

The existing analytical methods for strength and displacement calculation are detailed in Chapter 2. For ease of reference, they are summarized in Table 5.1 and Table 5.2 below.

Table 5.1 Summary of Analytical Method for Out-of-Plane Strength Calculation

Method	Out-of-Plane Strength (*kPa*)	Note
MSJC 2013	$q = 4.1 f_m'^{0.75} t^2 \left(\frac{\alpha}{l^{2.5}} + \frac{\beta}{h^{2.5}}\right)$	$\alpha = \frac{1}{h}(E_c I_c h^2)^{0.25} < 50$ $\beta = \frac{1}{l}(E_b I_b l^2)^{0.25} < 50$
Rigid Arching Mechanics (Drysdale and Hamid 2005)	$q = \frac{8C}{h^2}(\gamma t + \Delta_0)$	$C = f_c(1-\gamma)t$ $\Delta_0 = \frac{g_0 h}{4\gamma t}$ g_0 = axial shortening
Dawe and Seah (1989)	$q = 4.5 f_m'^{0.75} t^2 \left(\frac{\alpha}{l^{2.5}} + \frac{\beta}{h^{2.5}}\right)$	$\alpha = \frac{1}{h}(E_c I_c h^2 + G_c J_c t h)^{0.25} < 50$ $\beta = \frac{1}{l}(E_b I_b l^2 + G_b J_b t l)^{0.25} < 50$
Angel (1994)	$q = \frac{2 f_m'}{\left(\frac{h}{t}\right)} R_1 R_2 \lambda$	$R_1 = 1$ if $\delta/\delta_{cr} < 1$ (infill not cracked) Otherwise, $R_1 = \left[0.958 - 0.144\left(\frac{h}{l}\right)\right]^{\frac{\delta}{2\delta_{cr}}}$ $R_2 = 0.357 + 2.49\times10^{-14} EI \leq 1.0$ $\lambda = 0.154 \exp\left(-0.0985 \frac{h}{t}\right)$
Klingner et al. (1996)	$q = \frac{8}{h^2 l}\left\{\begin{matrix} M_{rv}[(l-h) + h\ln(2)] \\ +M_{rh}\left(\frac{x_{yv}}{x_{yh}}\right)\ln\left(\frac{l}{l-h/2}\right) l \end{matrix}\right\}$	$M_{rv} = \frac{0.85 f_m'}{4}\left(t - x_{yv}\right)^2$ $x_{yv} = \frac{t f_m'}{1000 E_m \left[1 - \frac{h}{2\sqrt{(h/2)^2 + t^2}}\right]}$
Mays et al. (1998)	$q = \left(1 + F_r\left(\frac{A_0}{A_p}\right)\right) \times q'$	- For Infills with Opening - $F_r = -3.07$ for blast-resisting opening - q' = Strength of the infill without opening

Table 5.2 Summary of Analytical Methods for Out-of-Plane Displacement Calculation

Method	Out-of-Plane Displacement (mm)	Note
Flanagan and Bennett (1999)	$\Delta_{ult} = \frac{0.002\left(\frac{h}{t}\right)}{1+\sqrt{1-0.001\left(\frac{h}{t}\right)^2}} \times h$	Valid for h/t ratios up to 25
Klingner et al. (1996)	$x_{yv} = \frac{tf'_m}{1000E_m\left[1-\frac{h}{2\sqrt{(h/2)^2+t^2}}\right]}$	- For one-way vertical arching - For one-way horizontal arching h is replaced with l

5.3 EVALUATION OF ANALYTICAL METHODS

Evaluation of the existing analytical methods is conducted in two-fold. First, the existing methods are assessed against the results obtained in this study. Secondly, in view of limited data points from this study, the methods are also assessed against experimental results reported in literature.

5.3.1 Evaluation Using Results from this Study

Table 5.3 provides the material and geometrical properties of the infilled specimens used for the evaluation of analytical methods. In the table, l, h, and t represent the length, height, and thickness of the infill. The modulus of elasticity of the infill (E_m) was calculated as $850f'_m$ in accordance with CSA S304-14. The shear modulus (G) of the concrete was determined based on E_b (=E_c) assuming that the Poisson's ratio of the concrete equals to 0.15.

Table 5.3 Material and Geometrical Properties of Specimens

ID	IF-ND	IF-W-ND	IF-D1	IF-D2
$t\ (mm)$	90	90	90	90
$h\ (mm)$	980	980	980	980
$l\ (mm)$	1350	1350	1350	1350
$f'_m\ (kPa)$	9400	9400	9700	9700
$E_m\ (MPa)$	7990	7990	8245	8245
$E_b = E_c\ (MPa)$	16911	16911	16911	20357
$I_b = I_c$ $(\times 10^6\ mm^4)$	87.5	87.5	87.5	87.5
$G_b = G_c\ (MPa)$	7352.6	7352.6	7352.6	7352.6
$J_b = J_c$ $(\times 10^6\ mm^4)$	147.6	147.6	147.6	147.6

A summary of evaluation results in terms of ratio of experimental to analytical values is presented in Table 5.4 for both out-of-plane strength and displacement calculation. Note that the experimental results, P_{ult} and Δ_{ult} represent the maximum load reached and the displacement corresponding to that load. The control specimen IF-ND was used to evaluate all methods whereas specimens IF-D1 and IF-D2 were used for Angel (1994) for damage consideration and IF-W-ND was used for Mays et al. (1998) for infill opening consideration.

Table 5.4 Summary of Analytical Methods Evaluation

ID	Experimental Results		Ratio of Experimental to Analytical Results								
			Out-of-Plane Strength							Out-of-Plane Displacement	
	P_{ult} (kPa)	Δ_{ult} (mm)	MSJC (2013)	Rigid Arching Mech. (Drysdale and Hamid 2005)		Angel (1994)	Dawe and Seah (1989)	Klingner et al. (1996)	Mays et al. (1998)	Klingner et al. (1996)	Flanagan and Bennett (1999)
				One-way	Two-way						
IF-ND	66.3	12.5	1.37	1.21	0.95	1.85	1.23	0.58	-	1.92	1.14
IF-W-ND	43.7	4.3	-	-		-	-	-	1.33	-	-
IF-D1	44.4	6.6	-	-		1.33	-	-	-	-	-
IF-D2	26.4	9.9	-	-		0.94	-	-	-	-	-

As seen in the table, for specimen IF-ND, the method proposed by Dawe and Seah (1989) and that based on arching mechanics (Drysdale and Hamid 2005) yielded the prediction closest to the experimental value. In the application of the rigid arching mechanics, both one-way and two-way arching results are presented. For one-way arching strength, it is considered that the predominant arching occurs along the direction with smallest length as the strength varies with the inverse of second power of slenderness ratio (equation in Table 5.1). To calculate the two-way arching strength, the participation of arching in the other direction in carrying out-of-plane load is calculated and added to the one-way arching strength by recognizing that the out-of-plane displacement for arching in both direction is the same. A sample calculation for both one-way and two-way arching strength can be found in Appendix A. The one-way arching strength based on the arching mechanics yielded an experimental-to-analytical ratio of 1.21, similar to that produced by the Dawe and Seah's method. The two-way arching strength based on the arching mechanics slightly

overestimated the strength with an experimental-to-analytical ratio of 0.95. This seems to indicate that the infill may not be able to develop a full two-way arching action.

It is also noted that the method proposed by Klingner et al. (1996) overestimates the strength whereas all others provide conservative estimate of strength. From a practical design standpoint, conservative estimate is more desirable. As Klingner et al.'s strength value is dependent on the out-of-plane displacement, an underestimation of displacement (also shown in the table) is attributed to the strength overestimation. On the other hand, the method proposed by Angel (1994) for a normal infill was too conservative. However, for the in-plane damage effect consideration, the Angel's method seemed to perform better with experimental-to-analytical ratios being 1.33 and 0.94 respectively for two specimens. The effect of damage is related through the factor R_1 which is in turn determined based on the in-plane lateral drift at the first crack and at the maximum drift the infill experiences during in-plane loading. Note that specimen IF-D1 sustained prior in-plane damage (a diagonal crack) before the out-of-plane loading whereas specimen IF-D2 reached its in-plane capacity where extensive diagonal cracking has occurred before the out-of-plane loading. The cracking displacements (δ_{cr}) for specimens IF-D1 and IF-D2 were 6.5 *mm* and 8.7 *mm* respectively and the maximum in-plane displacements (δ) for specimens IF-D1 and IF-D2 were 6.5 *mm* and 26.6 *mm* respectively. The Angel's method provided conservative strength estimate for specimen IF-D1 and overestimated the strength for specimen IF-D2 although not by a large degree. It suggests that the method is suited for evaluating prior damage occurred at the serviceability limit state and can be unsafe if used for damage occurred at the ultimate limit state. The method proposed by Mays et al. (1996) underestimated the strength of IF-W-ND with an experimental-to-analytical ratio of 1.33.

As for out-of-plane displacement, Flanagan and Bennett's method was more accurate than Klingner et al.'s method, even though the former is simpler. The inaccuracy of Klingner et al.'s method is due to the fact that the method considers only one-way arching condition, and hence, underestimates the out-of-plane displacement which is a result of deformation in both directions of the infill.

5.3.2 Evaluation Using Results from other Studies

It is noted that experimental studies on the subject of out-of-plane strength of unreinforced infills are limited and most were conducted before 1999 by a very few researchers. Only three experimental studies have been reported in the literature after 1999. A total of 7 studies involving 36 specimens were considered for this comparison. Table 5.5 shows a summary of geometrical and material properties of the specimens used in this evaluation. Specimen WE6 tested by Dawe and Seah (1989) had a 20 *mm* top gap which enabled an arching action in the horizontal direction (the out-of-plane displacement of this specimen was not reported however). Specimen TA5 tested by Hak et al. (2014) was a strip of masonry wall with a length of 1.38 *m* and height of 2.95 *m* built in tight against top and bottom beams and free at sides which corresponds to vertical arching condition. The rest of specimens were in tight contact at all boundaries with their bounding frames enabling the two-way arching condition.

Table 5.5 Summary of Infilled Specimens and Test Results from Other Studies

ID	Properties								Results	
	I_b (I_c) ($\times 10^6$ mm^4)	J_b (J_c) ($\times 10^6$ mm^4)	E_f (GPa)	E_m (GPa)	f'_m (MPa)	t (mm)	$\frac{h}{t}$	$\frac{h}{l}$	P_{ult} (kPa)	Δ_{ult} (mm)
Dawe and Seah (1989)										
WE2	45.4 (87.3)	0.22 (0.41)	200	23.0	28.1	190	14.7	0.78	19.2	50
WE4	45.4 (87.3)	0.22 (0.41)	200	13.8	22.7	140	20.0	0.78	11.2	90
WE8	45.4 (87.3)	0.22 (0.41)	200	16.2	27.4	140	20.0	0.78	13.4	60
WE5	45.4 (87.3)	0.22 (0.41)	200	15.6	20.2	90	31.1	0.78	7.8	80
WE6	45.4 (87.3)	0.22 (0.41)	200	17.2	22.3	190	14.7	0.78	10.6	-
Frederiksen (1992)										
F826	1.37 (1.37)	2.17 (2.17)	200	12.0	13.5	29.5	23.3	1.41	27.6	13.2
F861	1.37 (1.37)	2.17 (2.17)	200	11.0	10.6	29.5	23.3	1.41	16.6	15.5
F862	1.37 (1.37)	2.17 (2.17)	200	11.0	10.6	29.5	23.3	1.41	17.6	11.6
F863	1.37 (1.37)	2.17 (2.17)	200	11.0	10.6	29.5	23.3	1.41	18.0	13.6
F901	1.37 (1.37)	2.17 (2.17)	200	11.0	21.5	34.0	20.2	1.41	49.3	16.2
F902	1.37 (1.37)	2.17 (2.17)	200	11.0	21.5	30.1	22.8	1.41	35.5	17.0
F903	1.37 (1.37)	2.17 (2.17)	200	11.0	15.5	29.5	23.3	1.41	31.7	18.0
E901	1.37 (1.37)	2.17 (2.17)	200	12.0	16.0	31.0	22.2	1.41	32.9	15.9
E902	1.37 (1.37)	2.17 (2.17)	200	12.0	16.0	31.0	22.2	1.41	28.5	16.9
E903	1.37 (1.37)	2.17 (2.17)	200	12.0	16.0	31.0	22.2	1.41	23.7	16.0
F911	1.37 (1.37)	2.17 (2.17)	200	12.0	16.5	30.4	22.6	1.41	25.3	8.3
F912	1.37 (1.37)	2.17 (2.17)	200	14.0	21.2	30.4	22.6	1.41	35.2	14.7
F913	1.37 (1.37)	2.17 (2.17)	200	14.0	21.2	30.4	22.6	1.41	40.2	16.2
E911	1.37 (1.37)	2.17 (2.17)	200	12.0	26.6	31.1	22.2	1.41	40.0	13.1
E912	1.37 (1.37)	2.17 (2.17)	200	12.0	26.6	31.0	22.2	1.41	42.8	16.2
E913	1.37 (1.37)	2.17 (2.17)	200	12.0	26.6	31.0	22.2	1.41	38.7	15.0
Angel (1994)										
Test 1	963 (721)	1463 (1217)	33.5	7.8	11.5	46.0	34.0	0.67	8.2	16.0

Table 5.5 Summary of Infilled Specimens and Test Results from Other Studies [Cont'd]

ID	Properties								Results	
	I_b (I_c) ($\times 10^6$ mm^4)	J_b (J_c) ($\times 10^6$ mm^4)	E_f (GPa)	E_m (GPa)	f'_m (MPa)	t (mm)	$\frac{h}{t}$	$\frac{h}{l}$	P_{ult} (kPa)	Δ_{ult} (mm)
Flanagan and Bennett (1999)										
#22	556 (216)	1.18 (0.33)	200	5.0	5.6	330	6.8	1.00	39.5	49.5
#18	119 (71.1)	0.31 (0.26)	200	5.3	5.6	195	11.5	1.00	26.6	11.5
#25	119 (71.1)	0.31 (0.26)	200	5.3	5.6	93	24.4	1.00	8.1	25.3
Hak et al. (2014)										
TA5	1250 (1250)	2115 (2115)	32	5.3	6.6	235	12.6	2.14	16.0	17.5
Furtado et al. (2016)										
Inf_02	3125 (675)	2700 (1142)	24.7	1.4	0.5	150	15.3	0.55	7.0	15.0

The comparison results are presented in Table 5.6. For almost all of the experimental studies, the methods proposed by MSJC 2013 and Dawe and Seah yielded more accurate results with smallest coefficient of variations comparing to the other methods. The overall mean of experimental-to-analytical value by the MSJC is on the conservative side while slightly unconservative by the Dawe and Seah's method. It is not surprising that the two methods showed similar performance since the MSJC 2013 method adopted the Dawe and Seah's method with small modifications. The constant coefficient in the formulations is 4.1 for MSJC 2013 and 4.5 for Dawe and Seah's method. It must be noted that comparing to Dawe and Seah's method, omission of the second term ($G_c J_c th$ and $G_b J_b tl$) from α and β in MSJC 2013 method has an insignificant effect in α and β since their value is much smaller comparing to the first term ($E_c I_c h^2$ and $E_b I_b l^2$) for most practical cross-sections.

Table 5.6 Summary of Strength Evaluation

ID	P_{ult} (kPa)	Ratio of Experimental to Analytical Strength					
		Dawe and Seah (1989)	Angel (1994)	Klingner et al. (1996)	MSJC 2013	Rigid Arching Mech. (Drysdale and Hamid 2005)	
						One-way	Two-way
Dawe and Seah (1989)							
WE2	19.2	0.53	0.24	0.15	0.58	0.48	0.41
WE4	11.2	0.66	0.39	0.34	0.72	0.56	0.44
WE8	13.4	0.69	0.39	0.35	0.76	0.66	0.53
WE5	7.8	1.22	1.43	2.09	1.34	1.11	0.89
WE6	10.6	1.06	-	0.17	1.16	0.46	-
Avg.		0.83	0.61	0.62	0.91	0.65	0.57
CV (%)		35	90	133	35	41	39
Frederiksen (1992)							
F826	27.6	0.98	1.53	1.73	1.08	1.92	1.53
F861	16.6	0.79	1.32	1.32	0.87	1.47	1.17
F862	17.6	0.75	1.24	1.24	0.82	1.56	1.25
F863	18.0	0.77	1.27	1.27	0.85	1.59	1.27
F901	49.3	0.93	1.10	1.97	1.02	1.53	1.22
F902	35.5	0.85	1.16	2.71	0.93	1.47	1.18
F903	31.7	1.01	1.53	2.20	1.11	1.92	1.53
E901	32.9	0.93	1.31	1.69	1.02	1.71	1.36
E902	28.5	0.81	1.14	1.46	0.89	1.48	1.18
E903	23.7	0.67	0.94	1.22	0.74	1.23	0.98
F911	25.3	0.73	1.04	1.41	0.80	1.34	1.07
F912	35.2	0.84	1.13	1.71	0.92	1.45	1.16
F913	40.2	0.96	1.29	1.95	1.05	1.65	1.32
E911	40.0	0.77	0.96	2.71	0.85	1.24	0.99

Table 5.6 Summary of Strength Evaluation [Cont'd]

ID	P_{ult} (kPa)	Ratio of Experimental to Analytical Strength					
		Dawe and Seah (1989)	Angel (1994)	Klingner et al. (1996)	MSJC 2013	Rigid Arching Mech. (Drysdale and Hamid 2005)	
						One-way	Two-way
Frederiksen (1992)							
E91 2	42.8	0.83	1.03	2.90	0.91	1.34	1.07
E91 3	38.7	0.75	0.93	2.62	0.82	1.21	0.97
Avg.		0.84	1.18	1.88	0.92	1.51	1.20
CV (%)		12	16	31	12	14	14
Angel (1994)							
Test 1	8.2	1.21	2.61	1.14	1.33	2.86	2.28
Flanagan and Bennett (1999)							
#22	39.5	0.75	0.74	0.69	0.82	1.12	0.80
#18	26.6	0.82	0.58	0.61	0.90	0.91	0.48
#25	8.1	1.09	1.27	1.48	1.20	1.49	0.78
Avg.		0.89	0.86	0.93	0.97	1.17	0.69
CV (%)		20	42	52	21	25	26
Hak et al. (2014)							
TA5	31.9	1.06	-	1.59	1.34	1.12	-
Furtado et al. (2016)							
Inf_ 02	7.0	2.87	4.76	2.17	3.15	4.43	4.30
Avg.		0.94	1.16	1.42	1.03	1.61	1.22
CV (%)		46	74	60	46	52	62

The method by Angel (1994) overestimated specimens from Dawe and Seah (1989) and Flanagan and Bennett (1999) while underestimated those from Frederiksen (1992), Angel (1994) and Furtado (2016). Although the overall mean experimental-to-analytical ratio is 1.16, the coefficient of variation of 74% deems that the method is not reliable. The method

by Klingner et al. (1996) yielded the poorest estimation of strength for almost every individual specimen of each experimental program. The mechanics of rigid arching for two-way arching (and even in some cases for one-way arching) overestimated the strength of specimens by Dawe and Seah (1989) and Flanagan and Bennett (1999). This differed from the observation discussed earlier on results from this study. It is noted that in both the Dawe and Seah's and Flanagan and Bennett's studies, the bounding frames were steel frames with much smaller stiffness comparing with the concrete frame used in this study. It suggests that the bounding frame stiffness has a significant effect on the strength which relies on frame member to provide rigid support. This theory is supported by noting that the mechanics of arching provided more accurate results for Fredereksen (1992) specimens since their bounding frames were stiffer than those used in the former two studies in relation to the infills. For studies conducted by Angle, Hak et al. and Furtado et al. (3 specimens in total), reinforced concrete bounding frames were used and the experimental-to-analytical ratios by the mechanics arching method were all greater than unity, indicating a conservative estimate of the strength. This is in line with the observation of this study and further underscores that the bounding frame stiffness is an important factor in infill out-of-plane strength and the existing methods do not provide the strength estimate with a consistent safety margin. Overall, none of the existing methods yielded accurate and consistent results for the full range of parameters.

Table 5.7 summarizes the evaluation of methods proposed by Klingner et al. (1996) and Flanagan and Bennett (1999) for out-of-plane displacement calculation. The method proposed by Flanagan and Bennett (1999) slightly overestimates the displacement, although for most of the specimens (except Furtado et al.'s and Flanagan and Bennett's

specimens) the predicted values seem to be in an acceptable range. This method is used to predict the ultimate displacement of infills under two-way arching condition. As a result, the out-of-plane displacement of specimen TA5 from Hak et al. (2014) was not included in the evaluation as it was in one-way arching condition. Specimen WE5 from Dawe and Seah (1998) and Specimen 1 from Angel (1994) were also not included in the evaluation as their slenderness ratios were greater than the specified limit of 25. The method by Klingner et al. (1996) mostly underestimates the results which is expected since this method was developed for displacement calculation under one-way arching condition. Both methods have a large coefficient of variation of about 60%.

Table 5.7 Summary of Displacement Evaluation

ID	Δ_{ult} (mm)	Ratio of Experimental to Analytical Displacement	
		Klingner et al. (1996)	Flanagan and Bennett (1999)
Dawe and Seah (1989)			
WE2	50	1.96	1.15
WE4	90	1.96	1.43
WE8	60	1.26	0.95
WE5	80	1.41	-
Avg.		1.63	1.11
CV (%)		20	21
Frederiksen (1992)			
F82 6	13.2	1.46	0.69
F86 1	15.5	2.00	0.81
F86 2	11.6	1.50	0.61
F86 3	13.6	1.75	0.71
F90 1	16.2	1.19	1.03
F90 2	17.0	1.10	0.92
F90 3	18.0	1.59	0.94
E90 1	15.9	1.56	0.89
E90 2	16.9	1.65	0.95
E90 3	16.0	1.57	0.90
F91 1	8.3	0.77	0.45
F91 2	14.7	1.24	0.80
F91 3	16.2	1.37	0.89
E91 1	13.1	0.77	0.73
E91 2	16.2	0.95	0.91
E91 3	15.0	0.88	0.84
Avg.		1.33	0.82
CV (%)		27	18
Angel (1994)			
1	16	0.36	-
Flanagan and Bennett (1999)			
#22	49.5	5.45	3.21
#18	11.5	0.83	0.43
#25	25.3	0.86	0.37
Avg.		2.38	1.34
CV (%)		112	121
Hak et al. (2014)			
TA5	17.5	0.74	-
Furtado et al. (2016)			
Inf_02	15.0	2.21	0.40
Avg.		1.51	0.90
CV (%)		61	60

Table 5.8 summarizes the evaluation of the analytical method developed by Angel (1994) for prior in-plane damage effect. The literature review yielded only seven specimens tested in three programs where prior in-plane damage was considered as a parameter. It is noted that in Angel's method, δ_{cr} is the cracking drift, and δ is the maximum drift the specimen sustained from an in-plane loading. All of the specimens tested by Angel (1994) was loaded in-plane up to cracking drift (δ_{cr}), and then loaded up to twice the cracking drift as the maximum drift (δ). The difference between specimens 2b and 3b was the mortar type used in the construction which was Type N and lime respectively. The method provided conservative estimates for specimens 2b and 3b and better estimate for specimen 6b. They attributed the conservative estimate in specimen 2b and 3b to the high slenderness ratio of those two specimens which may result in a more flexural behaviour rather than arching action. The in-plane drift ratios prescribed for the three specimens tested by Hak et al. (2014) prior to out-of-plane loading were 1%, 1.5%, and 2.5%, which resulted in ratios of maximum drift to cracking drift of 1.7, 2.5, and 4.2 respectively. The method overestimated the strength of all three specimens. The in-plane drift of the specimen tested by Furtado et al. (2016) prior to out-of-plane loading was corresponding to the point of ultimate strength, which yielded a ratio of maximum drift to cracking drift of 3.3. The method provided an acceptable prediction of the specimen in a conservative side. Overall, for all seven specimens in the evaluation, the method slightly underestimated the strength but with a high coefficient of variation at 57%.

Table 5.8 Analytical Method Evaluation for Infills with Prior In-Plane Damage (Angel 1994)

ID	I_b (I_c) ($\times 10^6$ mm^4)	E_f (GPa)	f'_m (MPa)	t (mm)	$\frac{h}{t}$	$\frac{h}{l}$	δ_{cr} (mm)	δ (mm)	P_{ult} (kPa)	q_{ana} (kPa) (Angel 1994)	Ratio of experimental to analytical strength
Angel (1994)											
2b	963 (721)	33.5	10.9	46	34	0.67	2.8	5.6	4.0	2.8	1.43
3b	963 (721)	33.5	10.1	46	34	0.67	1.8	3.6	6.0	2.6	2.31
6b	963 (721)	33.5	4.6	92	17	0.67	2.0	4.1	12.4	12.8	0.97
										Avg.	1.57
										CV (%)	43
Hak et al. (2014)											
TA1	1250 (1250)	32.0	6.6	235	12.6	0.70	17.7	44.2	27.3	38.7	0.70
TA2	1250 (1250)	32.0	6.6	235	12.6	0.70	17.7	73.7	16.9	34.0	0.50
TA3	1250 (1250)	32.0	6.6	235	12.6	0.70	17.7	29.5	26.5	41.2	0.64
										Avg.	0.61
										CV (%)	17
Furtado et al. (2016)											
Inf_03	3125 (675)	24.7	0.5	150	15.3	0.55	4.6	15.0	1.7	1.5	1.13
										Avg.	1.10
										CV (%)	57

With the data presented in Table 5.8 as well as those obtained from this study, an attempt was made to develop a correlation between the prior in-plane damage and the reduction in the out-of-plane strength of the infill. Exclusion of some data points has to be made due to incomplete information. Specimen 6b from Angel (1994) and three specimens from Hak et al. (2014) were not used as their corresponding control specimens (undamaged) were not available. Figure 5.1 illustrated a preliminary correlation based on available data points. The prior in-plane damage is defined in terms of the lateral displacement experienced by the specimen before being subjected to out-of-plane loading, δ, over the lateral displacement of the control specimen corresponding to the ultimate strength, δ_{ult}. Note that in Angel (1994) experimental study, the specimens were loaded up to a drift of twice the cracking drift ($2\delta_{cr}$) before being subjected to out-of-plane loading and the displacement corresponding to the ultimate strength was not explicitly given. The in-plane results of several specimens tested by various researchers (IF-ND from this research; IFNG from Hu 2015; TA2 from Hak et al. 2014; Inf_03 from Furtado et al. 2016) showed that the ratio of drift at ultimate load over that at first major cracking is close to 2. Therefore, for Angel (1994) experimental study, it was assumed that $2\delta_{cr}$ corresponds to the in-plane drift of the control specimens at the ultimate strength, which led to a damage indicator of 1.0. In the case of specimen Inf_03 tested by Furtado et al. (2016), the specimen was loaded laterally to 15 mm which was 7.5 mm beyond the displacement at the ultimate strength, resulting in a damage indicator of 2.0. Figure 5.1 shows that the in-plane prior damage does have an impact on the infill out-of-plane strength; an increase in the damage indicator results in an increase in the degree of reduction. With the damage indicator defined herein,

a more or less linear trend is shown. It is, however, evident that more data points are needed to provide a better representation of the trend.

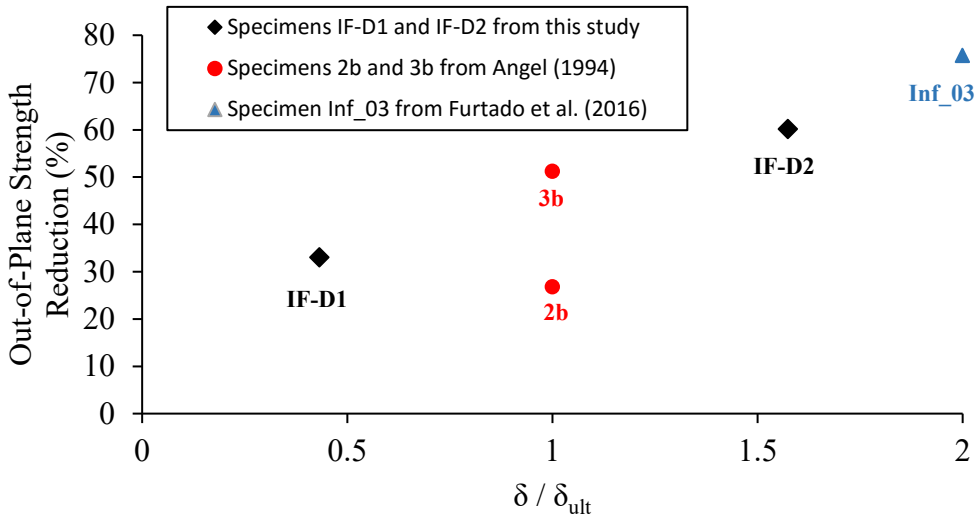

Figure 5.1 Relationship Between Prior In-Plane Loading and Out-of-Plane Strength Reduction

Table 5.9 summarizes the evaluation of Mays et al. (1998) method for infilled specimens with central opening. The evaluation indicates that the method highly underestimates the out-of-plane strength of infills with opening. This is in line with discussion on results of this study. However, for a better evaluation, more experimental results are required.

Table 5.9 Analytical Method Evaluation for Infills with Central Openings (Mays et al. 1998)

ID	I_b (I_c) ($\times 10^6$ mm^4)	E_f (GPa)	f'_m (MPa)	t (mm)	$\frac{h}{t}$	$\frac{h}{l}$	$\frac{A_0}{A_p}$	P_{ult} (kPa)	q' (kPa)	q_{ana} (kPa) (Mays et al. 1994)	Ratio of experimental to analytical strength
Dawe and Seah (1989)											
WE9	45.4 (87.3)	200	3.05	190	14.7	0.78	0.19	17.4	19.2	8.0	2.18
Akhoundi et al. (2016)											
SIF-A	262 (55)	-	1.0	-	-	0.68	0.13	8.9	9.9	5.9	1.51

CHAPTER 6 SUMMARY AND CONCLUSION

6.1 SUMMARY

This research was carried out to study the effect of damage due to prior loading and window opening on the out-of-plane behaviour and strength of masonry infilled RC frames. A total of four masonry infilled RC frame specimens were tested with different parameters. One was considered as a control specimen; one was built with a central window opening of 17% of the infill area; and the other two had sustained damage caused by either prior in-plane or out-of-plane loading. Of two specimens with prior damage, one was first subjected to in-plane loading until occurrence of a major diagonal crack, and then tested under out-of-plane pressure to failure. The other was first subjected to out-of-plane pressure until occurrence of a major horizontal crack around the midheight of the infill, and then tested under in-plane loading to failure. This specimen was then subjected to a second out-of-plane loading to complete collapse of the infill. All specimens had the same dimensions yielding a slenderness ration of 10.9 and an aspect ratio of 1.4. The infills were constructed using half scale standard 200 mm concrete units (CMUs) laid in the running bond. The infills of all specimens were ungrouted except for specimen IF-W-ND, in which the block cells in the courses above and besides the opening were grouted. The average compressive strength of masonry infills was about 9.5 *MPa*. The frame top beam and columns had a 180 *mm* square section, and the base beam had a 250 mm square cross-section. The average compressive strength of the concrete was about 40 *MPa*. The out-of-plane loading was achieved using an airbag that applied uniform out-of-plane pressure on the infill surface. The in-plane loading was done through application of monotonically increase lateral load

to the infilled system using a hydraulic jack. During the testing, the cracking pattern, failure mode, and load vs. displacement response were recorded. The accuracy MSJC 2013 method for strength calculation as well as existing analytical methods for out-of-plane strength and displacement calculation was studied using existing experimental results.

6.2 CONCLUSION

The following conclusions are drawn from this research:

Effect of prior damage and opening:

1. Compared with the infill with no prior damage, the prior damage sustained from in-plane loading up to the first major diagonal cracking resulted in a 33% reduction in the out-of-plane strength of the infill. This reduction was observed to be 60% when the prior in-plane loading reached the infill ultimate lateral capacity.

2. Compared with the infill with no prior damage, the prior damage sustained from out-of-plane loading showed negligible effect on the in-plane behaviour and strength of the infilled frame.

3. Compared with infill without opening, the presence of infill opening (16% opening) resulted in a 34% reduction in the out-of-plane strength and displacement of the infill.

Failure mode:

1. All specimens tested under out-of-plane loading had a sudden and volatile failure characterized by out-of-plane collapse of the infill. The initiation of the collapse was identified as web shear failure of the masonry units.

2. The failure under in-plane loading was characterized by corner crushing of infill at loaded corners.

3. The prior damage was shown to affect the cracking pattern under out-of-plane loading and also resulted in an unsymmetrical out-of-plane displacement of the infill.

Evaluation of analytical methods:

1. For standard specimens (with no opening, no prior damage), a total of 28 test results were used in the evaluation. The results showed that the coefficients of variation of the experimental-to-analytical ratios for all methods were very high, indicating that none of the methods are able to produce consistently accurate estimate over the entire data sets. Comparing with the other methods, MSJC 2013 and the method proposed by Dawe and Seah (1989) provided more accurate estimation of out-of-plane strength with smallest coefficient of variation.

2. For specimens sustained prior in-plane damage, a total of seven test results was used in the evaluation. The results showed that the only existing method for strength calculation (Angel 1994) which accounts for prior in-plane damage had an acceptable mean estimation of damaged specimens although the coefficient of variation was quite high. Based on the results of this experimental study, the above mentioned method underestimated the strength of the specimen with low degree of damage, while slightly overestimated the strength of the specimen with high degree of damage. A preliminary relationship between the reduction in out-of-plane strength and the prior in-plane damage was shown.

3. For specimens with openings, a total of three test results was used in the evaluation. The result showed that the existing method (Mays et al. 1998) underestimated the strength for all of the specimens.

4. The specimens involved in the evaluation had slenderness ratios (h/t) between 6.8 and 34, aspect ratios between (h/l) 0.55 and 2.14, and masonry compressive strength (f'_m) between 0.53 and 28.1 *MPa*. However, the number of specimens used in the evaluation is small. The findings presented above need to be verified with more experimental results. For example, more specimens covering a wide range of prior damages and/or openings need to be tested to provide a better correlation of the out-of-plane strength of the infills with these parameters. Further, more material and geometrical properties such as varying masonry compressive strength, aspect and slenderness ratio of the infill should be included as influential parameters to provide a better understanding of the out-of-plane behaviour and strength of infills.

REFERENCES

Akhoundi, F., Vasconcelos, G., Lourenco, P., Silva, L. (2016). Out-of-plane response of masonry infilled RC frames: Effect of workmanship and opening. 16th International Brick and Block Masonry Conference, Pádua, Italy.

Angel, R. (1994). Behavior of reinforced concrete frames with masonry infill walls. Ph.D. Dissertation, the University of Illinois at Urbana-Champaign.

ASTM C1314 (2016). Standard test methods for compressive strength of masonry prisms. ASTM International, West Conshohocken, PA.

ASTM C140/C140M (2016). Standard test methods for sampling and testing concrete masonry units and related units. ASTM International, West Conshohocken, PA.

ASTM C143/C143M (2015). Standard test method for slump of hydraulic-cement concrete. ASTM International, West Conshohocken, PA.

ASTM C270 (2014). Standard specification for mortar for unit masonry. ASTM international, West Conshohocken, PA.

ASTM C39/C39M (2016). Standard test method for compressive strength of cylindrical concrete specimens. ASTM International, West Conshohocken, PA.

ASTM E8 (2008). Standard test methods for tension testing of metallic materials. ASTM International, West Conshohocken, PA.

BS 5628 (2005). Code practice for Use of masonry: Structural use of unreinforced masonry. British Standard Institution, BSI, London.

CAN/CSA A165 (2015). CSA standards on concrete masonry units. Mississauga, ON, Canada: Canadian Standard Association.

CAN/CSA A23.3.14 (2014). Design of concrete structures. Mississauga, ON, Canada: Canadian Standard Association.

CAN/CSA S304.14 (2014). Design of masonry structures. Mississauga, ON, Canada: Canadian Standard Association.

Cohen, E., and Laing, E. (1956). Discussion to 'Arching action theory of masonry walls. Journal of Structural Division, ASCE, 82(5): 1067-28–1067-40.

Dafnis, A., Kolsch, H., and Reimerdes, H. (2002). Arching in masonry walls subjected to earthquake motions. Journal of Structural Engineering, ASCE,128(2): 153-159.

Dawe, J. L., and Seah C. K. (1989). Out-of-plane resistance of concrete masonry infilled panels. Canadian Journal of Civil Engineering, 16:854-864.

Drysdale, R.G., and Hamid, A.A. (2005). Masonry structures: behavior and design. Mississauga, Ontario: Canadian Masonry Design Centre.

Federal Emergency Management Agency (FEMA). (1994). NEHRP guideline for the seismic rehabilitation of buildings. FEMA-273, Building Seismic Safety Council, Washington, D.C.

Flanagan, R. D., and Bennett, R. M. (1999). Arching of masonry infilled frames: comparison of analytical methods. Practice Periodical on Structural Design and Construction, ASCE, 4(3):105-110.

Flanagan, R. D., and Bennett, R. M. (1999). Bidirectional behavior of structural clay tile infilled frames. Journal of Structural Engineering, ASCE, 125(3):236-244.

Frederiksen, V. T. (1992). Membrane effect in laterally loaded masonry walls: a second order phenomenon. Proceedings of the 6th Canadian Masonry Symposium, University of Saskatchewan, Saskatoon, Saskatchewan, 537–547.

Furtado, A., Rodrigues, and H., Arêde, A. (2016). Experimental evaluation of out-of-plane capacity of masonry infill walls. Journal of Engineering Structures, ELSEVIER, 111:48-63.

Gabrielsen, and Kaplan K. (1977). Arching in masonry walls subjected to out-of-plane forces. NBS Building Science Series 106, National Workshop on Earthquake Resistant Masonry Construction.

Gabrielsen, B., and Wilton C. (1976). Shock tunnel tests of arched wall panels. Report No 7030-19 URS Research Company, San Mateo, CA.

Gabrielsen, B., Wilton C., and Kaplan K. (1975). Response of arching walls and debris from interior walls caused by blast loading. Report No. 7030-23, URS Research Company, San Mateo, California.

Griffith, M. C., Vaculik, J., and Lam, N. T. K. (2007). Cyclic testing of unreinforced masonry walls in two-way bending. Journal of Earthquake Engineering and Structural Dynamics, Wiley, 36:801-821.

Hak, S., Morandi, P., and Magenes, G. (2014). Out-of-plane experimental response of strong masonry infills. Second European Conference on Earthquake Engineering and Seismology, Istanbul.

Henderson R. C., Fricke K. E., and Jones W. D. (2003). Summary of a large- and small-scale unreinforced masonry infill test Program. Journal of Structural Engineering, ASCE, 129(12): 0733-9445.

Hill, J.A. (1993). Full-scale testing of unreinforced masonry infill frame panels. Structural Engineering in Natural Hazards Mitigation, Proceeding of the Structures Congress.

Hu, C. (2015). Experimental study of the effect of interfacial gaps on the in-plane behaviour of masonry infilled RC frames. Master Thesis, Dalhousie University.

Klingner, R. E., Rubiano, N. R., Bashandy, T. R., and Sweeney, S. C. (1996). Evaluation and analytical verification of shaking table data from infilled frames. Part 2: Out of plane behavior. Proceeding 7th North American Masonry Conference, 521–532.

Masonry Standard Joint Committee (2012). Building code requirements for masonry structures. ACI 530/ASCE 5/TMS 402, American Concrete Institute, Detroit.

Mays, G. C., Hetherington, J. G., and Rose, T. A. (1998). Resistance deflection functions for concrete wall panels with openings. Journal of Structural Engineering, ASCE, 124(5):579–587.

Mazzoni, S., McKenna. F., Scott. M. H., Fenves. G. L. (2006). OpenSees command language manual. Pacific Earthquake Engineering Research (PEER) Center, Berkeley, CA.

McDowell, E. L., McKee, K. E., and Sevin, E. (1956). Arching action theory of masonry walls. Journal of the Structural Division, Proceeding of ASCE, 82(2)915-1-915-18.

Meisl, C. S., Elwood, K. J., and Ventura, C. E. (2007). Shake table tests on the out-of-plane response of unreinforced masonry walls. Canadian Journal of Civil Engineering, 34(11): 1381-1392.

Monk, C.B. (1958). Resistance of Structural Clay Masonry to Dynamic Forces. Research Report No.7, Structural Clay Products Research Foundation, Geneva, Illinois.

Rabinovitch, O., and Madah, H (2011). Finite element modeling and shake-table testing of unidirectional infill masonry walls under out-of-plane dynamic loads. Journal of Engineering Structures, Elsevier, 33(9):2683-2696.

Scawthorn, C. (2002). Reinforced concrete frame with masonry infills, digital image. < https://www.nexus.globalquakemodel.org/gem-building-taxonomy/overview/glossary/infilled-frame--lfinf >.

Steeves, R. J. (2016). Quasi-static testing of masonry infilled RC frames with interfacial gaps. Master Thesis, Dalhousie University.

World House Encyclopedia, Steel moment resisting frame with brick masonry partitions, digital image. < http://db.world-housing.net/building/95 >.

APPENDIX A MECHANICS OF RIGID ARCHING CALCULATION

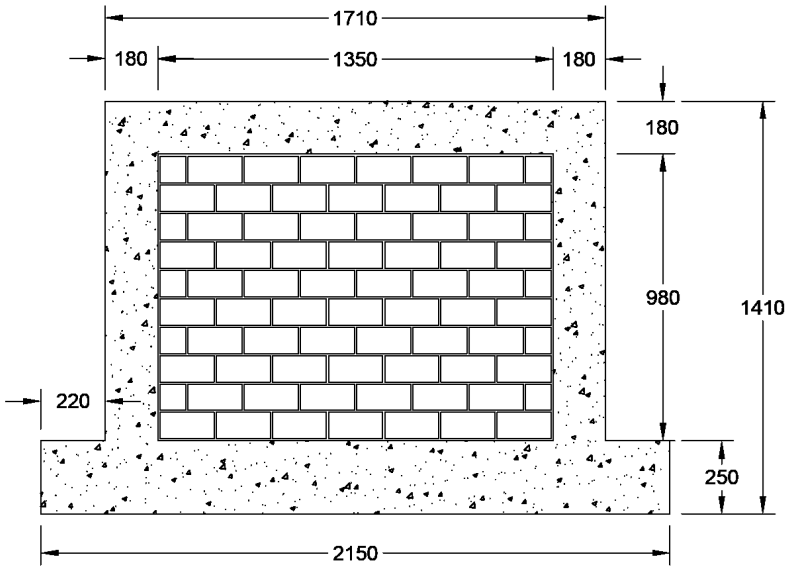

Figure A.1 Infilled Frame Specimen IF-ND (unit: *mm*)

Specimen IF-ND was taken as the example for the sample calculation.

Infill properties:

$f'_m = 9.4\ MPa \quad E_m = 7990\ MPa$

$t = 90\ mm \quad h = 980\ mm \quad l = 1350\ mm$

$\gamma = 0.9$ (recommended by British Standards Institution BS 5628)

Since $h < l$ vertical arching is more significant than horizontal arcing. Hence, the vertical arching strength is calculated and then the participation of horizontal arching is calculated and added. The vertical arching by considering the axial shortening is calculated as:

$$\varepsilon_m^v = \frac{f_m'}{E_m} \Rightarrow \varepsilon_m^v = \frac{9.4}{7990} = 0.00118$$

$$g_0^v = \varepsilon_m^v \times h = 0.00118 \times 980 = 1.153\ mm$$

$$\Delta_0 = \frac{g_0^v h}{4\gamma t} = \frac{1.153 \times 980}{4 \times 0.9 \times 90} = 3.487\ mm$$

$$C_v = \phi_m f_m (1-\gamma) t = 1 \times 9.4 \times 10^3 \times (1-0.9) \times 90 = 84600\ kN/m$$

$$q_v = \frac{8C_v}{h^2}(\gamma t - \Delta_0) = \frac{8 \times 84600}{980^2} \times (0.9 \times 90 - 3.487) = 54.7\ kPa$$

The extent at which the horizontal arching participates in load carrying capacity is calculated considering that the out-of-plane displacement for arching in both directions must be equal. So, by using the displacement obtained from vertical arching, the axial shortening of horizontal arching and the corresponding contribution of horizontal arching is calculated as:

$$\begin{cases} \Delta_0 = 3.487\ mm \\ \Delta_0 = \dfrac{g_0 l}{4\gamma t} \Rightarrow g_0^h = \dfrac{4\Delta_0 \gamma t}{l} \end{cases} \Longrightarrow g_0^h = \frac{4 \times 3.487 \times 0.9 \times 90}{1350} = 0.837\ mm$$

$$\varepsilon_m^h = \frac{g_0^h}{l} = \frac{0.837}{1350} = 0.00062$$

$$f_c = \varepsilon_m^h \times E_m = 0.00062 \times 7990 = 4.95\ MPa$$

$$C_h = \phi_m f_c (1-\gamma) t = 1 \times 4.95 \times 10^3 \times (1-0.9) \times 90 = 44550\ kN/m$$

$$q_h = \frac{8C_h}{h^2}(\gamma t - \Delta_0) = \frac{8 \times 44550}{1350^2} \times (0.9 \times 90 - 3.487) = 15.1\ kPa$$

Total out-of-plane strength is calculated as:

$$q = q_v + q_h = 54.7 + 15.1 = 69.8\ kPa$$

APPENDIX B YIELD LINE ANALYSIS OF FLEXURAL WALLS CORRESPONDING TO IF-ND AND IF-W-ND

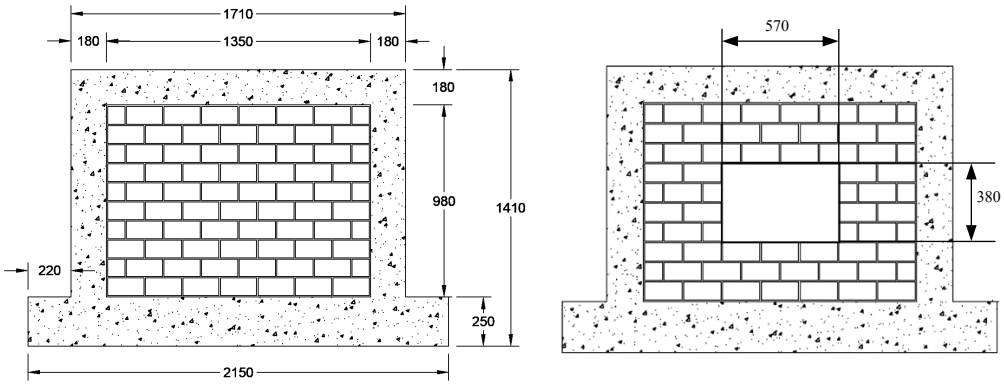

(a) IF-ND (b) IF-W-ND

Figure B.1 Infilled Frame Specimens (unit: *mm*)

For both specimens, it is assumed that the wall panel is simply supported along all four boundaries.

Wall properties:

$t = 90\ mm \quad t_f = 17\ mm$ (face shell thickness)

concrete block with Type S mortar ⟹ CSA S304.14 (2014):

$f_{tn} = 0.4\ MPa$ (flexural tensile strength of masonry normal to bed joints)

$f_{tp} = 0.8\ MPa$ (flexural tensile strength of masonry parallel to bed joints)

Moment of inertia of the wall for bending in both horizontal and vertical direction is:

$$I_m = \frac{10^3 \times 90^3}{12} - \frac{10^3 \times (90 - 2 \times 17)^3}{12} = 4.61 \times 10^7 \ \frac{mm^4}{m}$$

The section modulus of the wall is:

$$S = \frac{I_m}{t/2} = \frac{4.61 \times 10^7}{90/2} = 1.02 \times 10^6 \frac{mm^3}{m}$$

The moment resistant of the wall is:

$$M_{rh} = f_{tp} \times S = 0.8 \times 1.02 \times 10^6 = 8.2 \times 10^5 \ \frac{N.mm}{m} = 0.82 \ \frac{kN.m}{m}$$

$$M_{rv} = f_{tn} \times S = 0.4 \times 1.02 \times 10^6 = 4.1 \times 10^5 \ \frac{N.mm}{m} = 0.41 \ \frac{kN.m}{m}$$

Specimen IF-ND

The yield lines pattern of specimen IF-ND is illustrated in Figure B.2 in blue lines.

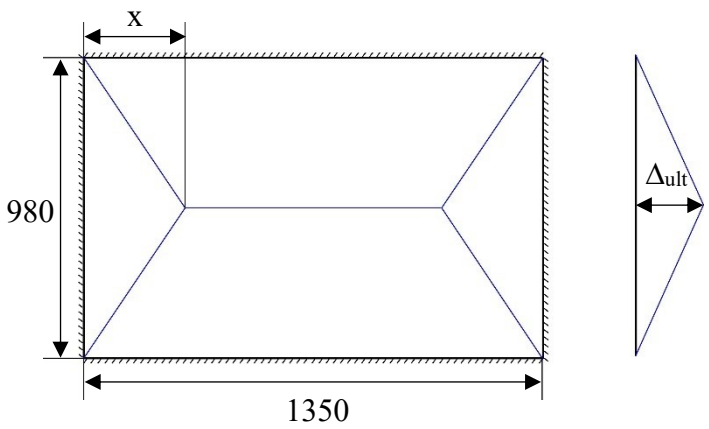

Figure B.2 Yield Lines of Specimen IF-ND (unit: *mm*)

q and x can be obtained by realizing that external work (load × deflection) equals internal work (moment × rotation). Due to the symmetry, it is only necessary to analyze the bottom half of the wall, thus:

$$2q\frac{490x}{2}\frac{\Delta_{ult}}{3}+2q\frac{490x}{2}\frac{\Delta_{ult}}{3}+q[490(1350-2x)]\frac{\Delta_{ult}}{2}$$

$$=2M_{rv}\frac{\Delta_{ult}}{490}x+2M_{rh}\frac{\Delta_{ult}}{x}(490)+M_{rv}(1350-2x)\frac{\Delta_{ult}}{490}$$

Δ_{ult} is removed from both sides of the equation. The distance x is the value that results in smallest out-of-plane strength. Therefore, it can be calculated by substituting M_{rv} and M_{rh} into the above equation, rearranging the equation base on q, differentiating q with respect to x and set it to zero, and then solving for x:

$$\frac{dq}{dx}=0\Longrightarrow x=653.6\,mm\Longrightarrow q=10.85\,kPa$$

Specimen IF-W-ND

The yield lines pattern of specimen IF-W-ND is illustrated in Figure B.3 in blue lines.

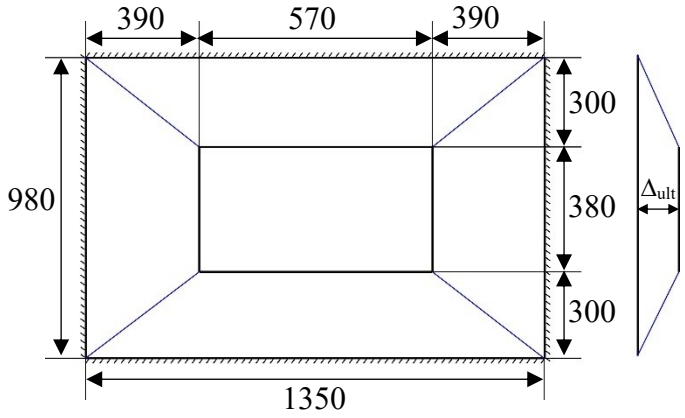

Figure B.3 Yield Lines of Specimen IF-W-ND (unit: *mm*)

q is calculated by setting external work equal to internal work:

$$2q(380\times390)\frac{\Delta_{ult}}{2}+2q(570\times300)\frac{\Delta_{ult}}{2}+8q\left(\frac{390\times300}{2}\right)\frac{\Delta_{ult}}{3}$$

$$=4M_{rh}\frac{\Delta_{ult}}{390}(300)+4M_{rv}\frac{\Delta_{ult}}{300}(390)$$

By removing Δ_{ult} form both side of the equation and solve the equation for q:

$$q=6.65\ kPa$$

APPENDIX C IN-PLANE ANALYIS OF MASONRY INFILLED FRAMES

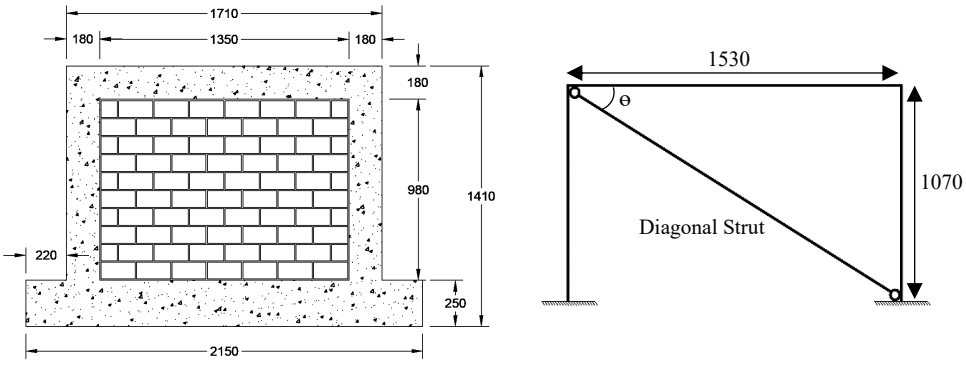

(a) (b)

Figure C.1 (a) Infilled Frame Specimen (IF-D1); (b) OpenSees Model (unit: *mm*)

For modeling and in-plane analysis of masonry infilled frames, the infill is replaced by an equivalent diagonal strut acting as a brace for the frame (CSA S304.14)

Infilled frame specimen properties:

Reinforcement: $E_s = 247357\ MPa \quad A_s = 100\ mm^2$

Concrete: $f_c' = 38.5\ MPa \quad E_f = 16911\ MPa$

Masonry wall: $f_m' = 9.7\ MPa \quad E_m = 8245\ MPa \quad t = 90\ mm \quad t_e = 34\ mm$

Since the bounding frame cracked prior to the occurrence of diagonal cracking, moment of inertia of the cracked section (I_{cr}) must be used. Gross moment of inertia (I_g) of the untracked section shown in Figure C.2 is calculated from:

$$\frac{E_s}{E_f} = \frac{247357\ MPa}{16911\ MPa} = 14.62$$

$\Longrightarrow A_s^{eq} = 4{\times}14.62{\times}100\ mm^2 = 5848\ mm^2$ (equivalent steel area)

Total equivalent cross-section area:

$$A^{eq} = A_s^{eq} + A_c = 5848 + [(180 \times 180) - 4{\times}100\ ] = 36860\ mm^2$$

$$I_g = 4{\times}14.62{\times}\left[\frac{\pi{\times}\left(\frac{11.3}{2}\right)^4}{4} + 100{\times}\left(\frac{107.4}{2}\right)^2\right]$$

$$+\left\{\frac{180^4}{12} - \left[\frac{\pi{\times}\left(\frac{11.3}{2}\right)^4}{4} + 100{\times}\left(\frac{107.4}{2}\right)^2\right]\right\}$$

$$= 7682818\ mm^4 + 87190830\ mm^4 = 1.01{\times}10^8\ mm^4$$

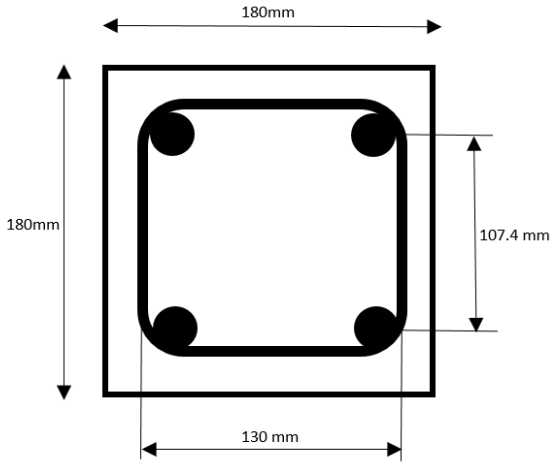

Figure C.2 Beam and Columns Cross-Section

Moment of inertia of the cracked section according to the Canadian Concrete Standard CSA A23.3-14 (2014) is calculated as:

$$I_{cr} = 0.35I_g = 0.35\times1.01\times10^8 = 3.54\times10^7\ mm^4$$

Calculation of width of equivalent diagonal strut in accordance with CSA S304.14

$$\theta = \tan^{-1}\frac{h}{l} = \tan^{-1}\frac{980}{1350} = 36°$$

$$\alpha_h = \frac{\pi}{2}\sqrt[4]{\frac{4E_cI_ch}{E_mt_e\sin 2\theta}} = \frac{\pi}{2}\sqrt[4]{\frac{4(20357)(1.01\times10^8)(980)}{8245(34)\sin 2(36)}} = 655\ mm$$

$$\alpha_l = \pi\sqrt[4]{\frac{4E_cI_bl}{E_mt_e\sin 2\theta}} = \pi\sqrt[4]{\frac{4(20357)(1.01\times10^8)(1350)}{8245(34)\sin 2(36)}} = 1419\ mm$$

The width of diagonal strut is:

$$\frac{w}{2} = min\begin{cases}\frac{1}{2}\sqrt{\alpha_h^2+\alpha_l^2} = \frac{1}{2}\sqrt{655^{\,2}+1419^{\,2}} = 781\ mm\\ \frac{1}{4}\sqrt{l^2+h^2} = \frac{1}{4}\sqrt{1350^2+980^2} = 417.05\ mm \rightarrow \boldsymbol{governs}\end{cases}$$

Calculation of diagonal cracking strength of the infill in accordance with CSA S304.14

$$h/l = \frac{980}{1350} \le 1$$

Then the infill is a squad wall. So, the diagonal cracking strength of the infill is calculated from:

$$V_r = \emptyset_m(v_mb_wd_v + 0.25P_d)\gamma_g \le 0.4\emptyset_m\sqrt{f'_m}b_wd_v\gamma_g\left(2 - h/l\right)$$

$\emptyset_m = 1$

$b_w = 90\ mm$ (actual thickness of the wall)

$d_v = 0.8l = 0.8{\times}1350 = 1080\ mm$ (effective depth for shear calculation)

$$\gamma_g = {A_e}\Big/{A_g} \leq 0.5 \Longrightarrow \gamma_g = \frac{2(17)}{90} = 0.378$$

$P_d = 0$ (axial compressive load on the section)

$$\frac{M_f}{V_f d_v} \geq 0.25 \Longrightarrow \frac{M_f}{V_f d_v} = 0.25 \Longrightarrow v_m = 0.16\left(2 - \frac{M_f}{V_f d_v}\right)\sqrt{f'_m} = 0.16(2 - 0.25)\sqrt{9.7}$$

$$= 0.87\ MPa$$

$$\Longrightarrow V_r = \begin{cases} 1.0(0.87{\times}90{\times}1080 + 0)(0.378) = 31.965\ kN\ \rightarrow \boldsymbol{governs} \\ 0.4(1.0)\sqrt{9.7}(90)(1080)(0.378)\left(2 - \dfrac{980}{1350}\right) = 58.317\ kN \end{cases}$$

V_r is the lateral load corresponding to diagonal cracking of the infill. The equivalent diagonal strut load corresponding to V_r is calculated from:

$$F_{strut} = \frac{V_r}{Cos\theta} = \frac{31.965}{Cos(36)} = 39.511\ kN$$

By using the properties of cracked section for the frame and equivalent diagonal strut for the infill, a computer model shown in Figure C.1 for the infilled frame was built in OpenSees software. By trial and error, the applied lateral load to the infilled system that produced an axial load equal to F_{strut} in the diagonal strut was calculated. The cracking load and lateral displacement of the infilled frame corresponding to the occurrence of diagonal cracking was calculated to be 39.98 *kN* and 0.92 *mm* respectively.